STUDY ON MODIFIED PVAs FROM TUNG OIL AND NATURAL RUBBER LATEX FOR COATING MATERIAL AND WATER RESISTANT FILM APPLICATIONS.

APICHAYA JIANPRASERT

A THESIS SUBMITTED IN PARTIAL FULFILLMENT
OF THE REQUIREMENT FOR THE DEGREE OF
DOCTORAL IN NANOSCIENCE AND NANOTECHNOLOGY
COLLEGE OF NANOTECHNOLOGY
KING MONGKUT'S INSTITUTE OF TECHNOLOGY LADKRABANG
2017

KMITL-2017-NT-D-001-002

หัวข้อวิทยานิพนธ์	การศึกษาการเตรียมพอลิไวนิลอัลกอฮอล์ที่ปรับปรุงด้วยน้ำมันทังและน้ำยางธรรมชาติสำหรับงานเคลือบผิวและฟิล์มต้านทานน้ำ
ชื่อนักศึกษา	อภิชญา เจียนประเสริฐ
รหัสประจำตัว	53670155
ปริญญา	ปรัชญาดุษฎีบัณฑิต
สาขาวิชา	นาโนวิทยาและนาโนเทคโนโลยี
พ.ศ.	2560
อาจารย์ที่ปรึกษาวิทยานิพนธ์	ผศ.ดร.ภัทธาวุธ มนต์วิเศษ

บทคัดย่อ

งานวิจัยนี้ศึกษาการเตรียมพอลิไวนิลอัลกอฮอล์ปรับปรุงสมบัติสำหรับงานเคลือบผิวและฟิล์มต้านทานน้ำ โดยเตรียมจากสารละลายพอลิไวนิลอัลกอฮอล์กับน้ำมันทังและ/หรือน้ำยางธรรมชาติในอัตราส่วนโดยน้ำหนัก 85:15 (ที่อัตราส่วนโดยน้ำหนักระหว่างน้ำมันทังต่อน้ำยางธรรมชาติเป็น 0:15, 5:10, 10:5 และ 15:0) ใช้โพแทสเซียมเปอร์ซัลเฟตเป็นตัวเร่งปฏิกิริยาแบบใช้ความร้อน หรือโพแทสเซียมเปอร์ซัลเฟต/โซเดียมไธโอซัลเฟตเป็นตัวเร่งปฏิกิริยาแบบรีดอกซ์ และใส่สารตัวเติมอนินทรีย์ (นาโนซิลิกา นาโนซิงค์ออกไซด์ และนาโนแคลเซียมคาร์บอเนต) เพื่อเพิ่มสมบัติเชิงกลและการต้านทานน้ำ นำพอลิไวนิลอัลกอฮอล์ปรับปรุงสมบัติที่เตรียมได้มาขึ้นรูปแผ่นฟิล์มบนจานเพาะเชื้อแล้วนำไปอบให้แห้งที่ 30 °C ถึง 80 °C ผลจากสมบัติการต้านทานน้ำแสดงให้เห็นว่าพอลิไวนิลอัลกอฮอล์สามารถเกิดโครงสร้างเชื่อมโยงโดยใช้ตัวเร่งปฏิกิริยาแบบใช้ความร้อนที่อุณหภูมิมากกว่า 60 °C และค่าสมบัติการต้านทานน้ำของพอลิไวนิลอัลกอฮอล์ปรับปรุงสมบัติเพิ่มขึ้นเมื่อใช้น้ำมันทังร่วมกับน้ำยางธรรมชาติ เทคนิคฟูเรียร์ทรานสฟอร์มอินฟราเรดสเปกโตรโฟโทเมทรี (Fourier Transform infrared Spectrophotometry, FTIR) สามารถยืนยันการเชื่อมโยงของน้ำมันทังที่มีผลต่อการปรับปรุงสมบัติการต้านทานน้ำและสมบัติเชิงกล นอกจากนี้ยังพบว่าการใช้น้ำมันทังร่วมกับน้ำยางธรรมชาติในพอลิไวนิลอัลกอฮอล์ปรับปรุงสมบัติสามารถเพิ่มสมบัติทางความร้อนและสมบัติเชิงกลที่ดีกว่าการใช้น้ำมันทังหรือน้ำยางธรรมชาติเพียงชนิดเดียว นอกจากนี้พอลิไวนิลอัลกอฮอล์ที่ปรับปรุงสมบัติด้วยน้ำมันทัง 15 % โดยน้ำหนักและนาโนซิลิกา 0-3 pph ให้สมบัติทางความร้อนและสมบัติเชิงกลที่ดี เมื่อนำพอลิไวนิลอัลกอฮอล์ปรับปรุงสมบัติมาทดสอบการเคลือบผิวกระดาษและเยื่อไม้อัดแล้วอบให้แห้งที่ 50 °C เป็นเวลา 60 นาที แล้วนำชิ้นงานที่เตรียมได้มาทดสอบพบว่าพื้นผิวที่ถูกเคลือบด้วยพอลิไวนิลอัลกอฮอล์ปรับปรุงสมบัติมีความชอบทั้งน้ำและน้ำมัน รวมทั้งมีอัตราการซึมผ่านของหยดน้ำและน้ำมันที่ช้าลง นอกจากนี้แผ่นฟิล์มต้านทานน้ำที่เตรียมด้วยระบบเชื่อมโยงโดยใช้แสงร่วมกับตัวเร่งปฏิกิริยาแบบรีดอกซ์สามารถปรับปรุงสมบัติการต้านทานน้ำและสมบัติอื่นๆของฟิล์มโดยประหยัดเวลาและพลังงาน

คำสำคัญ : ตัวเร่งปฏิกิริยา น้ำมันทัง น้ำยางธรรมชาติ พอลิไวนิลอัลกอฮอล์ปรับปรุงสมบัติ

Thesis Title	Study on modified PVAs from tung oil and natural rubber latex for coating material and water resistant film applications
Student Name	Miss. Apichaya Jianprasert
Student ID	53670155
Degree	Doctoral
Program	Nanoscience and Nanotechnology
Year	2017
Thesis Advisor	Asst. Prof. Dr. Pathavuth Monvisade

ABSTRACT

This research aims to prepare the modified PVA for coating material and water resistant applications. The modified PVAs were prepared by mixing poly(vinyl alcohol) solution (PVA) with tung oil and/or natural rubber latex at the weight ratio of 85:15 (Tung oil: natural rubber latex of 0:15, 5:10, 10:5 and 15:0 by wt.), cured by using potassium persulfate as a thermal catalyst or potassium persulfate/sodium thiosulfate as a redox catalyst. Nanosilica, nanozinc oxide or nanocalcium carbonate was used as a filler in various ratios to improve mechanical properties and water resistance. The modified PVA was casted onto the Petri dish and dried at several conditions; 30 $^{\circ}$C to 80 $^{\circ}$C, in an oven. The water resistant results showed the crosslinking reaction of PVA itself occurred when using thermal catalyst ($\geq$ 60 $^{\circ}$C) and the water resistance of the modified PVA was enhanced when tung oil and rubber were incorporated. FTIR results confirmed that the crosslinking reaction of tung oil in the modified PVA resulted in the improvement of water resistance. Moreover, the synergy of tung oil and rubber in the modified PVA gave better thermal behaviors and mechanical properties than those using only tung oil or rubber. In addition, 15% wt. of tung oil and 0-3 phr of nanosilica in the formula gained the better thermal and mechanical properties. After that, the chosen modified PVAs were applied by coating on paperboard and fiberboard and tested. The coated surface of modified PVAs showed both water and oil affinities and the decrease in water and oil absorption rates of those substrates. In addition, water resistant film was prepared through photocrosslinking reaction incorporating with redox catalyst improved the water resistance and other properties along with saving time and energy during process.

Key words: Catalyst, Tung oil, Natural rubber latex, The modified PVA

ACKNOWLEDGEMENTS

The author would like to take this opportunity to express sincere thanks to her advisors and people who gave useful advice and full support in this thesis.

The author wishes to express deep gratitude to her advisors, Asst. Prof. Dr. Pathavuth Monvisade and Prof. Yamaguchi Masayuki, for his valuable guidance, attention and encouragement throughout this thesis. It goes without saying to the thesis committee, Asst. Prof. Dr. Apiluck Eiad-Ua, Assoc. Prof. Dr. Naratip Vittayakorn, Asst. Prof. Dr. Darinee Phomyothin and Dr. Withawat Mingvanish for reading and criticizing the manuscript.

The author greatly appreciates the entire professors who have invaluable knowledge while studying in College of Nanotechnology, King Mongkut's Institute of Technology Ladkrabang. In the addition, thanks also to Scientific Instruments Service Center at Faculty of Science at King Mongkut's Institute of Technology Ladkrabang, Instrument Center at College of Data Storage Innovation at King Mongkut's Institute of Technology Ladkrabang and the School of Material Science, Japan Advanced Institute of Science and Technology (JAIST) for instrumental process and instrument analysis.

The author deeply appreciates the Thailand Research Fund (TRF) through the Royal Golden Jubilee Ph.D. Program for financial support.

The author also would like to give the special thanks to Mr. Sanit Sirapanichart, Miss Pitchaya Treenate and all of her friends at Polymer Synthesis and Functional Materials Research Unit (PSFMU) at department of Science at King Mongkut's Institute of Technology Ladkrabang who have been helping and encouraging her while studying the Ph.D. program at King Mongkut's Institute of Technology Ladkrabang.

Last but not least, the author would like to express the deepest appreciate her dearest family for love, care and encouragement that they have, which is the most important in her life forever.

MISS APICHAYA JIANPRASERT

Table of Contents

Table of Contents (CONT.)

Table of Contents (CONT.)

Page

Table of Contents (CONT.)

List of Tables

List of Figures

List of Figures (CONT.)

List of Figures (CONT.)

List of Figures (CONT.)

List of Figures (CONT.)

Abbreviations

PVA	:	Poly (vinyl alcohol)
PVAc	:	Polyvinyl acetate
$K_2S_2O_8$ or KPS	:	Potassium persulfate
$Na_2S_2O_3$	:	Sodium thiosulfate
SiO_2	:	Silicon dioxide
$CaCO_3$	:	Calcium carbonate
ZnO	:	Zinc oxide
FTIR	:	Fourier Transformed Infrared spectroscopy
DMA	:	Dynamic Mechanical Analysis
SEM	:	Scanning electron microscopy
E'	:	Storage modulus
E"	:	Loss modulus
Tan δ	:	Tan delta
T_g	:	Glass transition temperature
WVTR	:	Water Vapor Transmission Rate
WVP	:	Water vapor permeability

Chapter 1
Introduction

1.1 Research Motivation

Poly(vinyl alcohol) (PVA) is such a biodegradable polymer which is soluble in water. It has been widely used in various industrial applications, for instances, paper coating agent, adhesive, drug delivery carrier, flexible packaging film, etc. This is because PVA is environmental friendly and odorless. Moreover, it is easy to form film and its film has oil resistance property, good oxygen barrier, good transparency, printability, biodegradability and elasticity [1-4]. However, its shortcoming is poor water resistant property. Thus, the uses of PVA in commercial applications are limited. Many methods have been used to overcome this problem. For example, PVA was added by nanoparticles, crosslinked by heat, irradiation or chemicals to develop properties for its applications [5-7]. In terms of chemical crosslink methods, PVA can be crosslinked by several chemicals such as hexamethylene diisocyanate, glutaraldehyde and boric acid, etc [7-9]. However, their toxicity made them not suitable for packaging materials and human applications. Therefore, various natural hydrophobic chemicals [10-13] and/or many mineral fillers such as silica [14-16], calcium carbonate [17-18], etc. have been thoroughly studied to improve the hydrophobic property of PVA.

Natural rubber latex (R), a natural high elasticity material, is an unsaturated elastomer from natural sources. It can form hydrophobic film with high strength and high elongation at break after vulcanization process [19]. From the literatures, rubber has been blended with PVA to prepare multilayer films in order to improve their water resistant property [20-22]. However, rubber must be crosslinked under high temperatures (>120 ^{o}C) to achieve its reasonable water resistant property. Tung oil (T), a natural drying oil, is alternatively used as environmental-friendly coatings, varnishes, linoleum and a drying agent in paints [23-24]. The long carbon chain of tung oil provides not only a hydrophobic property but also a good crosslinker to form network structure because it has a conjugated double-bond structure which is able to generate free radicals and to crosslink itself into network structure resulting in film formations by temperature and oxygen [25]. As it can be crosslinked itself by heat and oxygen, this causes the surface to yield water resistant properties and reduce air/oxygen transmission. Tung oil was used to coat the surface or to blend with other polymers to improve gas barrier, water resistant and tensile properties of those surfaces or other polymers [26-27]. However, tung oil needs time and high temperatures to generate crosslinking in the structure of tung oil. Thus, the catalytic

systems and the modified structure of tung oil were studied to accelerate the crosslinking process [28-29].

Potassium persulfate (KPS) has been known as the thermal catalyst to activate double bond for free radical polymerization and also for crosslinking reaction [30-31]. However, it is necessary to use high temperatures to initiate the reaction. Since, it is not recommended to expose films, paperboards and fiberboards to high temperatures because they may be damaged. To lower the decomposition activation energy during free radical initiation process, the redox catalyst systems, such as couple KPS and sodium thiosulfate system, were of interest. Many researchers used this redox catalyst for crosslinking reaction [32-33]. Moreover, photoinitiator was also used to study photocrosslinking reaction by light radiation in many researches without applied temperatures [34-35].

Paperboards and fiberboards are widely beneficial in packaging because they are made from natural sources, easy recyclability, and degradable materials [36]. In contrast, they are hygroscopic and porous materials which incline to absorb humidity and applied printing ink. These caused the reduction of their mechanical strength and restriction to low-resolution printing, respectively [37]. The hydrophobic coating materials were applied to increase strength and reduce water absorption but they were poor at recyclability, difficult to process, low printability, and low oil resistance [37-40]. Furthermore, the most important problems concerned in their applications are toxic chemicals which caused some health problems. Thus, to produce coating materials more environmental-friendly, easy to recycle and promote printability, biodegradable hydrophilic polymers have been studied [41-43]. Even though they improved the recyclable property, oil resistance property, and environmentally friendly property, they have poor water resistance. To improve the water resistant property of coating materials, biodegradable polymers have been modified or blended with other materials or other additives [44-46].

Packaging films are also widely used in packaging industries because they are lightweight, easy to decorate with good transparency and protect food or many products from environmental conditions [47]. Good materials for packaging films are not only good film forming but also excellent barrier properties. Many petroleum materials were used to prepare packaging films such as polyethylene [48-49], polypropylene [50], polyamide [51], poly(ethylene terephthalate) [52], ethylene-vinyl alcohol [53]. However, most of petroleum materials are non-biodegradable polymers. They cause serious environmental problems. Thus, the biodegradable polymers have been used for packaging films instead of non-biodegradable polymers [54-56]. Although the biodegradable polymers are friendly to environment, their resistance to the humidity and mechanical properties are poor. It is clearly seen

that, new polymeric materials have been developed for coating materials and packaging films under the key advantage of their superior strength and water resistance.

Since PVA is a biodegradable polymer which has been used for coating materials and packaging films but their products have poor water resistant property. Therefore the combination of rubber and tung oil is an alternative way to improve water resistance of PVA. The aim of this work is to modify PVA for coating materials and water resistant films by rubber and tung oil at various rubber to tung oil ratios. Moreover, various nano-additives such as nanosilica, nanocalcium carbonate and nanozinc oxide, have been used in order to enhance the water resistant and the mechanical properties. Thermal catalyst (potassium persulfate, KPS) and redox catalyst (KPS and sodium thiosulphate) have been used to speed up the crosslinking reaction of these systems. The effects of catalytic systems (i.e., thermal and redox catalytic system), curing temperatures, types and contents of nano-additives were studied. Moreover, the presence of photoinitiators cooperating with catalytic systems (i.e. thermal and redox catalytic systems) and photocrosslinking times were studied. The chemical structure of modified PVA was characterized by FTIR. Water resistant property, mechanical thermal property, mechanical properties and hydrophobicity property of the modified PVA were evaluated. For applications, the suitable modified PVA were applied on paperboard. Water affinity and absorption rate by contact angle measurement of water or oil tests were investigated. Furthermore, water resistant films from a suitable modified PVA were prepared. Vapor permeability of their films was evaluated.

1.2 Objectives of the study

1. To modify PVA by using tung oil and natural rubber latex as coating materials and water resistant film applications.
2. To study the proper ratio of tung oil and natural rubber latex for modifying PVA.
3. To study the effect of catalytic systems (thermal and redox catalysts) on the properties of modified PVA of various curing temperatures.
4. To study the effect of nano-additives (nanosilica, nanocalcium carbonate and nanozinc oxide) on the properties of modified PVA.
5. To study the effects of photocrosslinking systems cooperating with thermal and redox catalytic systems on the properties of modified PVA at various exposure times.

1.3 Scopes of the study

1. The modification of PVA for coating material and water resistant film applications was prepared by using tung oil and natural rubber latex.

2. Thermal and redox catalytic systems were applied by varying the conditions of temperature as function of crosslinking agents.

3. Various nano-additives (nanosilica, nanocalcium carbonate and nanozinc oxide) were added to improve water resistant and mechanical properties.

4. The effects of ratios of tung oil to natural rubber latex, types and contents of nano-additives, types of catalyst and conditions of curing temperature on the properties of modified PVA were studied.

5. Photocrosslinking reaction was studied in the presence of photoinitiators cooperating with catalytic systems (i.e., thermal and redox catalytic systems) at various exposure times.

6. The chemical structure of modified PVAs was characterized by FTIR. Water resistant, thermal and mechanical properties of the modified PVAs were evaluated.

7. The suitably modified PVAs were applied on coating surfaces (i) paperboard and (ii) particleboard and then tested hydrophilic/hydrophobic properties and their morphology.

8. The suitably modified PVAs were casted to prepare the water resistant film in order to characterize and test for water resistant, thermal, mechanical and hydrophilic/hydrophobic properties.

1.4 Benefits of the study

1. Modified PVAs could be successfully prepared by using PVA, tung oil, natural rubber latex and mineral fillers with proper portions for coating materials and water resistant films.

2. Coating materials and water resistant films with reasonable water resistant and mechanical properties were achieved.

Chapter 2
Theory and Literature Reviews

2.1 Poly (vinyl alcohol) (PVA) [1-4]

Poly (vinyl alcohol) (PVA) is synthesized by polymerization of vinyl acetate monomer. Partial or complete hydrolysis of this polymer is used to prepare poly (vinyl alcohol) (Figure 2.1). The typically range hydrolysed alcohol product is 87% to 99% converted PVA.

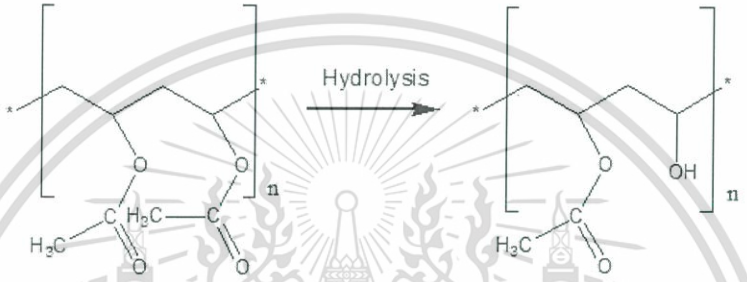

Figure 2.1 The preparation of PVA from poly (vinyl acetate).

PVA has excellent film forming, emulsifying, and adhesive properties. It is also resistant to oils, greases and solvents and it is odorless and nontoxic. Furthermore, this resin has high tensile strength, flexibility, high oxygen and aroma barrier. The physical properties of PVA, such as strength, water solubility, gas permeability and thermal characteristics vary with the degree of crystallinity, which is dependent on the degree of hydrolysis and the average molecular weight of the polymer. Partially hydrolysed grades contain residual acetate groups to reduce the overall degree of crystallinity. Thus, partially hydrolysed grades have lower strength and more increase in water solubility than those of the fully hydrolysed grades. However, PVA is fully degradable and it is a quick dissolver. PVA resins have a melting point of 230°C for the fully hydrolysed grades and 180–190°C for partially hydrolysed grades. The effects of molecular weight and hydrolysis level on the physical properties of PVA are summarized in Figure 2.2.

PVA is difficult to use in melt processing. Fully hydrolysed grades of PVA are more difficult to process than their partially hydrolysed grades due to their higher levels of crystallinity and consequent higher melting points. Plasticisers are incorporated into the polymer *via* a controlled process. Some other uses of (polyvinyl alcohol) include: paper adhesive, thickener, modifier, textile sizing agent, paper coatings, children's play putty, hard contact lens, fiber, surfactant, etc.

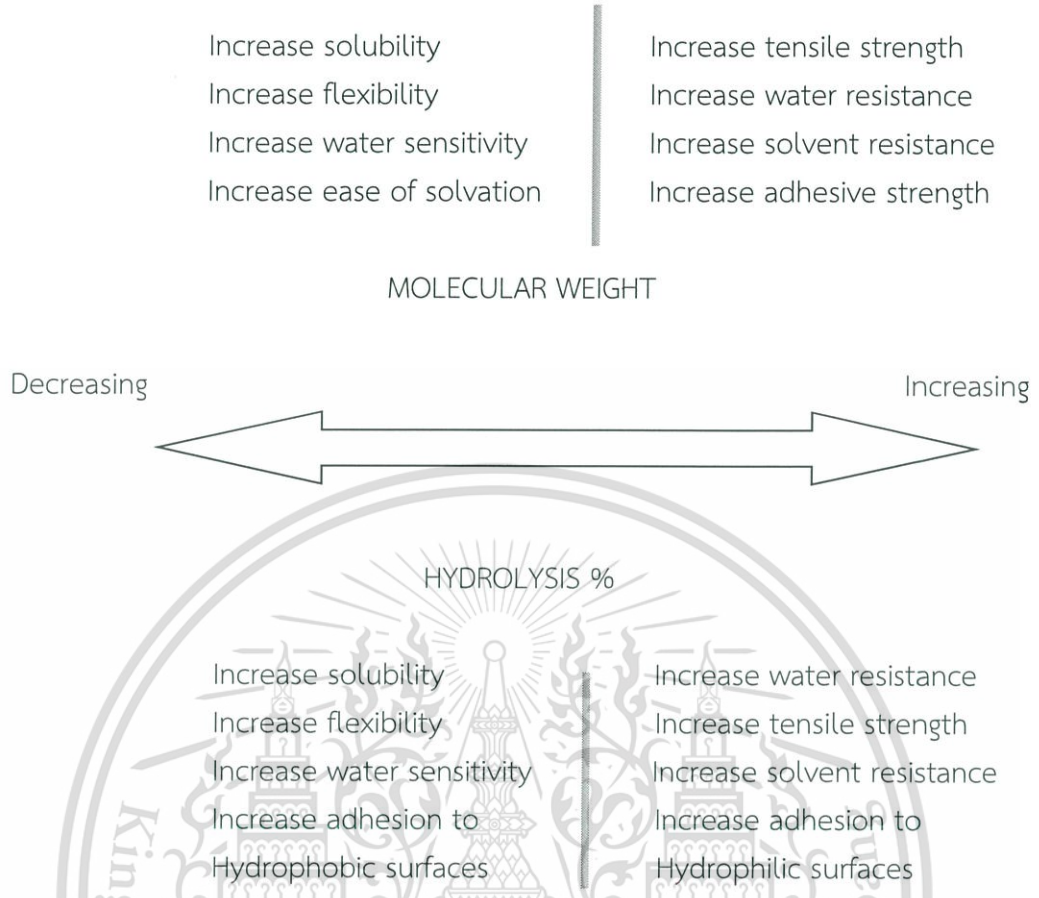

Figure 2.2 Effects of molecular weight and hydrolysis level on the physical properties of PVA.

Although PVA has excellent properties such as biocompatibility oil, grease and solvent resistance, low moisture permeation, oxygen barrier properties, and non-toxicity, it is able to dissolve in solvents with high polarity, such as water, dimethyl sulfoxide (DMSO), glycols, and dimethylformamide depending on the degree of polymerization (DP) and hydrolysis. In order to improve the performance of PVA, the modification of PVA was investigated in two categories:

Physical modifications

The physical modification is the preferred way to avoid toxic crosslinking agents for pharmaceutical and biomedical applications. These modifications cause a molecular rearrangement, forming more crystalline regions. The main physical modifications reported are as follows:

- Freeze-thawing

In this technique PVA is submitted to freezing and thawing cycles forming new crystalline regions. Moreover, this technique has been used to form hydrogels. This hydrogel is prepared by dissolving PVA and then submitted to freeze-thawing cycles to form a hydrogel.

- Annealing

This process relates to the heating of an aqueous PVA followed by a slow cooling until solvent was completely removed. Normally, this treatment prepares semipermeable membranes with many chain scissions. If this process is conducted alone, it is not reproducible due to the heterogeneous nature of the semicrystalline regions of the polymer produced leading to a membrane with diverse properties.

- Crosslinking by high energy radiation

High energy radiation on polymer enables numerous applications in industry, such as crosslinking of plastics, curing of coating, surface modification, sterilization and hydrogel formation. This method is better than the use of chemical crosslinking agents because of no chemical residue. When the radiation was applied, PVA absorbs energy and radicals are produced *via* the homolytic cleavage of a weak bond e.g. C–H bond alpha to the hydroxyl group. This is then followed by the coupling of two polymeric radicals, resulting in the formation of intermolecular crosslinks. The crosslinked polymer showed low mechanical properties, including elastic moduli, tensile strength and extensibility to break. Moreover, the radicals generated by irradiation might potentially attack and damage bioactive substances.

- Composites & blend

A composite and blend are homogeneous mixture generated from two or more hydrophobic materials such as additives, polylactic acid and caprolactone in order to improve water resistance and other properties of PVA, for example tensile strength, water barrier property.

Chemical modifications

The chemical modification is the easy way to prepare the stable macromolecular structure of PVA through intermolecular and intramolecular interactions. These modifications formed higher structure, leading to the better properties. The main chemical modifications reported are as follows:

- Crosslinking by chemical agents

Crosslinking leads to the formation of network or branched structures of PVA. PVA properties can be modified depending on the intended application. In theory, PVA structure could be reacted with hydroxyl groups by potential crosslinking agents. The most widely used crosslinking agents are glutaraldehyde, formaldehyde, acetaldehyde, glyoxal, boric acid, and isocyanates. When chemical agents are used to crosslink PVA, toxic residues could be presented in the final product and had undesirable effects. Therefore, this crosslinked product should not use for biomedical and pharmaceutics applications.

- Radical formation

This reaction occurred through the free radical polymerization. The free radical was generated to initiate by catalyst or initiator. The free radicals are abstracted to PVA, causing an internal polymerization, leading to an increase in the molecular weight and consequently, an increase in its hydrophobicity.

- Graft copolymerization

Graft copolymerization is a branched copolymer with a linear backbone of PVA and randomly distributed branches of two or more different types of hydrophobic monomers in order to have the new properties and improve water resistant properties.

2.1.1 Literature reviews

S.K. Ozaki *et* al. [57] studied on the environmentally friendly wood-based product composed of waste wood and poly(vinyl alcohol) (PVA) modified by phthalic anhydride (PA). Then Sugi (Criptomeria japonica) flour was added to the PA/ PVA reaction medium, and hot-pressed under 50 MPa at 180 ^{o}C. Varying the PA/ PVA ratio yielded composites with flexural modulus of elasticity (MOE) values of 13 GPa and modulus of rupture (MOR) of 90 MPa. The biodegradation was performed by the soil burial test. The changes in the composites' structures were investigated by infrared spectroscopy (IR), scanning electron microscopy (SEM) and the decrease in mechanical properties was monitored.

X. Liu *et* al. [58] studied on the wood adhesive which was prepared from PVA crosslinked with sodium silicate. This adhesive had the perfect bonding strength as well as water resistance. The results showed that the most suitable condition was the ratio of PVA: sodium silicate : OP-10 : weak acids = 20 : 3 : 0.05 : 2.5. The bonding strength of proper plywood reached 0.75 MPa and the 24 h thickness swell (TS) is 4.5% which was much better than the second class plywood standard.

H. Imam *et* al. [59] studied on wood adhesive prepared from a natural renewable resource. The characterization and the optimization of starch and poly(vinyl alcohol) (PVA) based crosslink adhesive suitable for wood-to-wood bonding in interior applications were described. The crosslinker, hexamethoxymethylmelamine produced effective crosslinking through a trans-esterification reaction between methoxy groups and hydroxyl groups in starch, PVA and wood, where hydroxyl groups replaced methoxyl groups forming ether bonds with the crosslinking. Optimal viscosity of the adhesive was obtained at 27% solid content. The optimum cure temperature and cure time were 175°C and 15 min, respectively. Wood samples were conditioned at 93.5% RH for 2 months exhibited >95% failure in wood but little in adhesive joints. Scanning electron microscopy revealed no visible growth of fungi or other microorganisms on the adhesive after 2 months exposure of samples at 97 %RH followed by 1 year at 50 %RH.

M. Krumova *et* al. [60] studied on the different degree of crosslinking poly(vinyl alcohol) crosslinked with hexamethylene diisocyanate. It was found that the variation of the thermal and mechanical properties of PVA with the crosslinking density suffer an initial decrease, due to the diminution of the crystallinity of the system, caused by the increasing of the crosslinking density. This behaviour is explained as a result of the competitive action of at least three factors during the crosslinking: (i) weakening of the existing physical network due to hydrogen bonding; (ii) formation of a chemical network; and (iii) introduction of flexible moieties due to the specific chemical structure of the crosslinker itself.

J. Wang *et* al. [5] studied on the synthesized high-performance graphene/PVA nanocomposites. These nanocomposites revealed increases of up to 212% in tensile strength and 34% in elongation at break with only 0.5 wt% graphene content. Water absorption measurements showed that the water absorption ratio of the graphene/PVA nanocomposites decreased from 105.2 to 48.8%, and the barrier properties were obviously improved. Contact angle measurements showed that the composites were hydrophobic (θ > 90°) in contrast to the highly hydrophilic (θ < 90°) pure PVA.

T.M.R Miranda *et* al. [6] studied on the crosslinked PVA in the presence of sodium benzoate and under ultraviolet irradiation (1 and 4 h.). Principal component analysis (PCA) is a mathematical procedure that allows treatment of the entire infrared spectrum and is very appropriate for analyzing the chemical reaction initiated by sodium benzoate which occurred in PVA upon UV irradiation. By PCA technique, it could clarify the mechanism of crosslinking of PVA. Moreover, it suggested that a free radical arising from the photolysis of sensitizer would abstract a

tertiary hydrogen atom from the polymer chain to yield a polymeric radical. This radical reacted with O-H groups, leading to the formation of ether bonds between the polymeric chains and hence to crosslinking and insolubilization of the PVA.

E.E. Shafee *et* al. [7] studied on poly(vinyl alcohol) (PVA) networks prepared by the reaction of PVA with hexamethylene diisocyanate in solution and casting. The dynamic-mechanical properties of PVA films used to investigate the interaction between water molecules and hydrophilic polymer network of crosslinked PVA. The calculated Flory–Huggins interaction parameter decreased with increasing the volume fraction of water in the hydrogel and increased slightly with increasing crosslink density. This attributed to the decreasing hydrophobicity of the network with increasing content of the hydrophobic crosslinking agent. For the water diffusion coefficients, D, in the networks obtained by means of dynamic sorption experiments increased with increasing water activity. The apparent diffusion coefficient was determined from dynamic sorption experiments, which increased with increasing water activity.

2.2 Tung oil [61-62]

Tung oil or **China wood oil** is a drying oil obtained by pressing the seed from the nut of the tung tree (*Vernicia fordii*) (Figure2.3). It belongs to the Euphorbia Family (Euphorbiaceae) along with the candlenut tree (A molucanna). Tung oil hardens upon exposure to air and polymerizes into a tough, glossy, waterproof coating. The resulting coating is transparent and plastic-like. This oil is widely used as the wood finishings, waterproof coatings, the component of caulk and mortar and the ingredient in oil paints and printing inks.

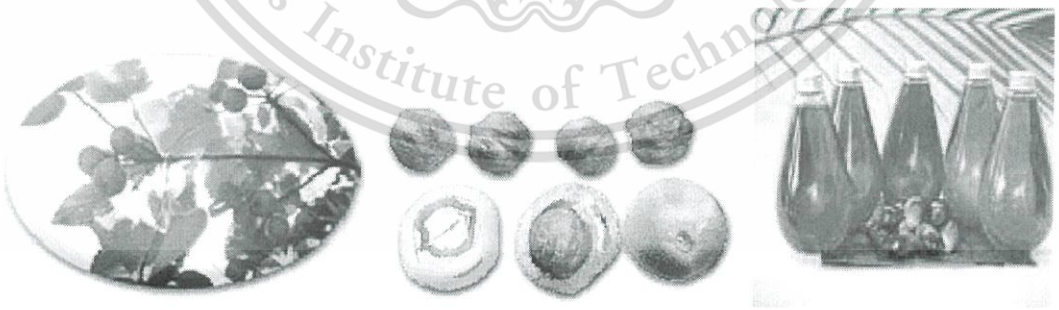

Figure 2.3 The tung tree, tung nut and tung oil.

Pure tung oil is water and alkali resistance. It resists penetrates well, builds quickly, consolidates the wood surface and builds the transparent matte finish. In addition, it contains no thinners or driers and it has a light nutty odor.

Tung oil is composed primarily of eleostearic acid, with smaller amounts of oleic, linoleic and palmitic glycerides. Eleostearic acid is the crystalline unsaturated

fatty acid that exists in two stereoisomeric forms: The alpha acid occurring as the glycerol ester especially in tung oil, and the beta acid obtained from the alpha acid by irradiation (9, 11, 13-octadecatrienoic acid). The amount of fatty acid compositions and chemical structures of tung oil are shown in Table 2.1 and Figure 2.4, respectively.

Table 2.1 The major fatty acid compositions of tung oil.

Compositions	%
Palmitic acid	5.5%
Oleic acid	4.0%
Linoleic acid	8.5%
alpha-Eleostearic acid	82.0%

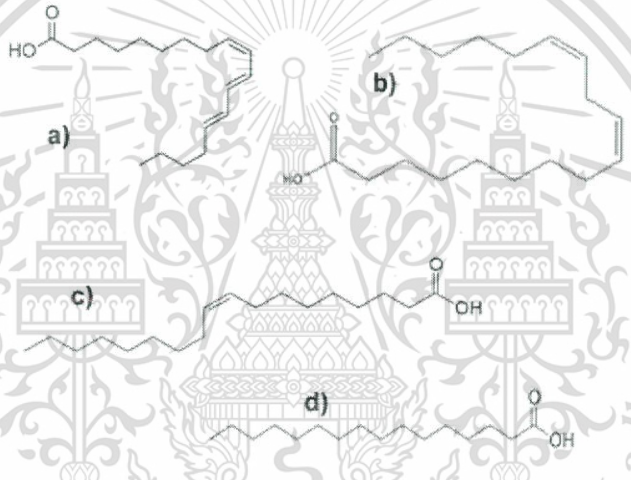

Figure 2.4 The structure of tung oil compositions; (a) Eleostearic acid, (b) Linoleic acid, (c) Oleic acid and (d) Palmitic acid.

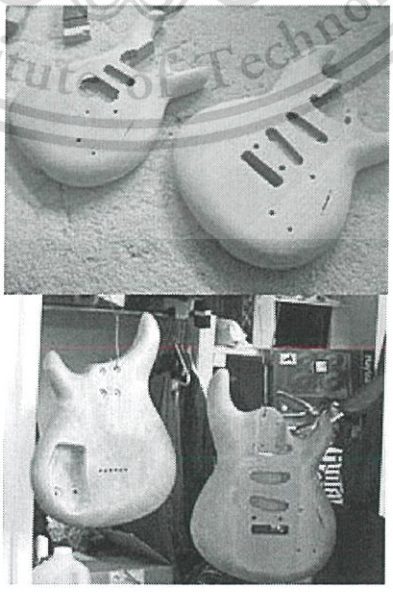

Figure 2.5 The tung oil coated specimen.

2.2.1 Application

The surface should be removed all loose particles such as any filling, sealing or staining. It should be rubbed with lightly sand over the wood and then cleaned by a soft rag before the oil is applied as shown in Figure 2.5. After that, the oil can soak in and then any excess is removed with clean soft rags. The surface let dry completely in 24-48 h. Tung oil is recommended for kitchen tables, chopping blocks and board. Because of its non-toxic nature, it is particularly made children's toys and furniture.

2.2.2 Literature reviews

Z.O. Oyman *et* al. [25] studied on the oxidation of non-conjugated drying oil (linseed oil) and conjugated drying oil (tung oil) by using Co(II)-2-ethylhexanoate (Co-EH) as the catalyst. For linseed oil, the broken hydrogen works throught arylic hydrogen atom. The higher oxygen content made hydroperoxide in which it then decomposed to be the antioxidant as alkoxy and peroxy product. For tung oil, the broken hydrogen is from monoallylic. Tung oil uses oxygen more than linseed oil. It was concluded that, free radical likely occured at conjugate double bond by replacing hydrogen atom of monoallylic.

XU Gui-zhuan *et* al. [63] studied on trans-esterification condition between tung oil and methanol using immobilizer lipase NOVO435 as the catalyst. It was found that the proper ratio between methanol and oil was 2.2:1 by using 14% of oil weight at 43°C. After eighteen hours, 67.5% of oil weight was changed into methyl ester (For the theory, 73.3% changed). From this experiment, lipase was removed and organic solvent was reused. The factors in this study were the ratio of methanol and tung oil, catalyst contents, temperature and time of process.

W. Chumchen [64] studied on the formaldehyde-free wood adhesive for wood joint. The adhesive was prepared from poly(vinyl alcohol) (the viscosity of solution are 500, 800, 1000, 2000 and 3000 Cps.) using tung oil as a crosslinking agent (0-20% w/w) and using the catalyst in the process. This adhesive was then tested for mechanical properties relevant to DIN EN 204-1991 standard (dry and wet state). It was found that tung oil could improve shear strength and water resistance of this adhesive. In summary, the formaldehyde-free wood adhesive using 15 and 20% w/w of tung oil could gain shear strength over the DIN EN 204-1991 standard (10 MPa at dry state and 8 MPa at wet state). The specimen prepared from 20%w/w of tung oil and compressed at 90°C for 2 h. gained the highest shear strength (13.0 MPa at dry state and 11.3 MPa at wet state).

R. Tongsuk *et* al. [65] studied on the formaldehyde-free wood adhesive prepared from poly(vinyl alcohol) using tung oil (15 and 20% w/w) as the crosslinking agent, using *p*-toluene sulfonic acid as the catalyst and using potassium persulfate as

the initiator. Sodium lauryl sulfate was also added as the surfactant to make a well-dispersed adhesive (1 and 2% w/w). After that, the adhesive was tested in various properties such as viscosity, solid content and % swelling of these adhesive films. Then particleboard was shaped by this adhesive (15, 20 and 25% w/w) and Eucalyptus flake. Later, this particleboard was examined followed JIS A 5908 and TISI 876 standard for particleboard. The sample was tested about density, moisture content, % swelling thickness, bending strength, bending modulus and internal bond. It was found that the specimen prepared from adhesive containing tung oil 15% w/w and SLS 2% w/w with Eucalyptus flake could pass both of JIS A 5908 and TIS 876 standards excepted for % swelling thickness.

P. Lakkanapornwisit [66] studied on the formaldehyde-free wood adhesive for particleboards. This adhesive was prepared from poly(vinyl alcohol) using drying oil (tung oil and linseed oil, 15 % w/w) as the crosslinking agent. The effect of silica (0-5% w/w) and *p*-toluene sulfonic acid (0 and 1% w/w) was investigated. The adhesive properties were evaluated such as viscosity, solid content and % swelling of adhesive films. After that, this adhesive was used to prepare particleboards with eucalyptus flake or rubber wood flake. The amounts of adhesive in the particleboard are 15 and 20% w/w. Finally, the particleboards were tested following JIS A 5908 and TISI 876 standard for particleboard for example, density, moisture content, % swelling thickness, bending strength, bending modulus and internal bond. It was clearly seen that the particleboard prepared with 15% of tung oil, 1% of silica and 20% w/w of adhesive in particleboard could pass both standards.

2.3 Natural rubber [19]

Natural rubber consists of the organic compound isoprene, with minor impurities of other organic compounds plus water. The major commercial source of natural rubber latex is the Pará rubber tree (*Hevea brasiliensis*) because it grows well and it can produce more latex for several years. The latex is a sticky, milky colloid by making incisions into the bark and collecting the fluid in vessels. The latex then is refined into rubber ready for commercial processing. Natural rubber is used extensively in many applications and products because it has a large stretch ratio, high resilience, and it is extremely waterproof.

Rubber exhibits the unique physical and chemical properties. Natural rubber has the presence of a double bond in each repeat unit and it is inclined to vulcanisation. The two main solvents for rubber are turpentine and naphtha (petroleum). Vulcanization of rubber creates disulfide bonds between chains, so it limits the degrees of freedom. This result shows that the chains tighten more quickly

for a given strain, thereby increasing the elastic force constant and making rubber harder and less extensible.

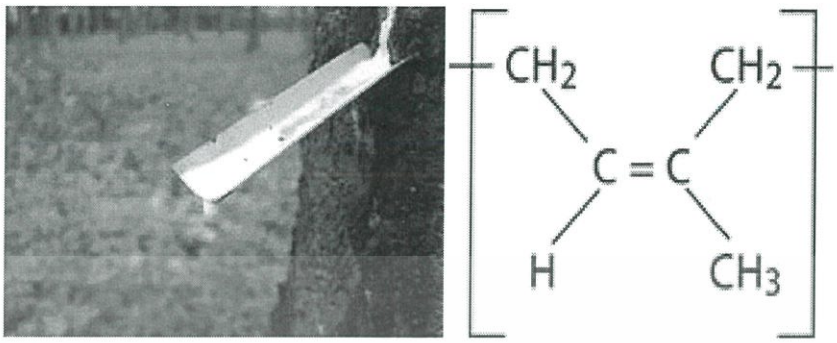

Figure 2.6 Physical appearance and repeating unit of rubber latex.

2.3.1 Chemical

Latex is an elastomer containing the chemical structure of cis-1,4-polyisoprene with a molecular weight of 100,000 to 1,000,000 daltons. Physical appearance and repeating unit of rubber latex are shown in Figure 2.6. Typically, a small percentage (up to 5% of dry mass) of other materials, such as proteins, fatty acids, resins, and inorganic materials (salts) are found in natural rubber. Polyisoprene can also be created synthetically, but the synthetic and natural routes are completely different. Synthetic cis-polyisoprene and natural cis-polyisoprene are derived from different precursors. Most rubber in everyday use is vulcanized to form thermoset polymer. If it is heated and cooled, it is degraded but not destroyed. The final properties of a rubber item depend not only on the polymer, but also on modifiers and fillers, such as carbon black, whiting, and a host of others.

2.3.2 Literature reviews

W. Simchareona *et* al. [20] studied on natural rubber latex (NRL) films prepared by the blend of deproteinized NRL (DNRL), hydroxypropylmethyl cellulose (HPMC), dibutyl phthalate (DBP), various enhancers, i.e., fatty acid (oleic acid), ester of fatty acid (isopropyl palmitate; IPP), fatty alcohol (propylene glycol; PG), hydrocarbon (olive oil), and terpene (menthol), using solution-casting technique. After that, the obtained films were studied the physical and mechanical properties. The results showed that DNRL could be compatible with all enhancers. Hence, the physical and mechanical properties of the blended films depended on types and concentrations of enhancers.

S.A. Riyajan *et* al. [22] studied on the semi-interpenetrating polymer network (semi-IPN) based on epoxidised natural rubber and poly(vinyl alcohol) containing maleic acid as a crosslinking reagent. The curing time and dose of maleic acid were

varied from 10 to 60 min and from 10 to 60% (w/w), respectively. The semi-IPNs exhibited good mechanical properties. The highest tensile strength of the semi-IPN based on ENR and PVA with 60% maleic acid was 32 MPa. The semi-IPN samples showed good thermal stability and there were no phase separation occurring.

2.4 Initiators [67-68]

For this research, the main modified PVA occurred through the reaction of active centers. The active centers could occur by thermal initiator, redox initiator or photoinitiator as follows:

2.4.1 Thermochemical reactions are brought about by molecular collisions. This may occur spontaneously by the absorption of heat. A thermal initiator is usually a weak organic compound that can be decomposed thermally to produce free radicals such as dialkyl peroxides (ROOR), diacylperoxides (RCO–O–O–CO–R), hydroperoxides (ROOH), and azo compounds (RN› NR). Equations 2.1–2.3 illustrate the mechanism of commonly used free radical initiators, benzoyl peroxide, azobisisobutyronitrile, and di-*t*-butylperoxide, respectively.

benzoyl peroxide (2.1)

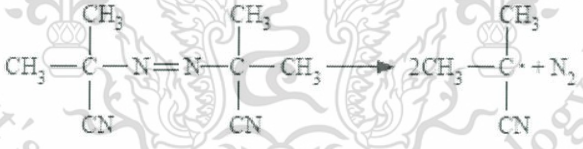

azobisisobutyronitrile (AIBN) (2.2)

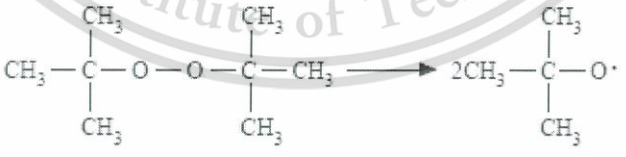

di-*t*-butylperoxide (2.3)

For example, the thermal decomposition of benzoyl peroxide, which takes place between 60 and 90 °C, involves the homolytic cleavage of the O–O bond to yield benzoyl free radicals that may react to yield phenyl radicals and carbon dioxide. Dinitrile or azo compounds such as 2,2′-azo-bis-isobutyronitrile, AIBN, require temperatures of about 70-80 °C to produce decomposition with free radical formation.

2.4.2 Redoxchemical reactions carry out usually in aqueous medium, the decomposition of peroxide or persulfate is greatly accelerated by the presence of a reducing system referred to as redox initiation. The initiation from the thermal decomposition of organic compounds discussed above is appropriate only for reactions carried out at room temperature or higher. The enhanced rate of free radical formation in redox reactions permits reaction at relatively lower temperatures. Equations 2.4–2.6 show typical redox reactions for emulsion polymerization.

$$S_2O_8^{2-} + HSO_3^- \longrightarrow SO_4^{2-} + SO_4^- + HSO_3 \quad (2.4)$$

$$S_2O_8^{2-} + S_2O_3^- \longrightarrow SO_4^{2-} + SO_4^- + S_2O_3^- \quad (2.5)$$

$$HSO_3^- + Fe^{3+} \longrightarrow HSO_3 + Fe^{2+} \quad (2.6)$$

For example, persulfate ion initiator (e.g., from $K_2S_2O_8$) reacts with reducing agent such as bisulfite ion (e.g., from $NaHSO_3$) to produce radicals for redox initiation (Equations 2.4 and 2.5). Ferric ion may also be used as a source of radicals (Equation 2.6). Other redox reactions involve the use of alkyl hydroxides and a reducing agent such as ferrous ion (Equation 2.7).

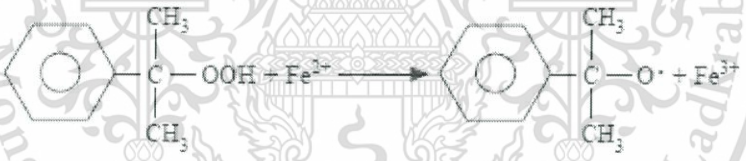

(2.7)

Moreover, the important parameters, considered to choose an initiator for free radical reaction, are the temperature range to be used for the reaction and the reactivity of the radicals formed. For example, the decomposition of benzoyl peroxide may be accelerated at room temperature by employing ternary or quaternary amines.

2.4.3 Photochemical reaction is the study of chemical reactions, isomerization & physical behavior that may occur under the influence of visible/ultraviolet light. The UV (wavelength 100-400 nm), visible light (400-750 nm), or infrared (750-2500 nm) radiation are mainly used in photochemical reactions. All photochemical reactions take place in two steps. Firstly, the reacting molecules are activated by absorption of UV, light or infrared radiation. Secondly, the activated molecules undergo a photochemical change. For example, in the combination of hydrogen and chlorine,

The first step is: $Cl_2 + h\nu \longrightarrow 2Cl^{\cdot}$ (2.8)

The activated chlorine atoms ($Cl^{\cdot}$) then undergo chemical reaction with activated hydrogen atoms ($H^{\cdot}$). It is evident from the above reaction that the second step can occur in absence of light. Moreover, there are five types of photochemical reactions as follows;

Types of photochemical reactions

1) Photo-dissociation

$A\text{-}B + h\nu \longrightarrow A^{\cdot} + B^{\cdot}$ (2.9)

2) Photo-induced rearrangements, isomerization

$A + h\nu \longrightarrow B$ (2.10)

3) Photo-addition

$A + B\text{-}C + h\nu \longrightarrow A\text{-}B + C$ (2.11)

4) Photo-substitution

$A + B + h\nu \longrightarrow A\text{-}B$ (2.12)

5) Photo-redox reactions

$A + D + h\nu \longrightarrow A^- + D^+ \longrightarrow \ldots$ (2.13)

$SC + h\nu \longrightarrow e^-_{cb} + h^+_{vb}\ A^- + D^+ \longrightarrow \ldots$ (2.14)

2.4.4 Potassium persulfate [69-70]

Figure 2.7 The structure of potassium persulfate.

Potassium persulfate ($K_2S_2O_8$) is a chemical compound. It is used in organic chemistry as an oxidizing agent for instance in the Elbs persulfate oxidation. It can also be used as an initiator in polymerization. The properties of potassium persulfate and the structure of potassium persulfate are shown in Table 2.2 and Figure 2.7, respectively.

Table 2.2 The properties of potassium persulfate

Appearance	white powder
Density	2.48 g/cm^3 solid
Melting point	100 °C (decomposes)
Solubility in water	4.7g/100g water
Molar mass	270.32 g/mol

Potassium persulfate is thermally sensitive and decompose to produce two free radicals. The temperature activity of potassium persulfate estimate more than 70 °C. In addition to thermal decomposition, it can be decomposed by activators or promoters at temperatures well below the normal decomposition temperature. A major application of these compounds is as free radical initiators in the polymerization of vinyl and diene monomers in the plastics and coatings industries. They are also used as crosslinking and modifying agents for polyolefins, as vulcanizing agents for elastomers, and as curing agents for polyester resins.

2.4.5 Sodium thiosulfate [71]

Sodium thiosulfate ($Na_2S_2O_3$) is a colorless crystalline compound. The thiosulfate anion is tetrahedral in shape and is notionally derived by replacing one of the oxygen atoms by a sulfur atom in a sulfate anion. Sodium thiosulfate is used in many applications such as "clock reaction", Iodometry, photographic processing, gold extraction, and is also used in analytical chemistry. Furthermore, it is used for medical, bleach, treat effluent from waste water and used as the strong oxidizing agent, etc. The structure and physical appearance of sodium thiosulfate and the properties of sodium thiosulfate are shown in Figure 2.8 and Table 2.3, respectively.

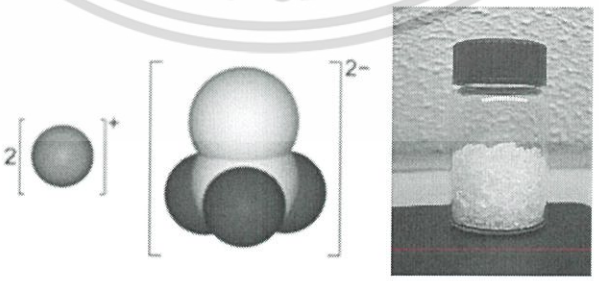

Figure 2.8 The structure and physical appearance of sodium thiosulfate.

Table 2.3 The properties of sodium thiosulfate.

Appearance	White crystals
Density	1.667 g/cm^3
Melting point	48.3 °C (pentahydrate)
Solubility in water	70.1 g/100 mL (20 °C) 231 g/100 mL (100 °C)
Molar mass	158.11g/mol (anhydrous) 248.18 g/mol (pentahydrate)

2.4.6 Literature reviews

S.A. Riyajan *et* al. [72] studied on the effect of potassium persulphate ($K_2S_2O_8$) on the physical property of crosslinked PVA. The viscosity of PVA solution in the presence of $K_2S_2O_8$ increased with increasing reaction time and PVA content in solution. The rate of crosslinked PVA was proportional to $K_2S_2O_8$ contents and temperature. The crystalline content of PVA dramatically increased after chemical modification confirmed by XRD.

N. Işıklan *et* al. [73] studied on the grafting of itaconic acid (IA) onto sodium alginate (NaAlg) using cerium(IV) ammonium nitrate/nitric acid (CAN/HNO_3) as redox system was carried out by free radical polymerization. The reaction conditions for maximum grafting were optimized by varying the reaction time, temperature, percentage of sodium alginate, monomer, initiator, and nitric acid concentrations. The optimum reaction conditions were obtained with reaction time of 5 h, reaction temperature of 30 °C, IA concentration of 0.92 M, CAN concentration of 1.368×10^{-1} M, HNO_3 concentration of 0.094 M and percentage of NaAlg 0.5 g/dL. The solubility test of NaAlg-g-PIA was also investigated using solvents. Moreover, the results indicated that prepared graft copolymer was non-soluble in the various solvents, while it was soluble only in saturated solution of NaOH.

L. Pengju *et* al. [33] studied on graft copolymers of chitosan with acrylonitrile (AN) prepared by free radical polymerization using ammonium persulfate and sodium thiosulfate as the redox system. The optimum reaction conditions were found using [AN] 0.9 mol/L, [CS] 13.3 g/L, [Initiator] 0.006 mol/L, 62±1 °C for 2 h. Then the solubility of chitosan-g-PAN was investigated by using several solvents. It was found that copolymer showed a good solubility in NaSCN and HNO_3 and good film-forming property.

Huiyu Bai *et* al. [74] studied on the preparation of composites based on poly(vinyl alcohol) (PVA) and micro- and nano-fibrillated cellulose (M/NFC). The addition of crosslinking HEMA monomers and a photoinitiator formed an interpenetrating network with PVA and thus improved the properties of the composite films. Photocrosslinked PVA/(M/NFC)/polyHEMA composite films were produced by casting followed by UV polymerization. Photocrosslinking reaction increased the interaction between PVA and (M/NFC) and improved the (M/NFC) distribution in PVA/(M/NFC)/polyHEMA composite films. Compared to PVA/(M/NFC) films, the photocrosslinked PVA/(M/NFC)/poly-HEMA systems exhibited improved water resistance with well thermal and barrier properties. Moreover, thermal results presented that the strong interaction between PVA and (M/NFC), mainly *via* hydrogen bonding or bond network from the photopolymerization of HEMA in the composite films are main factor in the formation of the IPNs.

2.5 Silicon dioxide [75]

Silicon dioxide, also known as silica (from the Latin *silex*), quartz, silicic oxide, silicon(IV) oxide, crystalline silica, is the oxide of silicon with the chemical formula SiO_2. It is manufactured in several forms including fused quartz, crystal, fumed silica, colloidal silica, silica gel, and aerogel. Silica is used primarily in the production of glass for windows, drinking glasses, beverage bottles, and many other uses. For example, in hydrated form, it is used in toothpaste as a hard abrasive to remove tooth plaque. In cosmetics, it is useful for its light-diffusing properties and natural absorbency. Colloidal silica is used as a wine and juice fining agent. In pharmaceutical products, silica aids powder flow when tablets are formed. Crystalline silica is used in hydraulic fracturing of formation which contains tight oil and shale gas. The physical appearance and structure of silicon dioxide and the properties of silicon dioxide are shown in Figure 2.9 and Table 2.4, respectively.

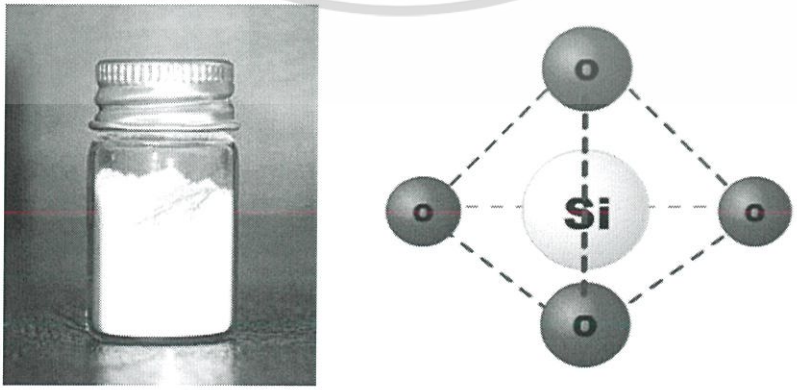

Figure 2.9 The physical appearance and structure of silicon dioxide.

Table 2.4 The properties of silicon dioxide.

Appearance	Transparent crystals
Density	2.648 g/cm^3
Melting point	1600-1725 °C
Molar mass	60.08 /mol

2.5.1 Literature reviews

M. Minelli. *et* al. [14] studied on the gas barrier properties of hybrid organic–inorganic coatings formed by poly(vinyl alcohol) (PVA) and SiO_2, obtained *via* sol–gel technique. It has been shown that the oxygen, nitrogen and carbon dioxide transfer rates of barrier polymers such as poly(ethylene terephthalate) and oriented polypropylene could be further reduced. Several polymeric films were evaluated as the supports and the addition of the coating results in a remarkable improvement of the oxygen barrier properties. On one hand, the trend of oxygen permeability and diffusivity indicated that the diffusivity decreased with increasing silica content, due to increased tortuosity. On the other hand, the solubility increased with increasing silica content, due to physical adsorption onto silica. As a result, the permeability decreases with silica weight fraction for the hybrid coating with lower silica content (30%), whereas for a content of silica of 50% the permeability was higher than that measured on a pure PVA coating. Interestingly, the oxygen permeability of the hybrid coatings remained extremely good even after a prolonged immersion in either liquid water or saturated water vapor. This is a good indication that the present materials can offer the exceptional barrier properties of the organic phase (PVA) without being plasticized and dissolved by water.

F. Liu *et* al. [15] studied on the improvement of poly(vinyl alcohol) (PVA)/silica (SiO_2) composite polymer coating on wooden substrates with super repellency water, low sliding angles, low contact angle hysteresis and relatively better mechanical robustness. In this study, the produced wood surfaces exhibited with a contact angle of 159° and a sliding angle of 4°, and the relatively better mechanical robustness.

J. Li *et* al. [16] studied on the modified organic PVA using inorganic silica sol. The tensile strength and Young's modulus of these hybrid films were improved compared with the neat PVA film. It was found that PVA matrix contains 20wt% silica was considerable increased in tensile strength and Young's modulus by factors of 1.9 and 3.2, respectively. The solubility measurements of the hybrid showed the enhancement of water resistance. The solubility and degree of swelling decreased with the addition of silica. Strong interfacial bonding between the silica and the PVA

matrix and homogenous distribution of the silica particles in PVA improved mechanical strength.

2.6 Calcium carbonate [76]

Calcium carbonate is the chemical compound with the formula $CaCO_3$. It is a common substance found in rocks in all parts of the world and it is the main component of shells of marine organisms, snails, coal balls, pearls, and eggshells. The physical appearance and structure of calcium carbonate and the properties of calcium carbonate are shown in Figure 2.10 and Table 2.5, respectively.

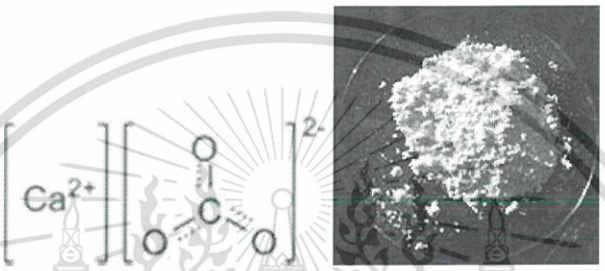

Figure 2.10 The physical appearance and structure of calcium carbonate.

Table 2.5 The properties of calcium carbonate.

Appearance	Fine white powder; chalky taste
Density	2.711 g/cm^3 (calcite) 2.83 g/cm^3 (aragonite)
Melting point	825 °C (aragonite) 1339 °C (calcite)
Molar mass	100.869 Ol

2.6.1 Preparation

The majority of calcium carbonate used in the industry which is extracted by mining or quarrying. Pure calcium carbonate can be produced from a pure quarried source. Alternatively, calcium carbonate is prepared from calcium oxide. Water is added to give calcium hydroxide and carbon dioxide is passed through this solution to precipitate the desired calcium carbon. From natural, there are many sources to find calcium carbonate for instance, rock include limestone, chalk, marble, eggshells, snail shells, corals and most seashells. For its applications, there are the use in the construction industry, oil industry, a major component of blackboard chalk, a common filler material in glove, paper for saving in material and production costs or

improve the properties such as print ability mechanical properties (tensile strength and elongation), rigidity and electrical properties, etc.

2.6.2 Literature reviews

B. Shi *et* al. [17] studied on using inorganic fillers such as $CaCO_3$ and talc to facilitate the plasticized PVA processing for blown films. It was found that the presence of $CaCO_3$ in PVA film could improve water resistant property. The filled PVA films can delay or reduce water solubility (7 to 10 mim) whereas the neat PVA films are soluble in water suddenly. Thus the product could use for specialty applications such as packaging of pesticides during shipping and storage. In conclusion, PVA films with $CaCO_3$ could improve the processability for the melt extrusion which produced PVA film should cost less than the solution-cast PVA films.

G.Q. Zheng *et* al. [18] studied on the composites of poly(vinyl alcohol) (PVA) and calcium carbonate ($CaCO_3$) prepared by *in situ* synthesis of $CaCO_3$ in PVA solution. X-ray diffraction analysis revealed that calcium carbonate was mainly composed of aragonite and calcite. The composites had good mechanical properties when they were increased with higher content of calcium carbonate.

2.7 Zinc oxide [77]

Zinc oxide, a white powder that is insoluble in water, is an inorganic compound with the formula ZnO. It is widely used as an additive in numerous materials and products including plastics, ceramics, glass, cement, lubricants, paints, ointments, adhesives, sealants, pigments, batteries, fire retardants, and first aid tapes. It occurs naturally as the mineral zincite but the most zinc oxide is produced synthetically. The physical appearance of zinc oxide and the properties of zinc oxide are shown in Figure 2.11 and Table 2.6, respectively.

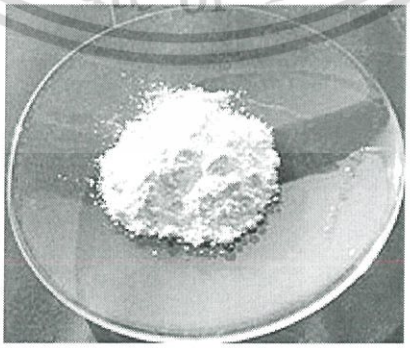

Figure 2.11 The physical appearance of zinc oxide.

Table 2.6 The properties of zinc oxide.

Appearance	White solid
Density	5.606 g/cm^3
Melting point	1975 °C (decomposes)
Molar mass	81.408 mol

2.7.1 Literature reviews

J. Sawa *et* al. [78] studied on the particles of ZnO coated with carbon (ZnOCC) prepared and evaluated for their antibacterial activity. ZnO powder and poly (vinyl alcohol) (PVA) were mixed at the mass ratio (ZnO/PVA) of 1 and heated at 500-650 °C for 3 h under argon gas with a flow rate of 50 ml/min. The antibacterial activity of ZnOCC powder against Staphylococcus aureus was evaluated quantitatively by measuring the change in the electrical conductivity of the growth medium caused by bacterial metabolism (conductimetric assay). In this study, ZnO was immobilized on materials approximately 10-50% and the antibacterial activity decreased compared with that of the original ZnO. The ZnOCC particles contained approximately 95% ZnO and possessed antibacterial activity similar to that of pure ZnO. The carbon-coating treatment could maintain the antibacterial efficacy of the ZnO and may be useful in the development of multifunctional antimicrobial materials.

2.8 Application for packaging [79-83]

Packaging is responsible for, not only containing food products, but also their preservation and quality maintenance, their appearance and convenience, and for protecting and providing the product information to the consumer. The most common packaging materials are glass, wood, metal, plastics, paper and other flexible packages such as coatings and adhesives. The design and manufacture of packaging materials should meet all required properties. Among all required properties of packaging materials, there are five of the most important properties to mention:

1. Mechanical properties
2. Thermal properties
3. Gas and aroma barrier properties
4. Water and water vapor barrier properties
5. Grease and oil barrier properties

2.8.1 Food packaging

Food packaging is the main product in the field of packaging. There are several critical aspects required in food packaging are summarized in Table 2.7. In order to retain the food quality, packaging materials have to control these chemical reactions which influence food quality, like the gaseous atmosphere around foods (oxygen, carbon dioxide, and nitrogen), water activity, light, and temperature are the affecting issues. Furthermore, physical changes are not independent of chemical ones. Therefore, controlling chemical reactions and microbial deterioration can also ensure physical stability, which is another food quality demand.

Table 2.7 Food packaging requirements.

ASPECT	REQUIREMENT
Food quality	Maintain or enhance sensory properties (e.g. appearance, flavor, texture) Maintain the necessary microbiological standards
Manufacturing	Offer simple, economic processes for package formation Give compatibility in product filling
Logistical	Facilitate distribution
Marketing	Enhance point of sale appeal
Environment	Not endanger human safety Use resources responsibly Facilitate waste management
Legislation	National laws
Financial	Cost effectiveness

2.8.2 Conventional packaging materials

The common packaging materials used today can be divided into four groups: paper/paperboard, plastic, metal, and glass packages. Among all packaging materials only paper/paperboard, and some plastic packages are biodegradable. Therefore, the dominating materials used in packaging industries are fossil fuel-based, especially plastics including flexible film and rigid containers. These packagings are practically undegradable for which the option of composting is eliminated.

2.8.3 Biopackaging

In the recent years, new bio-based packaging materials from renewable resources are aimed to extend the shelf life and enhance food quality with reducing

packaging waste. To replace the conventional food packaging materials with biobased ones, the major challenges is the durability of food packages, with respect to its mechanical and barrier properties, and function properly during storage and usage. Another challenge is biodegradability which constrains biopolymers applications to short-term use. There are several factors which affect biodegradation as well as deterioration rate such as water activity, microorganisms, temperature, etc. Therefore, the biopackaging developments must be considered to supply consumers with mandatory and optional information. Furthermore, biobased materials have basically repeating chemical units like synthetic ones, but demonstrate different chemical and physical properties. The processing and product development are not always cost effective as shown in Table 2.8, potential biobased products and their major processing routes are listed.

Table 2.8 The major processing routes to potential biobased products.

PROCESSING ROUTE	PRODUCT EXAMPLES
(Co-)Extruded film	Packaging film
Cast film	Packaging film
Thermoformed sheets	Trays, cups
Blown films	Packaging film
Injection (blow-)moulding	Salad pots, cutlery, drinking beakers, cups, plates, drinks bottles, trays
Fibers and non-wovens	Agricultural products, diapers, feminine hygiene products, certain medical plastics, clothing
Extrusion coating	Laminated paper or films

2.8.4 Films and coating materials

Biopolymers are alternative way to use in packing applications because they are extracted from natural sources constitute a good option to obtain less contaminant. However, some properties should be improved, for example, durability, mechanical properties, barrier properties, etc. In this research, the development of biodegradable packaging is focused on two types: films and coatings. The main difference between films and coatings is that films are stand-alone and not dependent on their intended use. On the contrary, coatings refer to the formation of a film directly over the surface of the final product, so that it may improve or protect final product.

Paper will stay an important biobased packaging material. Paper and board materials perform excellent mechanical properties, but the gas barrier properties are

not suitable for many applications because of the hydrophilic nature of paper. Nowadays, paper-based materials, which have to resist water vapor and gas, are being coated with a thin layer of synthetic plastic. To obtain fully biobased packaging materials, biomaterials are applied as coating on paper and board. The main purpose of coating is to improve the surface quality of paper or board. The quality improvement can be aimed at optical properties such as brightness, gloss or opacity, at tactile properties such as smoothness. When the surface is smooth by coating, paper and board can be upgraded to a higher quality level with added value. Furthermore, printing on packaging paper and board has the functions of advertising, delivering information, and showing data such as barcodes. For specialty papers, the coat layer can have functional properties. Examples are the thermosensitive layer of thermal papers or the capsule-containing coat layer of carbonless papers.

In case of the films products, they are widely used in packaging applications such as shopping bags, garbage bags, etc. The films of renewable polymers based on biodegradable polymer have been successfully introduced. They have promising properties, like excellent transparency. However, regarding the other requirements of a barrier film, it is believed that no single biobased polymer can be both water vapor and gas barrier. Therefore, in this case, the use of co-extrusion can lead to laminates which meet the requirements. In addition, barrier dispersion coating is an interesting alternative, where a barrier material is applied onto plastic films using different coating techniques like blade, rod or curtain coating. During drying, water is removed and a barrier layer is created.

2.8.5 Literature reviews

J.W. Rhima *et* al. [84] studied on the effect of biopolymer coating on the water barrier and mechanical properties of paperboards used as corrugated fiberboard box liners. Paperboards were coated with alginate or soy protein isolate (SPI) and studied with or without further treatment (cross-linking through $CaCl_2$ or formaldehyde treatment). The organically modified montmorillonite (OMMT) was also used for improving water resistance. It was found that the tensile strength (TS) of the coated paperboards decreased from 37.5% to 12.5% of the uncoated paperboards but the ring crush strength was not decreased. In addition, wetting properties, dynamic change in contact angle, water vapor permeability (WVP), and water absorptivity were also affected by biopolymer coating, but the degree of change was dependent on the coating materials and treatment methods. In conclusion, SPI-coated paperboards were more water-resistant than alginate coated ones.

H.D. Huang *et* al. [85] studied on the preparation of high barrier graphene oxide nanosheet (GONS)/poly(vinyl alcohol) (PVA) nanocomposite films. Transmission electrical microscope (TEM) and two-dimensional wide angle X-ray diffraction techniques 2D-WAXD techniques showed that GONSs were full exfoliation, uniform dispersion and high orientation along the surface of films in PVA matrix. Fourier-transform infrared spectroscopy (FTIR) and differential scanning calorimetry (DSC) measurements indicated the existence of strong H-bonding interaction between GONSs and PVA matrix. The barrier properties of GONS/PVA nanocomposite films were improved. Both O_2 and water vapor permeability coefficients of PVA film decreased about 98% and 68%, respectively at a GONS loading of 0.72 vol%. This is because the complete exfoliation, homogeneous dispersion and high orientation and interactions between GONSs and PVA matrix, rather than changes in crystallinity and crystalline structure of PVA matrix.

A. Musetti *et* al. [86] studied on the development of a thin and water-resistant food-grade poly(vinyl alcohol) (PVA)-based matrix. This film was prepared by blending PVA and poly(ethylene glycol) (PEG) with citric acid as crosslinking agent. The thickness of casted film was 60 μm and it showed a good transparency. After immersion in water for 72 h at room temperature, water content, degree of swelling, and crosslink density of the crosslinked film were improved comparing with its original one. It proved that the presence of PEG diminishes the hydrophilic behavior of the material. Moreover, the mechanical properties of the wet and dry film were better than its original one.

A. Jansson *et* al. [87] studied on the preparation of plastisol coatings based on oxidized and hydroxypropylated potato starch and poly(vinyl alcohol). Poly(alkyl methacrylate) was used to improve the water vapour barrier of the coated materials. Plastisol coatings were produced by two different routes: (1) by adding a liquid plasticizer (glycerol or poly(ethylene glycol)) to the starch/poly(vinyl alcohol)-based powder and (2) by mixing the dry starch/poly(vinyl alcohol)-based powder with the dry poly(alkyl methacrylate) powder and subsequently adding a mixture of liquid plasticizers (glycerol and dipropylene glycol benzoate) to the powder mixture. Two different base-papers were investigated; greaseproof paper and paperboard. The coated paper was prepared by double coatings, the first plastisol layer was a pure starch/poly(vinyl alcohol) plastisol according to route 1 and the second layer was a pure poly(alkyl methacrylate) plastisol according to route 2. The plastisol coatings resulted in improvements in the water vapour and oxygen barrier properties of greaseproof paper and paperboard.

G.D. Miller *et* al. [88] studied on the coating adhesive prepared from poly(vinyl alcohol) (PVA) which is a water soluble synthetic polymer that exhibits oil,

grease and solvent resistance. PVA was compatible with common coating raw materials, provided water retention and viscosity modification. Furthermore, it exhibited outstanding adhesion to cellulose and provided high pigment binding strength making it the unique binder or co-binder for pigmented size press and surface coatings. Moreover, poly(vinyl alcohol) provided the unique enhancement of optical brightening agents and fluorocarbon grease repellent performance. For applications, it is used in clear and pigmented size press treatments, water box applications and pigmented surface coatings of paper and paperboard.

From previous literature reviews, the properties of PVA for coating materials and films for packaging applications can be enhanced by modifying with other substances. In this research, the modification of poly(vinyl alcohol) with tung oil and/or natural rubber latex was studied to improve the water resistant and mechanical properties. Various fillers, such as nanosilica, nanocalcium carbonate and nanozinc oxide and crosslinking systems (thermal, redox and photoinitiators) were studied for enhancing water resistance, mechanical properties and other properties.

Chapter 3
Research methodology

3.1 Chemicals and materials

1. Poly(vinyl alcohol) (PVA), Nippon synthetic chemical industrial Co, Ltd., GL-05 grade, GOSENOL®, Partially saponified type, MW=29,600 g·mol^{-1}, Viscosity (4 % aqueous solution) at 20 °C = 4.8 – 5.8 mPa·s
2. Natural rubber latex, Lucky four Co. Ltd., High ammonia Grade, 60 wt% dry rubber content
3. Tung oil, UV photographic Co. Ltd., Commercial Grade
4. Potassium persulfate [$K_2S_2O_8$], CARLO ERBA reagent, Analytical Grade, 99 % assay
5. Sodium thiosulfate, Ajax Fine chem Ltd., Analytical Grade. , 99.5 % assay
6. Coconut oil, Ampol Food, Commercial Grade, 100 % assay
7. Photoinitiator, Twins Co. Ltd., Commercial Grade
8. Premium white paperboard (Card pro paper), SCG Paper Co. Ltd., 240 grams, thickness 320 μm
9. Fiberboard (Commercial grade)
10. Nanozinc oxide, College of Nanotechnology, KMITL, Synthesis Grade, Particle size 50-70 nm
11. Nanosilica, Chemical Village Co. Ltd., Commercial Grade

Table 3.1 The specific properties of nanosilica.

Items	HL-200
Specific surface area (BET)	200±20 m^2/g
Particle size	20-30 nm
pH value in 4% dispersion	3.7-4.5
Loss on drying (2 h, 105 °C)	≤2.0%
Loss on ignition (2 h 1000 °C, based on material dried for 2 h, 105 °C)	≤2.0%
Sieve residue (45um)	≤0.04%
Silica content (based on ignited material)	≥99.8%
Tamped density (based on material dried for 2 h, 105 °C)	40-60 g/L
Carbon content (based on material dried for 2 h, 105 °C)	≤0.15%

12. Nanocalcium carbonate, Behn Meyer Chemical (T) Co.,Ltd., Commercial Grade

Table 3.2 The specific properties of nanocalcium carbonate.

Items	NPCC-101
Particle shape	Cubic
Particle size	40 nm
% Whiteness	>90
Density	2.5-2.6 g/cm^3
% $CaCO_3$	>97
pH	8.0-9.5

3.2 Instruments

1. Balance, model SI-234, DENVER instrument
2. High speed Agitator with propeller, model RW 20 digital, IKA
3. Magnetic Stirrer with magnetic bar, model C-MAG HS 7, IKA
4. Homogenizer, model T 25 digital ULTRA TURRAX, IKA
5. Universal Testing Machine, LLOYD Instrument
6. Fourier Transform Infared Spectrometer, FTIR Spectrum GX, Perkin Elmer
7. Tensile oscillatory rheometer, model DVE-E4000, UBM, Japan
8. Contact angle analyzer, model OCA 20, Data physics instruments
9. EVO® HD scanning electron microscopy, model EVO® MA 10, LaB6, resolution 3 nm, maximum magnification 3000, Carl Zeiss model
10. Hot air oven, model UN-55, Memmert
11. Micrometer, model G-7C, Peacock, Ozaki MFG Co., Ltd.
12. Wooden box with 20 tubes of 18 W fluorescent tubes
13. Desicator
14. Glassware

Figure 3.1 Wooden box with 20 tubes of 18 W fluorescent tubes.

3.3 Studied factors

In this thesis, the experiment could be divided into 3 main sections as follows:

1. Preparation and characterization of raw materials

2. Preparation of modified PVA

2.1 For PVA/tung oil sheet (PT sheet), various preparation compositions were carried out, i.e.

2.1.1 PVA : Tung oil ratios: 100:0, 95:5, 90:10 and 85:15 (Tung oil contents: 0, 5, 10 and 15 %w/w)

2.1.2 Catalytic systems: thermal catalyst and redox catalyst

2.1.3 Curing temperatures: 30, 40, 50, 60, 70 and 80 °C

2.2 For PVA/tung oil/rubber sheet (PTR sheet), various preparation compositions were carried out, i.e.

2.1.1 Tung oil : natural rubber latex ratios: 0:15, 5:10, 10:5 and 15:0 (The weight ratio of PVA to tung oil/rubber was fixed at 85:15)

2.1.2 Catalytic systems: thermal catalyst and redox catalyst

2.1.3 Curing temperatures: 30, 40, 50, 60, 70 and 80 °C

2.3 For PVA/tung oil sheet (PT sheet) and PVA/tung oil/rubber sheet (PTR sheet) with nano-additives, various preparation compositions were carried out, i.e.

2.1.1 Tung oil contents: 0, 5, 10 and 15 %w/w

2.1.2 Tung oil : natural rubber latex ratios: 0:15, 5:10, 10:5 and 15:0 (The weight ratio of PVA to tung oil/rubber was fixed at 85:15)

2.1.3 Nano-additive contents in PVA mixtures: 0, 1, 2, 3, 5 and 7 pph (SiO_2, $CaCO_3$ and ZnO)

2.1.4 Catalytic systems: thermal catalyst and redox catalyst

2.1.5 Curing temperatures: 30, 40, 50, 60 and 70 °C

The characterization and other properties of modified PVA were investigated, i.e. water resistance testing by % solid remain, chemical structure by FTIR, mechanical properties by universal testing machine, thermal properties by DMTA, and morphology by SEM-EDS.

3. Application of modified PVA as coating materials and water resistant films

3.1 For coating materials, modified PVA was coated on white paperboard and fiberboard. The effects of the compositions on coated surface morphology were examined by SEM-EDS. Hydrophilic/hydrophobic properties of the coated surface were investigated by water and oil contact angle measurement.

3.2 For water resistant films, the water resistant films were prepared by casting and the modified PVA films were cured by heat and light radiation. The effects of the compositions and curing conditions on different properties of the water resistant

films were investigated, i.e. water resistance testing by % solid remain and % swelling, chemical structure by FTIR, mechanical properties by universal testing machine, thermal properties by DMTA, moisture resistance testing by moisture content and water vapor permeability (WVP), morphology by SEM-EDS, and hydrophilic/hydrophobic properties by water and contact angle measurement.

3.4 Preparation and characterization of raw materials

PVA (150 g) was slowly added into distilled water (850 g) and stirred at 500 rpm. After that, the mixture was heated to 90 °C under constant stirring until the clear solution was obtained. PVA solution was then casted and characterized by FTIR. To study the effect of humidity on the T_g of PVA, PVA sheets were kept in several conditions, i.e. at 25 °C and 50 %RH, 25 °C and 20 %RH, and 90 °C and 0 %RH before evaluation by DMA.

Figure 3.2 PVA solution preparation.

Tung oil was casted at room temperature until it dried for preparing crosslinked tung oil, while natural rubber latex was casted at 60 °C until it dried. After that, crosslinked tung oil and rubber were characterized by DMA and FTIR.

3.5 Preparation of modified PVA

Modified PVA was prepared by weighing the components following the Table 3.3. PVA solution and each of nano-additives (nanosilica, nanozinc oxide or nanocalcium carbonate) were well mixed by using homogenizer at 10,000 rpm. Then, natural rubber latex and tung oil were added and mixed by using homogenizer. Subsequently, thermal catalytic system (potassium persulfate) or redox catalytic system (potassium persulfate and sodium thiosulfate at equimolar amount) was added into the mixture and further homogenized for 15 min. The texture of the modified PVA is shown in Figure 3.3. After that, all modified PVA was casted onto the Petri dish and dried at several conditions; 30, 40, 50, 60, 70 and 80 °C (for sheets), and room temperature and 50 °C (for films) in an oven where the sheets or films were allowed to dehydrate. The thickness of samples was

approximately 350±50 μm (sheets) and 100±10 μm (films). Each sample was measured at five different points using a micrometer.

For studying the photocrosslinking reaction, photoinitiator was added into each mixture with well stirring and the mixture was then cast into the Petri dish and dried at 30 °C for 24 h to achieve the films. In comparison, the films without photoinitiator added were also prepared. These films were subsequently crosslinked by exposure to light radiation for 10 and 30 min. The light radiation process was implemented by utilizing a wooden box with 20 x 18 W of fluorescent lamps. The thickness of the films measured at five different points using a micrometer was approximately 100±10 μm.

Table 3.3 The composition of the modified PVA.

Formula	PVA solution (wt%)	Tung oil (wt%)	Natural rubber latex (wt%)	Nano-additive (pph)	Catalytic system
P100	100	0	0	0	none
P100-t					t
P100-r					r
P95T5	95	5			none
P95T5-t					t
P95T5-r					r
P90T10	90	10			none
P90T10-t					t
P90T10-r					r
P85T15	85	15			none
P85T15-t					t
P85T15-r					r
P85T10R5		10	5		none
P85T10R5-t					t
P85T10R5-r					r
P85T5R10		5	10		none
P85T5R10-t					t
P85T5R10-r					r
P85T0R15		0	15		none
P85T0R15-t					t
P85T0R15-r					r

Table 3.3 (Cont.)

Formula	PVA solution (wt%)	Tung oil (wt%)	Natural rubber latex (wt%)	Nano-additive (pph)	Catalytic system
P85T15Si1	85	15	0	Si1	none
P85T15Si1-t					t
P85T15Si1-r					r
P85T15Si2				Si2	none
P85T15Si2-t					t
P85T15Si2-r					r
P85T15Si3				Si3	none
P85T15Si3-t					t
P85T15Si3-r					r
P85T15Si5-r				Si5	
P85T15Si7-r				Si7	
P90T10Si1-r	90	10		Si1	
P90T10Si3-r				Si3	
P90T10Si5-r				Si5	
P90T10Si7-r				Si7	
P95T5Si1-r	95	5		Si1	
P95T5Si3-r				Si3	
P95T5Si5-r				Si5	
P95T5Si7-r				Si7	
P85T15Ca1	85	15		Ca1	none
P85T15Ca1-t					t
P85T15Ca1-r					r
P85T15Ca2				Ca2	none
P85T15Ca2-t					t
P85T15Ca2-r					r
P85T15Ca3				Ca3	none
P85T15Ca3-t					t
P85T15Ca3-r					r
P85T15Zn1				Zn1	none
P85T15Zn1-t					t
P85T15Zn1-r					r

Table 3.3 (Cont.)

Formula	PVA solution (wt%)	Tung oil (wt%)	Natural rubber latex (wt%)	Nano-additive (pph)	Catalytic system
P85T15Zn2	85	15	0	Zn2	none
P85T15Zn2-t					t
P85T15Zn2-r					r
P85T15Zn3				Zn3	none
P85T15Zn3-t					t
P85T15Zn3-r					r
P85T0R15Si1		0	15	Si1	none
P85T0R15Si1-t					t
P85T0R15Si1-r					r
P85T5R10Si1		5	10		none
P85T5R10Si1-t					t
P85T5R10Si1-r					r
P85T10R5Si1		10	5		none
P85T10R5Si1-t					t
P85T10R5Si1-r					r

where P : PVA
T : tung oil
R : natural rubber latex
t : thermal catalytic system
r : redox catalytic system
Si : nanosilica
Ca : nanocalcium carbonate
Zn : nanozinc oxide

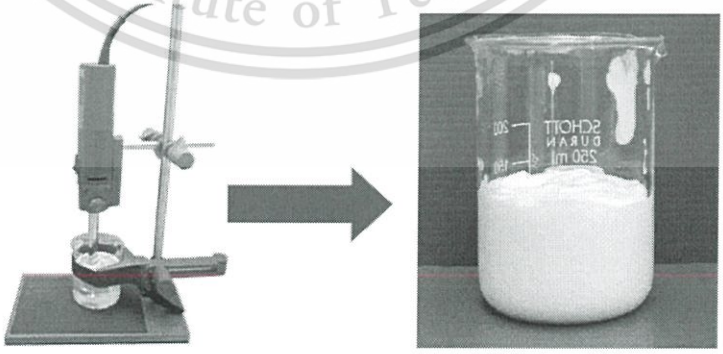

Figure 3.3 Preparation of modified PVA.

For coating application, 1 g of selected modified PVA was coated on white paperboard and fiberboard (8 cm x 5 cm). The coated materials were dried under

different conditions, including hot-air oven, drying at 50 °C for 60 min. The thickness of coated materials was approximately 70-80 μm by measurement at five different points using a micrometer and then the coated materials were subsequently conditioned in a desiccator for at least 7 days at ambient conditions before the measurement were made.

3.6 Characterization and testing of modified PVA sheets and films

3.6.1 Water resistance testing

The PVA and modified PVA sheets and films were cut into a rectangular shape (1.5x2 cm). Each of the specimens was weighed before immersed in distilled water (pH 7) at room temperature for 24 h to ensure that the film had reached the equilibrium state of swelling through absorption of water into it. The specimen was later dried in an oven to achieve constant weight. The percentage of solid remain was calculated as follows:

$$\%\ Solid\ remain = \frac{W_2}{W_1} \times 100 \qquad (3.1)$$

where W_1 : Dry weight (g) before immersion in water

W_2 : Dry weight (g) after immersion in water for 24 h

In case of swelling behavior, after the selected modified PVA films were soaked in water for 24 h, the swollen film was weighed to estimate the degree of swelling. The swelling degree (% Swelling) was calculated as follows:

$$\%Swelling = \frac{W_2 - W_1}{W_1} \times 100 \qquad (3.2)$$

Where W_1 : Dry weight (g) before swelling in water

W_2 : Swollen weight (g) after the equilibrium swelling in water for 24 h

3.6.2 Mechanical properties

The modified PVA sheets were cut into Dumbbell shape following to ISO 37-2005 while the modified PVA films were cut into rectangular shape (1.5x5 cm) following to ASTM standard method D882 [89]. These selected films were then kept in 0 %RH at ambient conditions for at least 7 days before the measurement. The ultimate tensile strength and Young's modulus of modified PVA sheets and films based on the stress–strain behavior were measured at a crosshead speed of

500 mm/min with a load cell of 1 kN and an initial gauge length of 20 mm using a universal testing machine, LLOYD Instrument. The specimens were measured for each particular specimen and the average values were reported with standard deviation showing the error range.

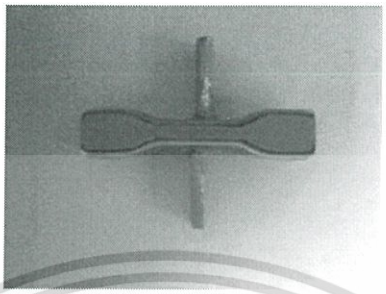

Figure 3.4 Dumbbell-shaped specimen following to ISO 37-2005.

3.6.3 Fourier Transformed Infrared spectroscopy (FTIR)

The chemical structure of raw materials and modified PVA films were characterized using a Perkin Elmer FTIR Spectrum GX spectrometer within the wave number region of 400–4000 cm^{-1} at the number of scan of 32 with a resolution of 4 cm^{-1}.

3.6.4 Dynamic mechanical thermal analysis (DMTA) [90]

The dynamic mechanical thermal properties, which are storage modulus (E'), loss modulus (E'') and damping factor (tan δ) of modified PVA sheet and films were carried out at 1 Hz as a function of temperatures using a tensile oscillatory rheometer (DMA, DVE-E4000, UBM, Japan) from -100 to 150 ^{o}C at a heating rate of 2 ^{o}C/min. in nitrogen atmosphere using the bending mode and dynamic strain control of 0.03%. The glass transition temperature (T_g) was determined from a temperature peak of tan δ.

3.6.5 Moisture content

The PVA and modified PVA films were cut into square shape (2x2 cm). Before the measurement, these specimens were kept to afford constant weight in 0 %RH at ambient conditions for at least 7 days and weighed to record as the dried film. The samples were placed into a desiccator (75 %RH, ambient conditions). These samples were weighed at selected times to obtain the adsorbing weight. The percentage of moisture content of the films was calculated as follows:

$$\%\ moisture\ content\ = \frac{W_2 - W_1}{W_1} \times 100 \qquad (3.3)$$

where W_1 : Dry weight (g) at 0 %RH

W_2 : Adsorbing weight (g) after held in a desiccator 75 %RH for the selected times

3.6.6 Water vapor permeability (WVP) [91]

Water vapor permeability was evaluated at 25 °C and 75 %RH, following ASTM E96/E96M method. The PVA and modified PVA films were cut into circular shapes with an area of 0.0141 m^2, then placed and sealed using epoxy glue on the top of the cups containing 10 g of anhydrous $CaCl_2$ (0 %RH). These cups were weighed before being placed in a desiccator containing saturated NaCl solution (NaCl – 75 %RH). The film-coated cups were weighed at the selected times and the weight change of these cups was recorded and plotted as a function of time. The slope of each line was calculated by linear regression and the water vapor permeability (WVP) was determined from the weight gain of the cup according to Eq. (3.4) and (3.5):

$$WVTR = \frac{G}{t \times A} \qquad (3.4)$$

$$WVP = \frac{WVTR \times L}{S \times (R_2 - R_1)} \qquad (3.5)$$

where G/t : the amount of gain-water per unit time of transfer (g/day)

A : the permeation area (m^2)

L : the film thickness (m)

R_1 : relative humidity at the source expressed as a fraction (0 %RH)

R_2 : relative humidity at the vapor sink expressed as a fraction (75 %RH)

S : the water vapor pressure difference between both sides of the film at 25 °C (kPa) [91].

3.6.7 Scanning electron microscopy (SEM)

Cross-sectional and topographical phase morphologies of the selected modified PVA sheets including coated paperboard at various magnifications were

studied by Carl Zeiss model EVO® MA 10, LaB6, resolution 3 nm, maximum magnification 3000. The specimens were fractured in liquid nitrogen and the cross-sections or the surface were mounted on SEM stubs with double-sided adhesive tape, and then coated with a thin gold layer using sputter coater.

3.6.8 Water and oil contact angle measurement [92]

The initial contact angle of water and oil on the surface and contact angle change rates (k) of coated paperboard and fiberboard were evaluated with a contact angle analyzer (model OCA 20, Data physics instruments) at 25 °C. These samples were conditioned in 0 %RH at ambient conditions for at least 7 days before the measurement. A distilled water drop or oil drop of ca. 3 μL was place on the surface of them using micro-syringe. The contact angle of the drop was measured on both sides of the drop and averaged. The reported contact angle value is the average of at least three measured data. Contact angle change rates (k) was measured by recording the contact angle change of a water drop with time within 300 s at room temperature and reported value is the average of at least three measured data.

Chapter 4

Main Results and Discussion

This research studied the modification of PVA for coating material and water resistant film applications by using tung oil and natural rubber latex. Thermal catalytic system (potassium persulfate, KPS), redox catalytic systems (KPS and sodium thiosulphate) and the systems of photoinitiators cooperating with catalytic systems (i.e., thermal and redox catalytic system) were utilized to study the crosslinking reaction of modified PVA. Moreover, each of nano-additives (nanosilica, nanocalcium carbonate and nanozinc oxide) was also used to improve the properties. For applications, the suitable modified PVA was applied on paperboards and prepared for water resistant films before being characterized and evaluated, water resistant, thermal and mechanical properties. The details are as follows:

4.1 Characterization and thermal properties of PVA, tung oil and rubber as raw materials

PVA, tung oil and natural rubber latex were characterized by FTIR and tested for mechanical thermal properties by DMA.

4.1.1 Fourier Transformed Infrared spectroscopy (FTIR)

The chemical structures of PVA, tung oil and rubber in the film form were characterized by using FTIR. The FTIR spectra of PVA, tung oil and rubber films are shown in Figure 4.1. For PVA (Fig 4.1a), the broad peak at around 3200-3600 cm^{-1} indicates the presence of hydroxyl groups of PVA and the peaks at 1450 and 1375 cm^{-1} are attributed to $-CH_2-$ bending vibration. Moreover, the absorptions in the range of 2,960 to 2,850 cm^{-1} are symmetric and asymmetric C–H stretching vibrations of methyl and methylene groups. [72]. For tung oil (Figure 4.1b), the infrared spectra of symmetric and asymmetric C–H stretching vibrations of methyl and methylene groups are in the range of 2,960 to 2,850 cm^{-1} while the vibration of the carbonyl group of ester are visible at 1,745 cm^{-1}. Besides these bands, the characteristic peaks corresponding to the double bonds of tung oil are visible at 3012 cm^{-1} (**–C=C–**H stretching), 992 cm^{-1} (conjugated trans: trans –C=**C–H** bending), and 965 cm^{-1} (conjugated cis: trans –C=**C–H** bending), which was allowed to follow a crosslinking reaction of tung oil [25, 93]. In case of rubber (Figure 4.1c), the absorption peak at 2965 cm^{-1} is the asymmetrical vibration

absorption of the saturated hydrocarbon -CH_3 group and the absorption peak at 2868 cm^{-1} is the symmetrical vibration absorption of the methylene group. Besides, the absorption peaks at 1450 and 1375 cm^{-1} are the -CH_3 absorption. Furthermore, the characteristic peaks corresponding to double bonds of rubber are visible at 3037 cm^{-1} (-C=**C**-**H** stretching) and 1663 cm^{-1} (-**C**=**C**-H stretching) which were allowed to follow a crosslinking reaction of rubber [94].

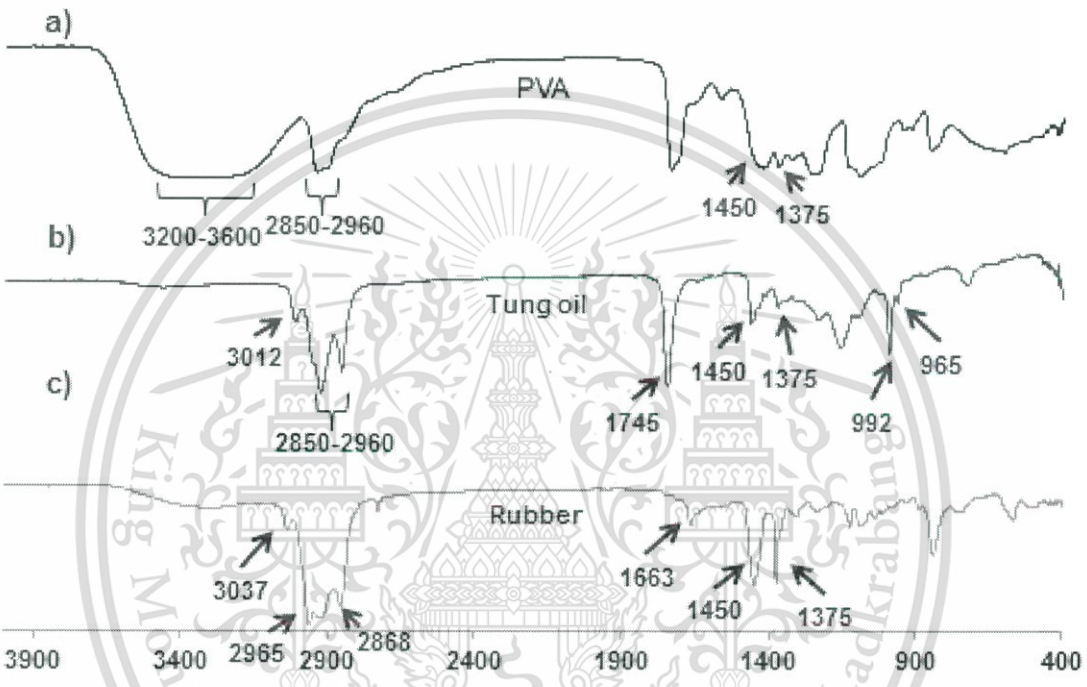

Figure 4.1 FTIR spectra of raw material films; (a) PVA, (b) tung oil and (c) rubber.

4.1.2 Dynamic mechanical analysis (DMA)

The dynamic mechanical analysis is a sensitive method that can detect the molecular relaxations, the glass transition temperature T_g, and the crosslink reaction of the polymer. Figure 4.2 shows the temperature dependence of storage modulus (E'), loss modulus (E'') and tan δ values for crosslinked tung oil and rubber. In this study, the tan δ values of tung oil (Figure 4.2a), ascribed to the glass to rubber transition (T_g), was detected around 10 °C, while the T_g of rubber was detected around -69 °C (Figure 4.2b). Furthermore, storage modulus (E') value, is directly related to the elastic portion, of tung oil was higher than that of rubber, while loss modulus (E'') value, is directly related to the viscous portion, of tung oil was lower than that of rubber. This is because tung oil

was crosslinked by oxygen to form film, while rubber could form film without curing reaction. Thus the structure of crosslinked tung oil was difficult to move compared with the structure of rubber.

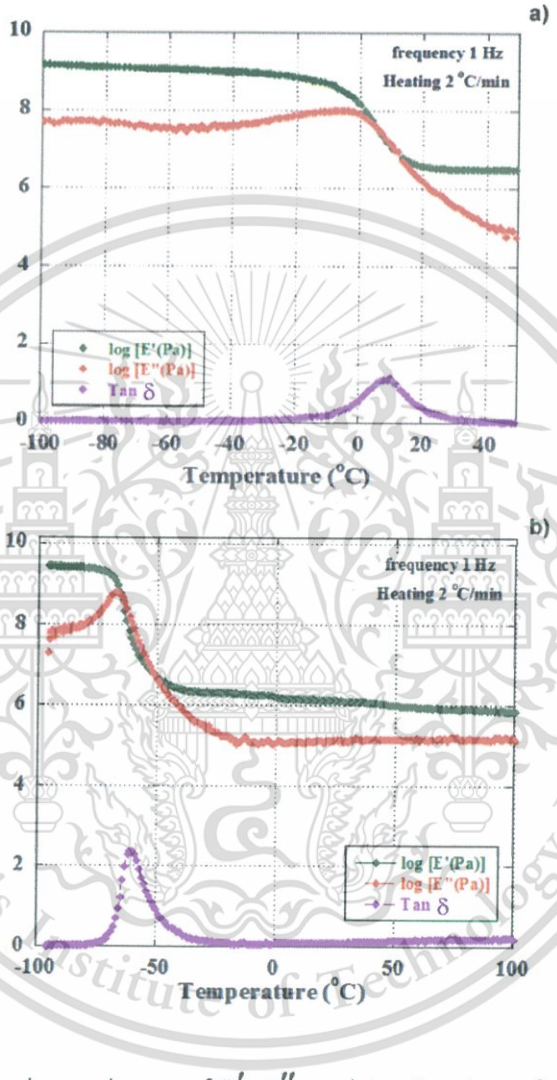

Figure 4.2 Temperature dependence of E', E'' and tan δ values for (a) crosslinked tung oil and (b) rubber.

4.1.3 The effect of humidity on T_g of PVA sheet (P100)

Figure 4.3 shows the thermograms of PVA sheet without addition of catalysts for studying the effect of humidity on storage modulus (E'), loss modulus (E'') and T_g of PVA (P100). Above this critical temperature (ca.40 °C), the storage modulus (E') for the moisture-exposed samples (50 %RH and 20 %RH) was lower than that of the dried

sample (0 %RH) because of the plasticization effect of moisture containing in the P100 sheet. Furthermore, the T_g values of P100 were detected around 37 °C, 52 °C and 85 °C for conditions at 25 °C with 50 %RH, 25 °C with 20 %RH, and 90 °C with 0 %RH, respectively. This effect can be ascribed to the plasticization effect of moisture on the cooperative motions of the main chains. Moreover, this effect also enhances the intensity of the molecular motions within this temperature region, leading to an increase in the relaxation strength with increasing moisture content. These effects are also very well visible in the curves of the storage modulus versus the temperature, as shown in Figure 4.3. Therefore, the T_g values of PVA decreased significantly with an increase in humidity. It could be concluded that the humidity in PVA film behaves as the nano-plasticizer.

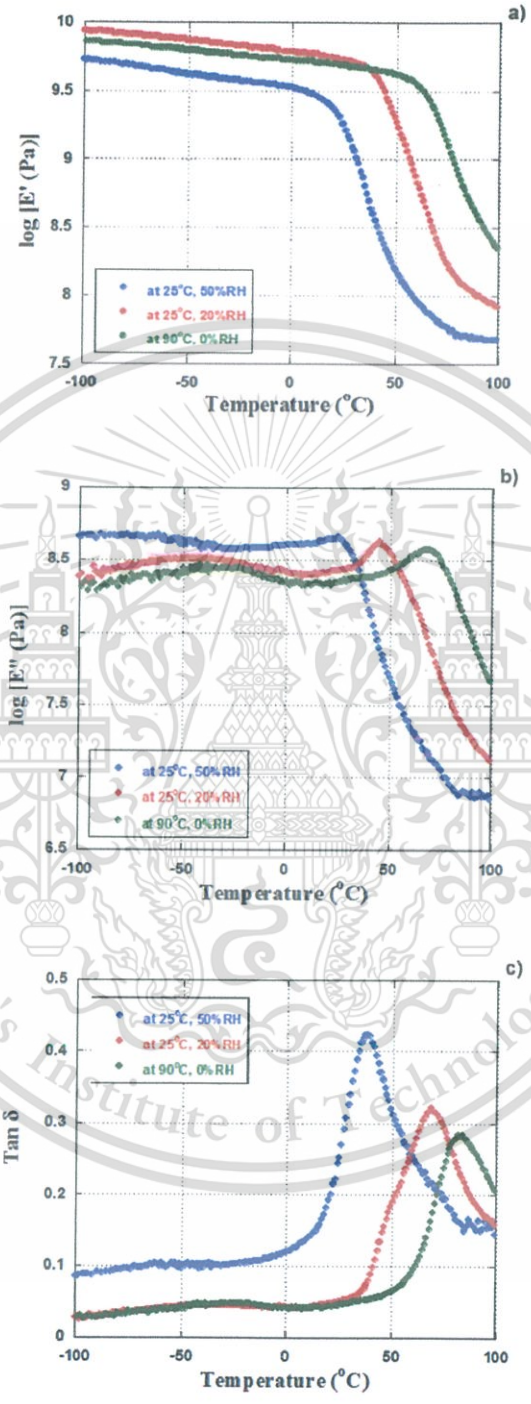

Figure 4.3 Temperature dependence of PVA sheet kept in various conditions; (a) E', (b) E'' and (c) tan δ values.

4.2 The modified PVA

4.2.1 Effect of tung oil contents, catalytic systems and curing temperatures on the properties of PVA/tung oil sheet (PT sheet)

In this part, the modified PVA based on the mixture of tung oil and PVA at various tung oil contents (0, 5, 10 and 15% w/w) cured by using thermal catalyst (potassium persulfate) or redox catalysts (potassium persulfate and sodium thiosulfate) were prepared by solution casting and then dried at different curing temperatures (from 30 °C to 80 °C) to form PT sheets. The effects of tung oil contents, types of catalysts and curing temperatures on the water resistant, thermal and mechanical properties were investigated.

4.2.1.1 Water resistance testing

Water resistant property of P100 and PT sheets after curing at different temperature was measured and reported in terms of the percentage of solid remains shown in Figure 4.4. In case of PVA sheets without applied catalysts (P100), they could totally dissolve in water, thus, the % solid remains could not measure. As adding catalysts into P100 sheet, the results suggested that the crosslinking of PVA could occur at some given curing temperature, especially when the curing temperatures were ≥ 60 °C. In case of P100 sheets cured by using thermal catalyst (P100-t), KPS was firstly activated by heat and then converted to free radicals. These free radicals further reacted with main chain and hydroxyl groups of PVA to generate the new free radicals on the PVA chains. Finally, these free radical chains continued to react with each other and form the crosslinking resulting in the difficulty to dissolve in water (see Figure 4.5).[72] The % solid remains of P100 sheets cured by using redox catalyst (P100-r), on the other hand, had much lower values than those cured by using thermal catalyst (P100-t) at high temperatures (≥ 60 °C). It can be pointed that thermal catalyst has an influence in the crosslinking reaction of PVA rather than redox catalyst, preferably at high curing temperatures.

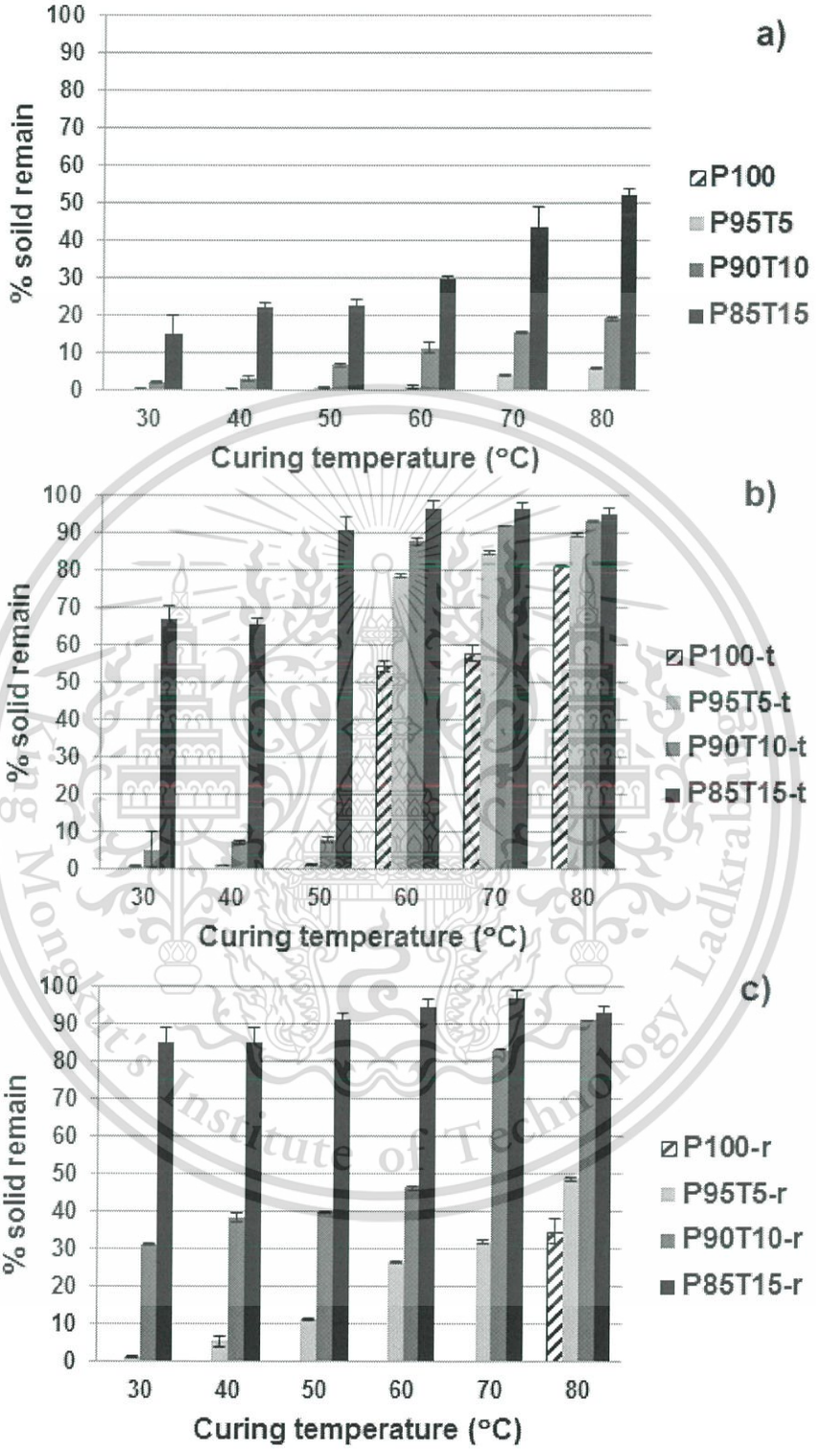

Figure 4.4 The percentage of solid remains of PT sheets after immersion in water at 25 °C for 24 h; (a) no catalyst system, (b) thermal system and (c) redox system.

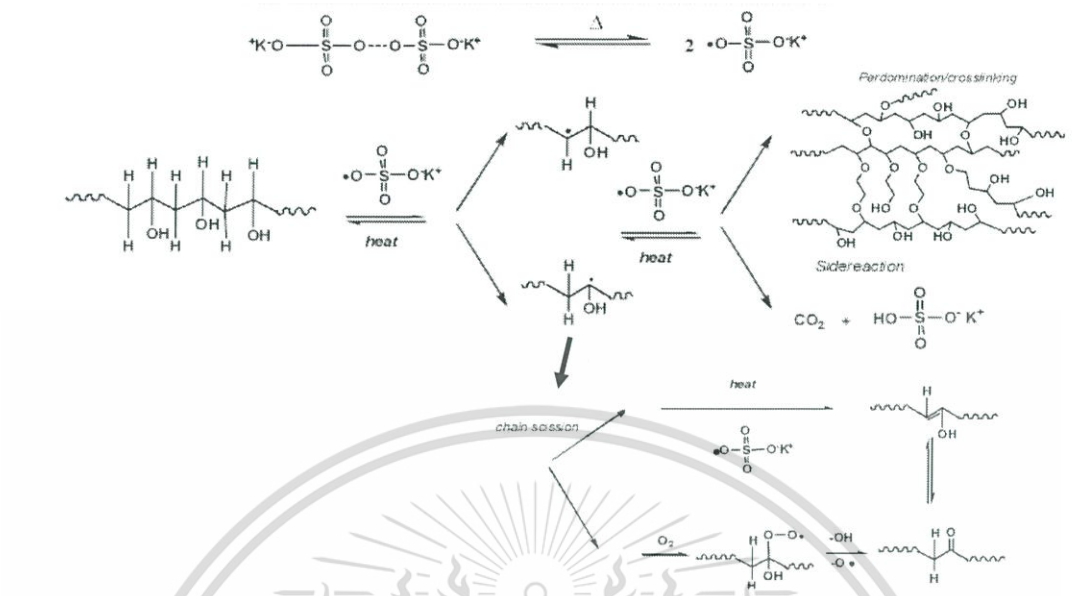

Figure 4.5 The mechanism of the reaction between PVA and KPS [95].

In terms of tung oil contents, the % solid remains of PT sheets without catalyst were found at the low level of 0–50% depending on curing temperatures and tung oil contents. The results suggested that higher curing temperatures promoted the more network formation at the conjugated double bonds of tung oil by autooxidative curing. When the oxidation of tung oil takes place, oxygen attacks at an active center on a fatty acid chain and then creates the network structure of tung oil. PVA chains were retained within the crosslinked structure resulting in difficulty to dissolve into water. Not surprisingly, the presence of higher tung oil contents could gain the increase of crosslink density within the PT sheets. Hence, the better water resistant property would be obtained.

As compared with the PT sheets without catalyst, the PT sheets cured by using catalysts showed dramatic enhancement of water resistant properties. It could be pointed that the efficiency of crosslinking reaction among the double bonds of tung oil increased when the catalyst was involved. The crosslinking reaction of tung oil in the presence of thermal catalyst or redox catalyst is based on free radical mechanism. The catalysts firstly decomposed to generate free radicals by the elevated temperature and immediately abstracted allylic hydrogen atoms from the backbone of tung oil to produce free radicals. These radicals instantaneously terminated, forming crosslinking, with either intramolecular or intermolecular chains. Tung oil was subsequently changed to be solid. When crosslinking reaction occurred, PVA chains were retained within the

crosslinked structure of tung oil by interlocking network among them. It caused PVA to be difficult to dissolve in water.

With different types of catalysts, the water resistant property of the PT sheets cured by using redox catalytic system is better than those cured by using thermal catalytic system, especially at low curing temperatures. This is reasonable because thermal catalyst can be dissociated efficiently at elevated temperatures whereas redox catalyst can be broken down well even at low temperatures.[33] It can be proposed that the reactivity of tung oil cured by using redox catalytic system is faster than that cured by using thermal catalytic system at lower curing temperatures. Although the crosslinking reaction of tung oil cured by using redox catalyst is better than cured by using thermal catalyst, PVA could preferably crosslink itself by using thermal catalyst at the temperature ≥60 °C. For the reasons above, both P85T15-t and P85T15-r cured at ≥60 °C gained the similar values of the % solid remains.

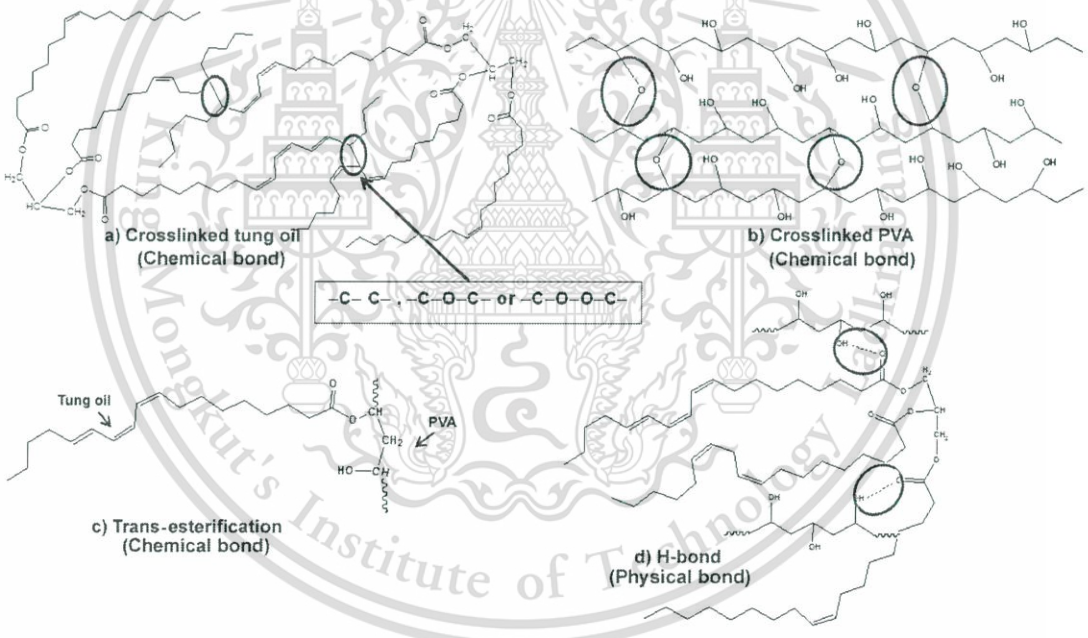

Figure 4.6 Schematic illustration of the reactions within PVA/tung oil sheets; (a) crosslinked tung oil, (b) crosslinked PVA, (c) trans-esterifications, and (d) hydrogen bond between tung oil and PVA.

The model of the reactions within PT sheets crosslinked by thermal catalyst and redox catalyst are illustrated in Figure 4.6. The network structures of thermal crosslinked PT sheets including the crosslinking reaction of tung oil, the crosslinking reaction of PVA, trans-esterifications and hydrogen bond between tung oil and PVA are

illustrated in Figure 4.6. As for crosslinked PT sheets cured by using redox catalyst system, the network structures are in the same manner as the thermal crosslinked PT sheets excluding the crosslinking reaction of PVA.

4.2.1.2 Fourier Transformed Infrared spectroscopy (FTIR)

The chemical structures of PT sheets were characterized by using FTIR as shown in Figure 4.7. The –**C=C**–H and –C=**C–H** vibration in the structure of tung oil were allowed to follow the formation of crosslinking. When the crosslinking reaction occurred, the characteristic peaks corresponding to double bonds of tung oil at 3012 cm^{-1} (–**C=C**–H stretching), 992 cm^{-1} (conjugated trans: trans –C=**C–H** bending), and 965 cm^{-1} (conjugated cis: trans –C=**C–H** bending) would be changed. In the case of P85T15-t, curing at 30 °C, all of the peaks related to –C=**C–H** and –**C=C**–H vibration of tung oil still appeared at the similar patterns (Figure 4.7a). On the other hand, for redox system (P85T15-r), at the same temperature, the decreases in the intensity at 992 and 3012 cm^{-1} were observed while the peak at 965 cm^{-1} almost ceased (Figure 4.7b). It implied that, at ambient temperature, the redox catalytic system could initiate the crosslinking reaction at unsaturated position greater than that in the thermal catalytic system. Moreover, the peak at 3012, 992 and 965 cm^{-1} of P85T15-t vanished (Figure 4.7a) when the curing temperatures were raised above 60 °C. On the other hand, for the redox system, the peaks at 3012, 992 and 965 cm^{-1} almost ceased when the curing temperature was raised to 60 °C (Figure 4.7b). It could be suggested that crosslinking network in the films would occur *via* the addition reaction at the double bonds of tung oil, and the redox system exhibited a higher efficiency of crosslinking reaction than that using thermal catalyst when low curing temperature was applied (<60 °C).

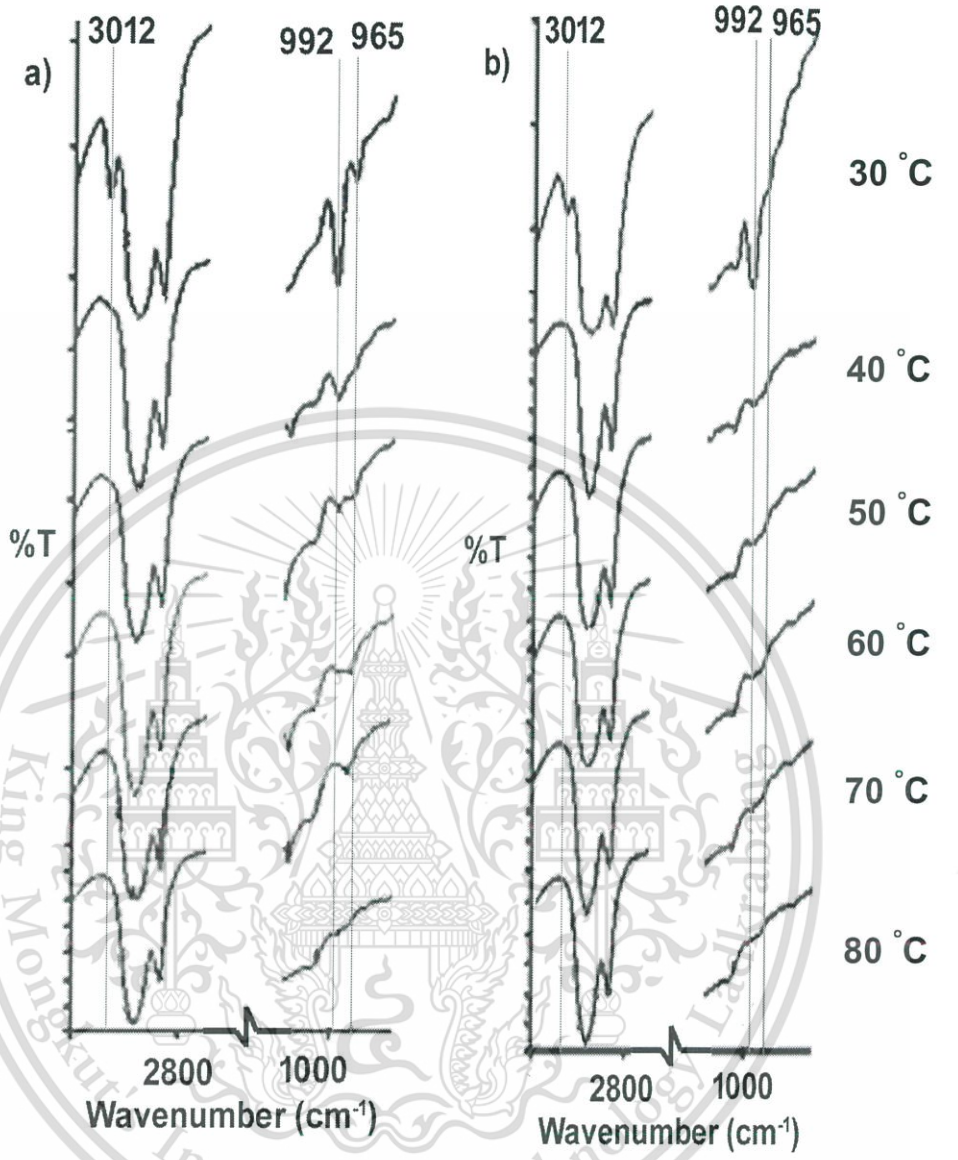

Figure 4.7 FTIR spectra of P85T15 sheet cured by using; (a) thermal catalytic system and (b) redox catalytic system at various curing temperatures.

4.2.1.3 Dynamic Mechanical Analysis (DMA)

To confirm the occurrence of crosslink reaction, the thermal properties of PT sheets were investigated by DMA. Figure 4.8 - 4.10 showed the tan δ values of PVA and PT sheets as a function of catalytic systems. For PVA sheets (Figure 4.8), the T_g values of PVA part (37 °C for neat PVA without catalyst) increased by the thermal catalytic systems. This is reasonable because, at ≥60 °C, thermal catalyst could generate a large number of free radicals easily resulting in the higher extent of crosslinking in PVA.

Moreover, with the increase of temperature, the mobility of macro radicals would be enhanced, leading to more crosslinking reaction between the free radicals. Therefore, the shift of T_g values towards higher curing temperatures was obtained. For the redox system, at 60 °C, the shift of T_g values of PVA is lower than PVA sheets cured by using thermal catalyst due to the favored chain termination reactions of redox catalyst [29]. However, it shifted to higher temperature after curing at 80 °C suggesting that KPS in redox system preferred relatively high temperature to generate the crosslinking reaction in PVA sheets. It can be pointed that the crosslink reaction of PVA itself occurred by using the thermal catalysts rather than by using redox catalyst.

In case of P85T15, the tan δ values of P85T15 sheets as a function of catalytic systems were investigated by DMA as shown in Figure 4.9. The T_g peaks of tan δ values corresponded to the motion of tung oil and PVA. In P85T15 (catalyst not applied) cured at 80 °C, the T_g of value tung oil was detected at about 2 °C while the T_g value of PVA was found at about 53 °C. In comparison with P85T15, the T_g values of tung oil in P85T15-t and P85T15-r shifted to the values of 4 - 11 °C while the T_g values of PVA were found in the range of 63 - 68 °C. The increase in T_g values of tung oil and PVA meant that crosslinking reaction occurred efficiently resulting in cumbersome movement of both tung oil and PVA segments. With different catalytic systems, the raised shift in T_g value of tung oil was detected when redox catalyst was applied rather than thermal catalyst. It is claimed that the reactivity of redox catalyst is greater than that by thermal catalyst corresponding to the FTIR results.

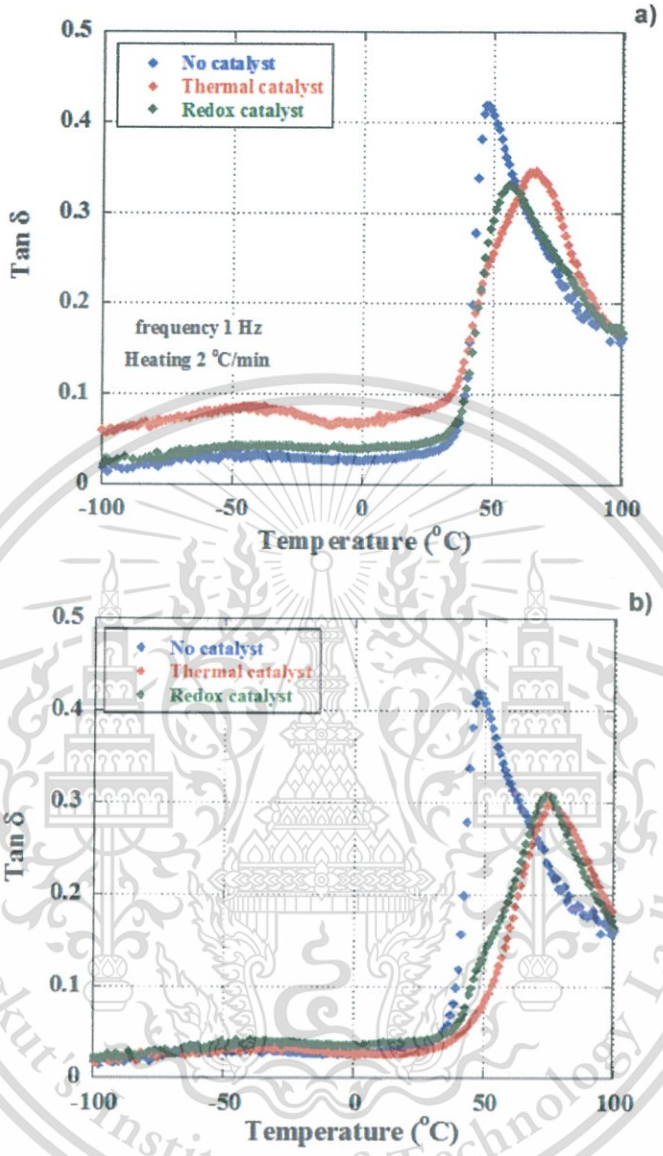

Figure 4.8 Temperature dependence of tan δ values for PVA sheets for different catalytic systems; (a) cured at 60 °C and (b) cured at 80 °C.

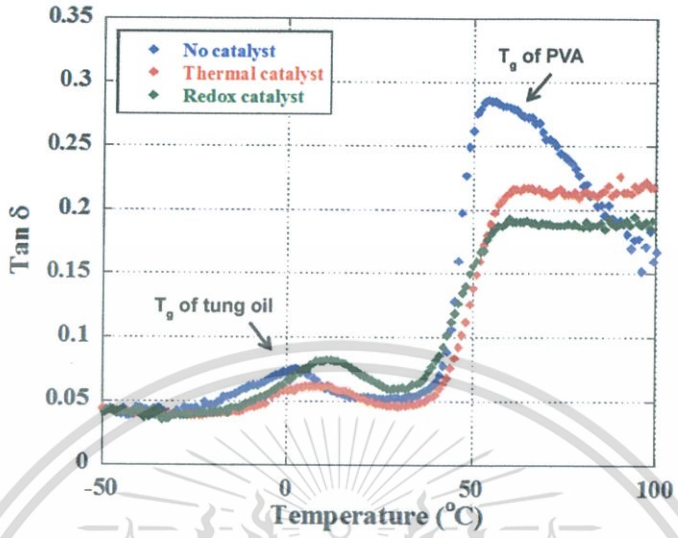

Figure 4.9 Temperature dependence of tan δ values for P85T15 sheets for different catalytic systems cured at 80 °C.

As a function of curing temperature, as shown in Figure 4.10, the T_g values of PVA and tung oil were raised by the raise of curing temperature irrespective of the type of catalytic system. In addition, Figure 4.10 shows the comparative transition temperatures and heights of tan δ values for P85T15-t and P85T15-r. The increase in the T_g and the decrease in the heights at β transition peak of tung oil and at a transition peak of PVA cured by using thermal and redox catalytic system were revealed. The lower heights at α transition peak of PVA, the higher crosslink reaction. It meant that the reactivity of redox catalyst is greater than that by thermal catalyst. It caused the reduction in the molecular motions of the amorphous phase of tung oil's side chains and the backbone of PVA chains.

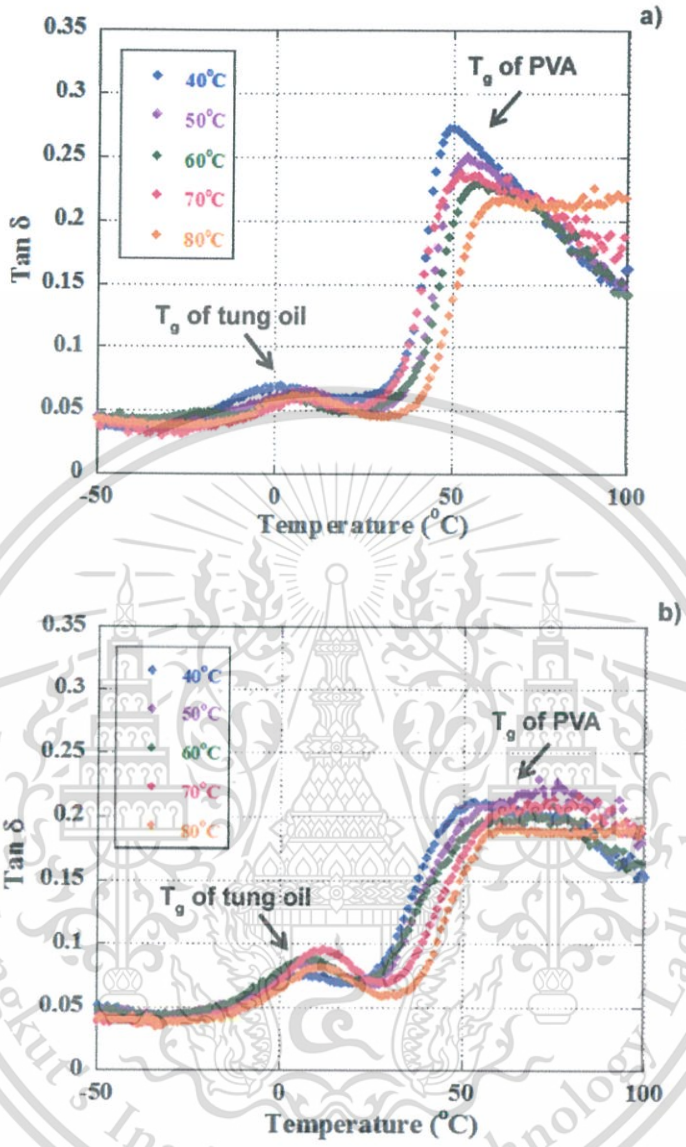

Figure 4.10 Temperature dependence of tan δ values for P85T15 sheets for different curing temperatures in; (a) thermal system and (b) redox system.

4.2.1.4 Mechanical properties

The tensile strength and Young's modulus of P85T15 as the function of curing temperatures and catalytic systems are demonstrated in Figures 4.11(a) and (b), respectively. The tensile strength and Young's modulus of P85T15-t and P85T15-r were found to be increased (116–164% for tensile strength and 81–88% for Young's modulus) as the curing temperatures increased from 40 to 80 °C. As known that, the material with higher amount of crosslink density commonly shows better mechanical properties

such as tensile strength and Young's modulus. This indicated the increase in reactivity of double bonds of tung oil for crosslinking reactions, thus increase in crosslink density corresponding to FTIR results. Moreover, there is also the influence of the retained structure of PVA within the network structure of tung oil, as shown in Figure 4.6. In the case of catalytic systems, it could be seen that these mechanical properties of the sheets cured by using redox system (6.3–16.1 MPa for tensile strength and 69.3– 129.2 MPa for Young's modulus) were higher than those of the sheets cured by using thermal system (5.4–11.7 and 60.3–113.5 MPa for tensile strength and Young's modulus, respectively). Comparing at the same curing temperatures, referring to the previous discussion in water resistant section, the reactivity of tung oil cured by using redox catalytic system was greater than that cured by using thermal catalytic system, resulting in more increase of crosslink density within the P85T15-r. Hence, the higher the crosslink density of the P85T15-r, the better mechanical properties would be obtained.

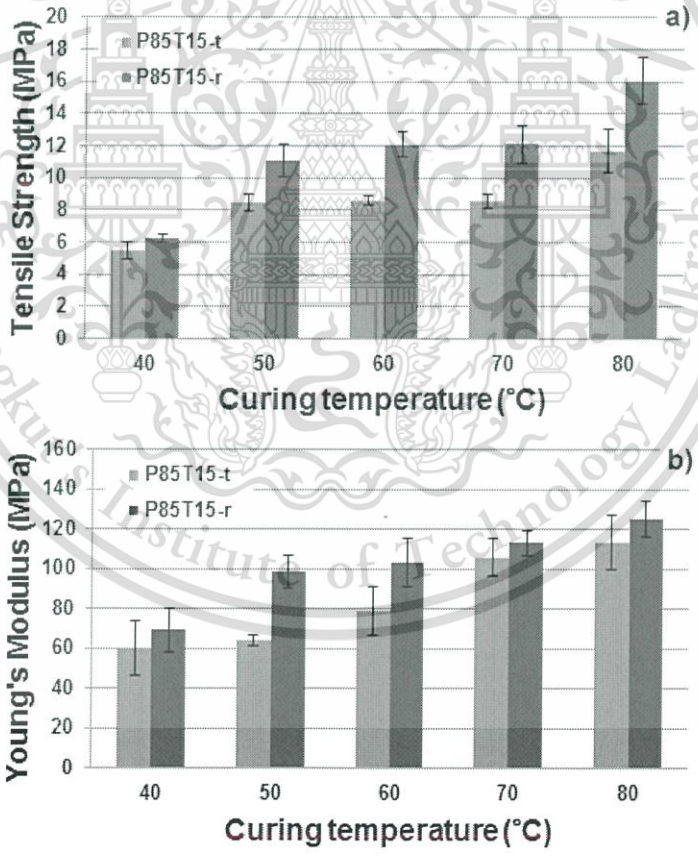

Figure 4.11 Mechanical properties of P85T15 sheets using various catalytic systems; (a) tensile strength and (b) Young's modulus.

Among all results this section, the 15% wt. of tung oil in the formula gained the best properties. The next section, natural rubber latex will be applied instead of tung oil in various weight ratios (0:15, 5:10, 10:5, 15:0) by fixing the weight ratio of PVA to tung oil/rubber at 85:15. Water resistant, thermal and mechanical properties will be evaluated.

4.2.2 Effect of tung oil/natural rubber latex ratio on the properties of PVA/tung oil/rubber sheet (PTR sheet)

The PTR sheets based on PVA, tung oil and rubber (with PVA : tung oil/rubber weight ratio of 85:15) at various tung oil:rubber ratios (0:15, 5:10, 10:5, 15:0) cured by using thermal catalyst (potassium persulfate) or redox catalyst (potassium persulfate and sodium thiosulfate) were prepared by solution casting and then dried at different curing temperatures (from 30 °C to 80 °C). The effects of tung oil:rubber ratios, types of catalyst and curing temperatures on the water resistant, thermal and mechanical properties were investigated.

4.2.2.1 Water resistance testing

The water resistance of the PTR sheets was investigated in terms of the % solid remains as shown in Figure 4.12. Considering to rubber and tung oil structures, they have hydrophobic structures. Thus, the addition of rubber and/or tung oil would be expected to improve the water resistance of PVA. As observed in Figure 4.12, the % solid remain values of PTR sheets were higher than that of neat PVA. In comparison between tung oil and rubber, the results showed that the presence of tung oil incorporating with rubber dramatically increased the % solid remain values rather than the existence of the sole rubber or tung oil, especially at low curing temperatures without catalytic system (Figure 4.12a). This is because tung oil could partially crosslink to be the network structures at the conjugated double bonds of tung oil through free radical mechanism [25, 72]. Rubber stayed as the large hydrophobic structure where its chain entangled with crosslinked tung oil. PVA chains were thus retained within the crosslinked tung oil structures and hydrophobic structure of rubber causing more difficulty to dissolve in water of the PTR sheets.

When apply catalysts, the % solid remain values of PTR sheets with higher tung oil contents showed dramatic enhancement of water resistant properties (Figure 4.12 (b) and (c)). It could be pointed out that the efficiency of crosslinking reaction among the double bonds of tung oil increased when both catalysts were involved rather

than those of rubber. For thermal catalytic system, high temperatures (≥60 °C) were preferred while even low temperatures (≥30 °C) could be applied for redox catalytic system. With crosslinking reaction of tung oil, PVA and/or rubber chains were retained within the crosslinked structure of tung oil by interlocking network [28]. In addition, PVA part could crosslinked by thermal catalyst at ≥ 60 °C. These brought about the difficulty of PVA and/or rubber chains to dissolve in water. Therefore, the similarly high % solid remain values of PTR sheets cured by both thermal and redox catalysts at ≥ 60 °C, would be obtained.

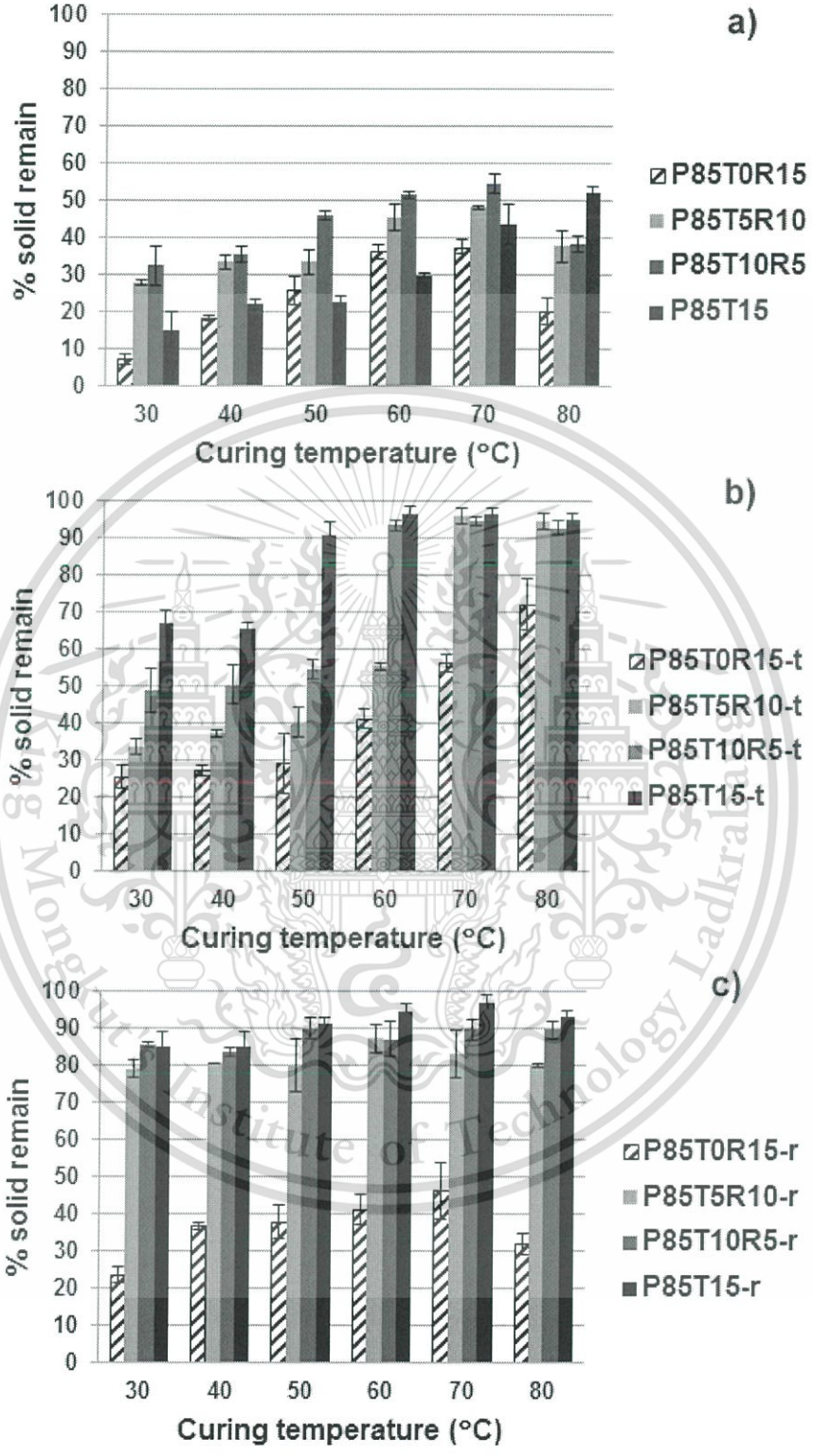

Figure 4.12 The percentage of solid remains of PTR sheets after immersion in water at 25 °C for 24 h; (a) no catalyst system, (b) thermal system and (c) redox system.

4.2.2.2 Fourier Transformed Infrared spectroscopy (FTIR)

The FTIR spectra of PTR sheets as a function of rubber:tung oil ratios are shown in Figure 4.13. The -**C=C**-H and -C=**C-H** vibrations in the structures of tung oil and rubber were allowed to follow the crosslinking reaction. At 50 °C, the pattern of the characteristic peaks of tung oil (3012 cm^{-1} for -**C=C**-H stretching, 992 cm^{-1} for conjugated trans: trans -C=**C-H** bending and 965 cm^{-1} for conjugated cis: trans -C=**C-H** bending) of P85T15-r disappeared while the characteristic peaks of tung oil at 992 cm^{-1} of P85T15-t still appeared. It implies that the crosslinking network in the films would occur *via* the addition reaction at the double bonds of tung oil, especially in redox catalytic system. On the contrary, P85T0R15-t and P85T0R15-r still showed characteristic peaks corresponding to double bonds of rubber at 3036 cm^{-1} (-C=**C-H** stretching) and 1663 cm^{-1} (-**C=C**-H bending). It is suggested that the crosslinking reaction at double bonds of rubber did not predominate. In case of P85T5R10 and P85T10R5 with either thermal or redox catalysts, only the characteristic peaks of tung oil depleted whereas those of rubber remained, suggesting that the crosslinking reaction of tung oil was predominant, especially in redox catalytic system.

From the previous results (water resistance testing and FTIR), the model of the reactions within PTR sheets crosslinked by either thermal catalyst or redox catalyst at 50 °C are illustrated in Figure 4.14. The network structures of thermally crosslinked PTR sheets included the crosslinking reaction of tung oil, trans-esterifications and hydrogen bond formation between tung oil and PVA. As for crosslinked PTR sheets cured by using redox catalyst system, the network structures are in the same manner as the thermal crosslinked PTR sheets with higher crosslink density of tung oil because of the relatively high reactivity of redox catalyst. However the crosslinking reaction of rubber could not be proved in both catalytic systems. This is suggested that rubber might not be crosslinked by assigned catalysts with the moderate temperature (50 °C).

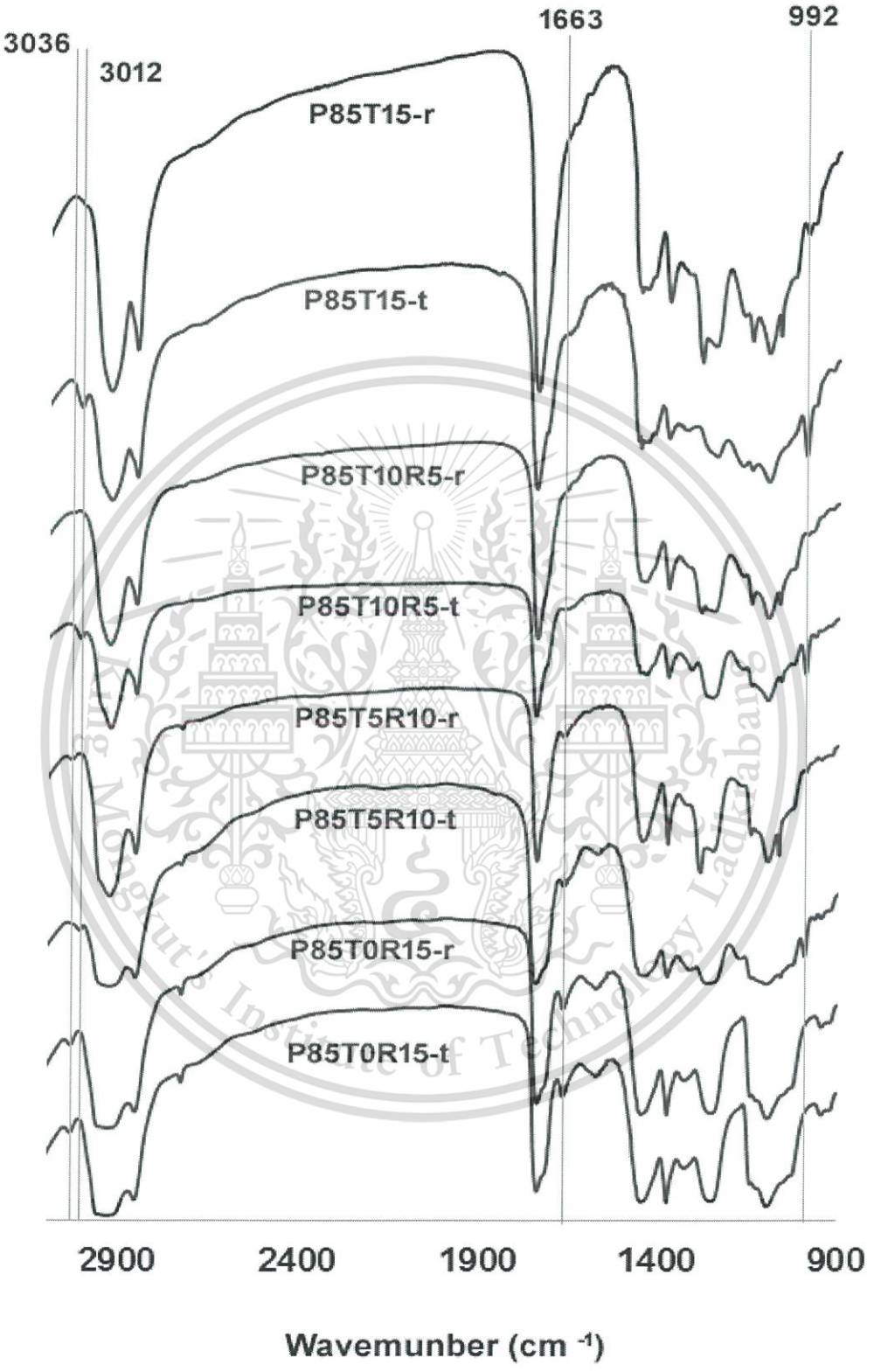

Figure 4.13 FTIR spectra of PTR sheets cured at 50 °C.

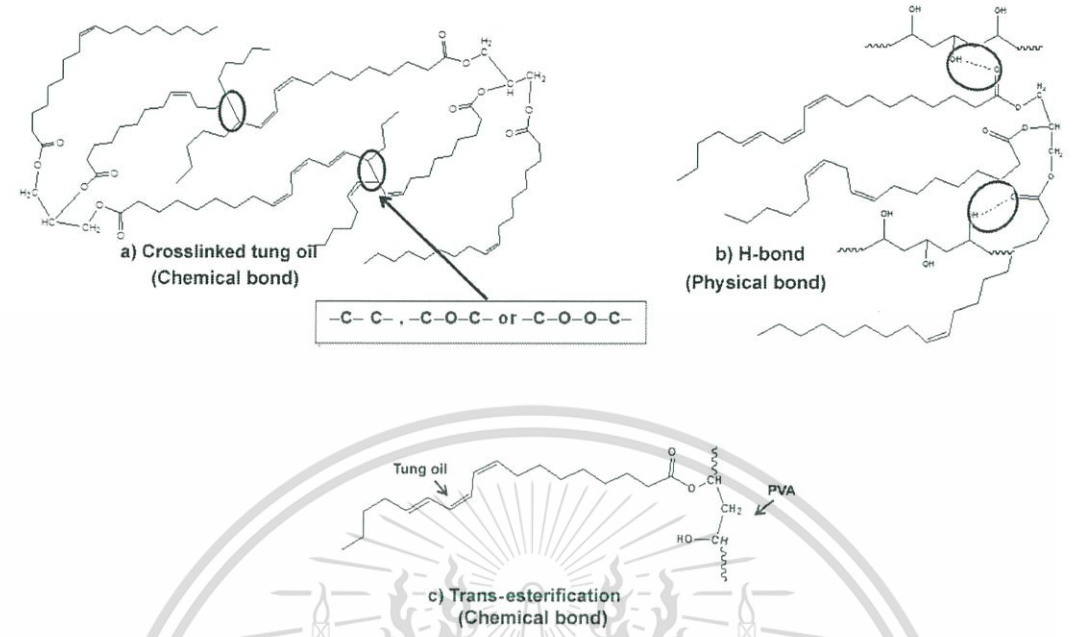

Figure 4.14 Schematic illustration of the reactions within PTR sheets; (a) crosslinked tung oil, (b) trans-esterifications, and (c) hydrogen bond between tung oil and PVA.

4.2.2.3 Dynamic Mechanical Analysis (DMA)

The storage modulus (E') and tan δ values of PTR sheets with various ratios of rubber:tung oil were investigated by DMA, as shown in Figure 4.15. It was found that the T_g values of PVA in PTR sheets increased from 53 °C to 71 °C with increasing tung oil contents. This suggested the occurrence of the crosslinking points of tung oil and the entanglement of rubber and PVA chains within the crosslinked tung oil structures resulting in the restriction of movement of rubber and PVA chains. As a function of tung oil to rubber ratio, the storage modulus of P85T0R15-r showed the lowest value than those of other PTR sheets since rubber was found hardly to crosslink at relatively low curing temperatures as discussed in FTIR session. The combination of tung oil and rubber, on the other hand, in the PTR sheets displayed a high level of E' as compared to both P85T0R15-r and P85T15-r. This phenomenon was due to the crosslinked structures of tung oil within the PTR sheets and strong interactions among tung oil, rubber and PVA resulting in enhancing storage modulus. In addition, the intensities of tan δ peak of PVA in PTR sheets with higher tung oil contents exhibited a decreasing trend as compared to that of the P85T0R15-r meaning the increase in network chain by the crosslinking reaction. With different curing temperatures, as shown in Figure 4.16, T_g of tung oil and PVA in P85T5R10-r sheets increased with increasing curing temperatures

irrespective of the types of catalytic system. This is because the higher curing temperatures, the better crosslink reaction. The results of other PTR sheets are in the same manner.

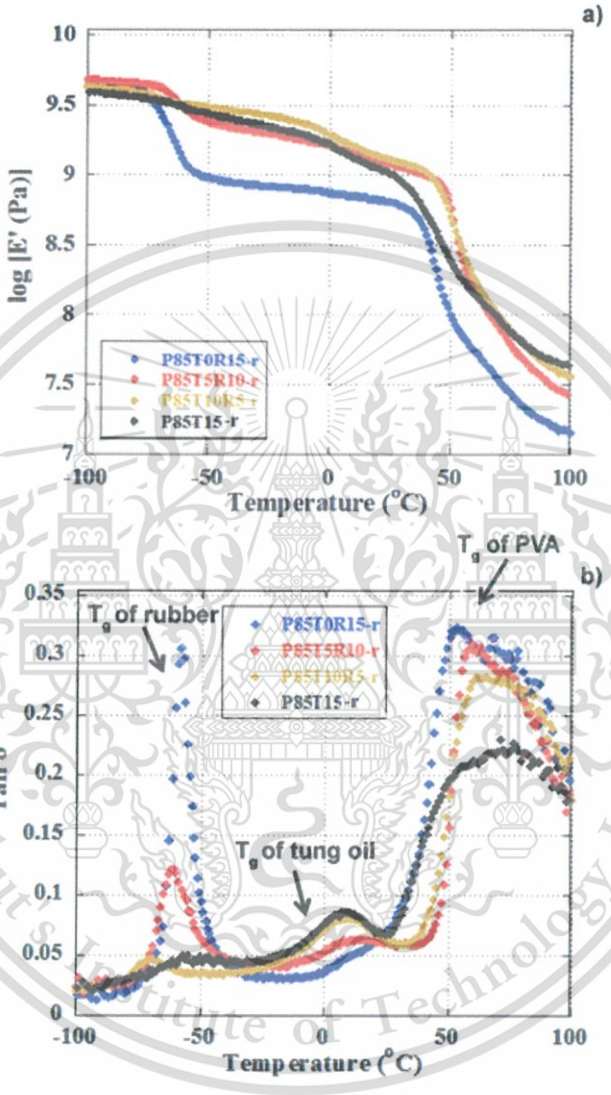

Figure 4.15 Temperature dependence of E′ and tan δ values for PTR sheets cured by redox catalyst at 50 °C.

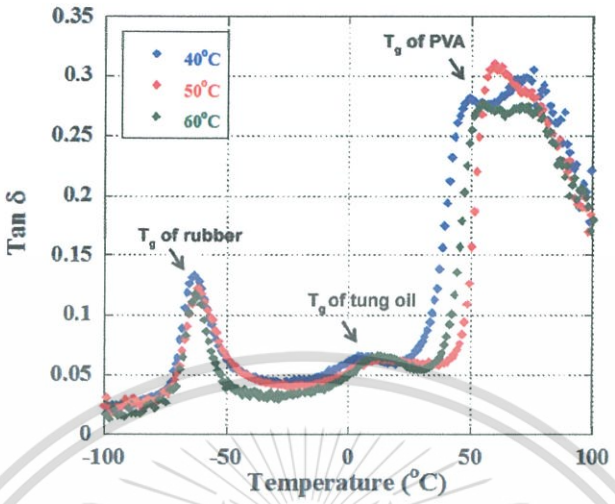

Figure 4.16 Temperature dependence of tan δ values for P85T5R10-r sheets for different curing temperature.

4.2.2.4 Mechanical properties

The tensile properties of the PTR sheets were evaluated by the values of tensile strength and Young's modulus as shown in Figure 4.17 and 4.18, respectively. It was clearly indicated that the tensile strength and the Young's modulus increased with increasing curing temperatures. When the curing temperatures varied from 40 to 70 °C, the tensile strength of P85T0R15-t increased at about 41% and the tensile modulus enhanced at about 68%. Meanwhile, for P85T0R15-r, the tensile strength represented a ~24% enhancement, and the tensile modulus indicated a ~62% increment. For P85T15-t, the tensile strength increased at about 57% and the tensile modulus enhanced at about 76%. Meanwhile, for P85T15-r, the tensile strength represented a ~93% enhancement, and the tensile modulus indicated a ~64% increment. It was found from Figure 4.17 and 4.18 that the presence of tung oil in the PTR sheet and an increase in temperatures would gain relatively high values of the mechanical properties especially in the P85T10R5 sheet, while the effect of different catalytic systems in the PTR sheets on the mechanical properties was small. The results implied that tung oil and PVA could be rather crosslinked by catalyst at high temperatures than rubber. Moreover, the combination of tung oil and rubber enhanced the tensile strength and the Young's modulus. This proposed that incorporating tung oil and rubber into the PVA matrix results in strong interactions between the modifiers and the matrix, and consequently restricts the motion of the matrix and promotes rigidity. In addition, as

using different catalytic systems, the tensile strength and the Young's modulus of the PTR sheets cured by using redox catalyst was slightly higher than those using thermal catalyst. The crosslink of tung oil was found to be predominated in redox system, while PVA could crosslink in thermal system as discussed in the earlier section. These results suggested that the crosslinking as of tung oil was more effective than the crosslinking reaction of PVA. Hence, the higher crosslink density of the PTR sheets cured by using redox catalyst could be obtained resulting in the better mechanical properties.

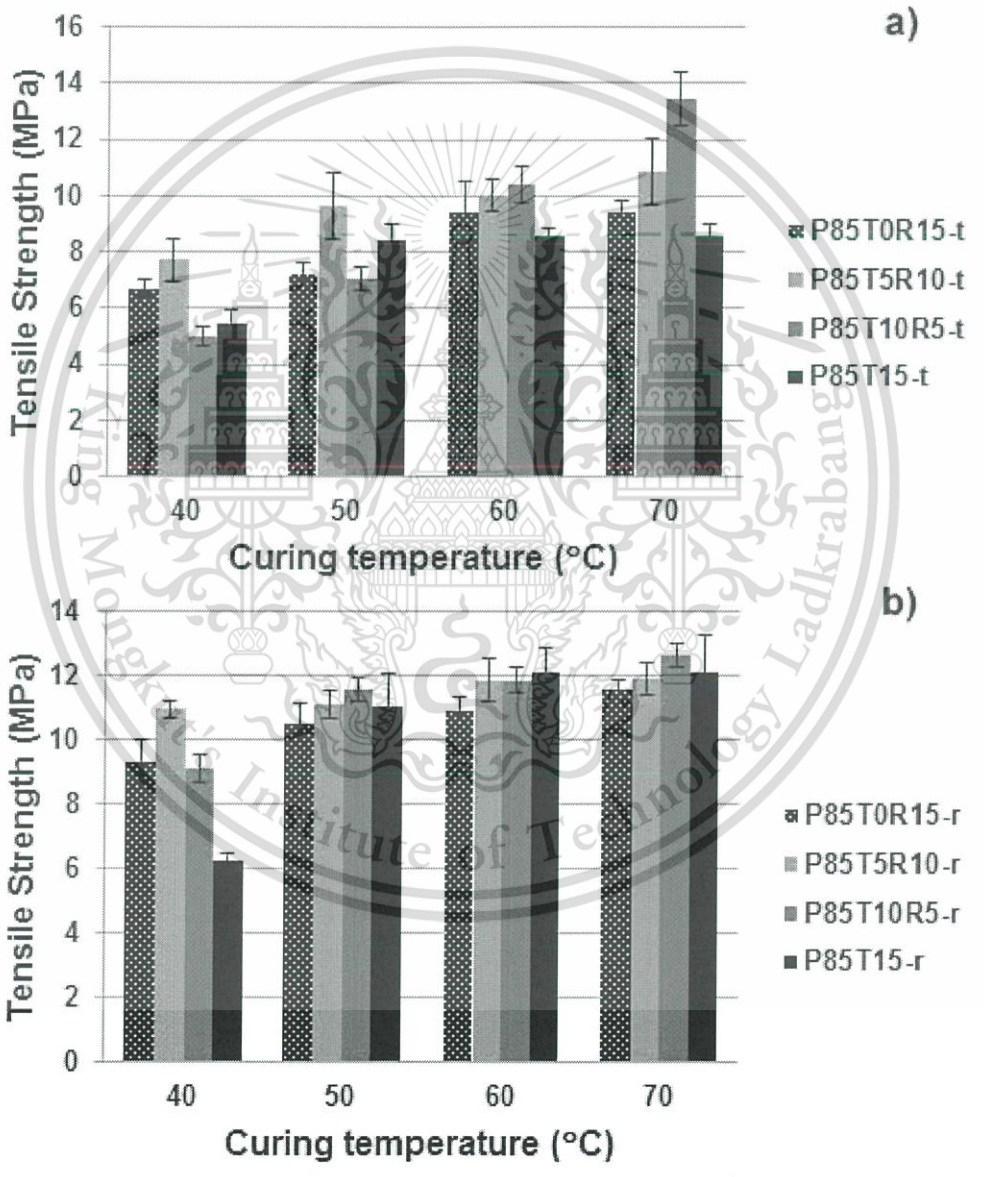

Figure 4.17 Tensile strength of PTR sheets catalyzed by; (a) thermal system and (b) redox system.

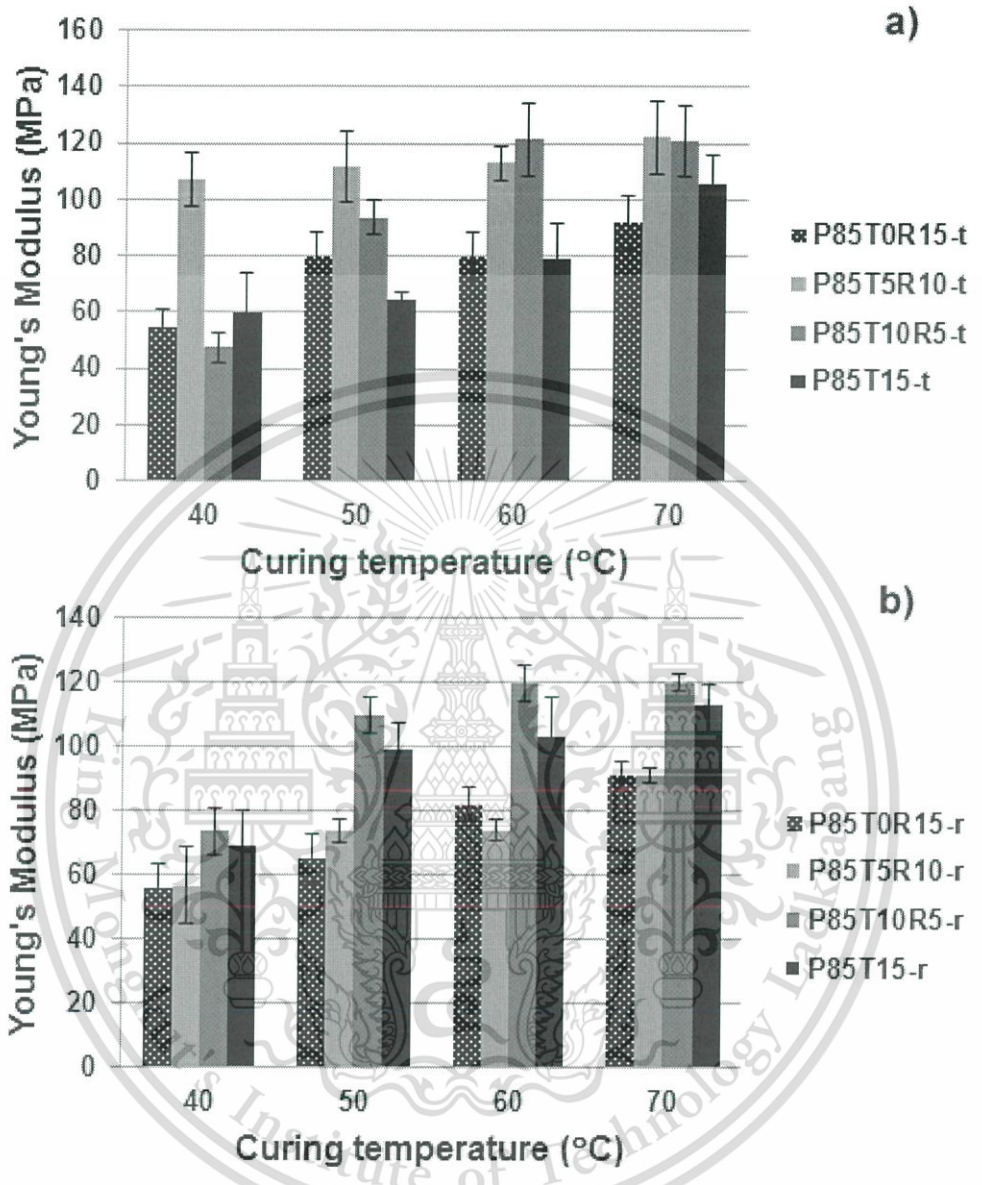

Figure 4.18 Young's modulus of PTR sheets catalyzed by; (a) thermal system and (b) redox system.

4.2.3 Effect of nano-additives on the properties of the PVA/tung oil sheets (PT sheets) and PVA/tung oil/rubber sheets (PTR sheets)

In this part, the sheets prepared from the modified PVAs based on the mixtures of tung oil, rubber and PVA at various tung oil:rubber ratios (0:15, 5:10, 10:5, 15:0) with the addition of nano-additives (nanocalcium carbonate, nanozinc oxide and nanosilica) by using thermal catalyst (potassium persulfate) or redox catalyst (potassium persulfate

and sodium thiosulfate) were prepared by solution casting. Curing temperatures applied during drying step were ranged from 30 °C to 70 °C to achieve nano-additive PT and PTR sheets. The effects of types of nano-additive, nano-additive contents and curing temperatures on the water resistant, thermal and mechanical properties were investigated.

4.2.3.1 Water resistance testing

Water resistance of nano-additive P85T15 sheets was defined as the % solid remain after dissolving in water for 24 h as shown in Figure 4.19 – 4.23. Figure 4.19 (a) and (b) show the % solid remains of P85T15Zn (nanozinc oxide contained) cured by using thermal and redox catalysts, respectively while Figure 4.20 (a) and (b) display the % solid remains of P85T15Ca (nanocalcium carbonate contained) cured by using thermal and redox catalysts, respectively. These results indicated that the % solid remains of P85T15Zn and P85T15Ca sheets decreased as compared those of P85T15 sheets. These suggested that nanocalcium carbonate and nanozinc oxide have high surface energy and they are easy to aggregate, leading to their poor dispersion in P85T15 sheets. This phenomenon hindered the crosslinking reaction of tung oil and it might generate voids among the interfaces of the matrix (PVA and tung oil) and nanozinc oxide or nanocalcium carbonate. When P85T15Zn and P85T15Ca sheets were immersed in water, water could penetrate throughout these voids, leading to the dissolution of the matrix especially PVA. With different curing temperatures, the % solid remains of P85T15Zn and P85T15Ca sheets cured by using thermal catalyst were slightly enhanced with increasing curing temperatures, whereas those cured by using redox catalyst hardly changed. It was suggested that, at lower curing temperatures, the reactivity of redox catalyst is better than that of thermal catalyst and higher curing temperatures had less effect on the % solid remains of P85T15Zn and P85T15Ca sheets cured by using redox catalyst. In case of the nano-additive contents, it showed less effect on the % solid remains of the sheets, except for the P85T15Zn cured by using thermal catalyst. In this case, the higher content of nanozinc oxide, the higher % solid remains.

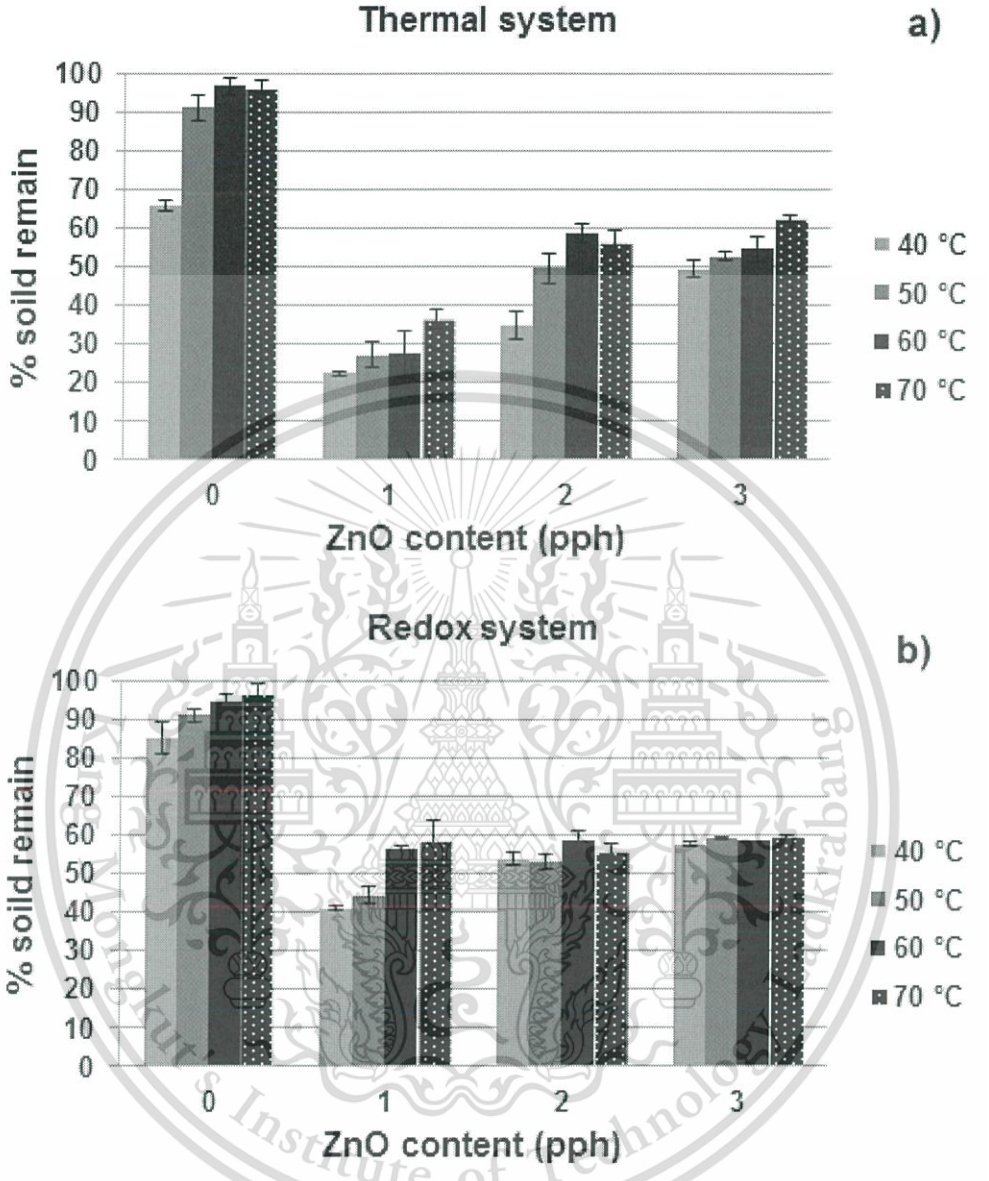

Figure 4.19 The percentage of solid remains of P85T15Zn sheets after immersed in water at 25 °C for 24 h; (a) thermal system and (b) redox system.

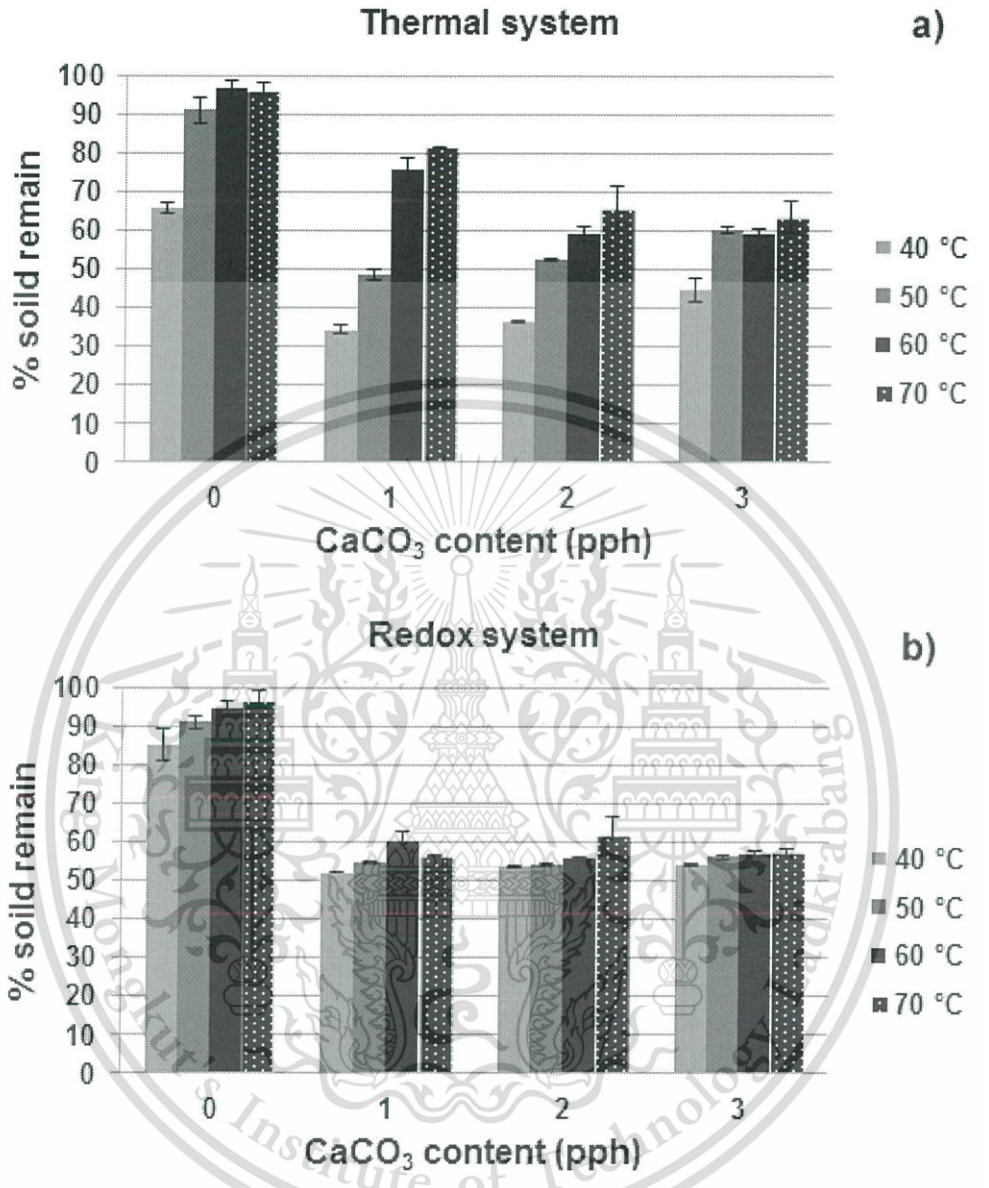

Figure 4.20 The percentage of solid remains of P85T15Ca sheets after immersed in water at 25 °C for 24 h; (a) thermal system and (b) redox system.

Figure 4.21 (a) shows the % solid remains of nanosilica contained-PT sheets cured by using redox catalyst and dried at 50 °C (the suitable curing temperature referring to the section 4.2.1.2). It was found that the PT sheets contained relatively high tung oil contents exhibited high values of % solid remains. The higher tung oil contents, the higher crosslinking reactions. As a function of nanosilica amount added into the PT sheet, the % solid remain values showed in different way depending on the amount of

tung oil in the PT sheet. The PT sheets containing higher tung oil content (P85T15 sheets) gained the decrease in % solid remains when the nanosilica amount was raised. On the other hand, sheets containing the lower tung oil content sheets (P95T5 and P90T10 sheets) gave higher % solid remain values as higher amounts of nanosilica was applied. It proposed that nanosilica preferred dispersion in PVA matrix to tung oil because of the interaction between silanol groups on the surface of silica and hydroxyl groups of PVA.

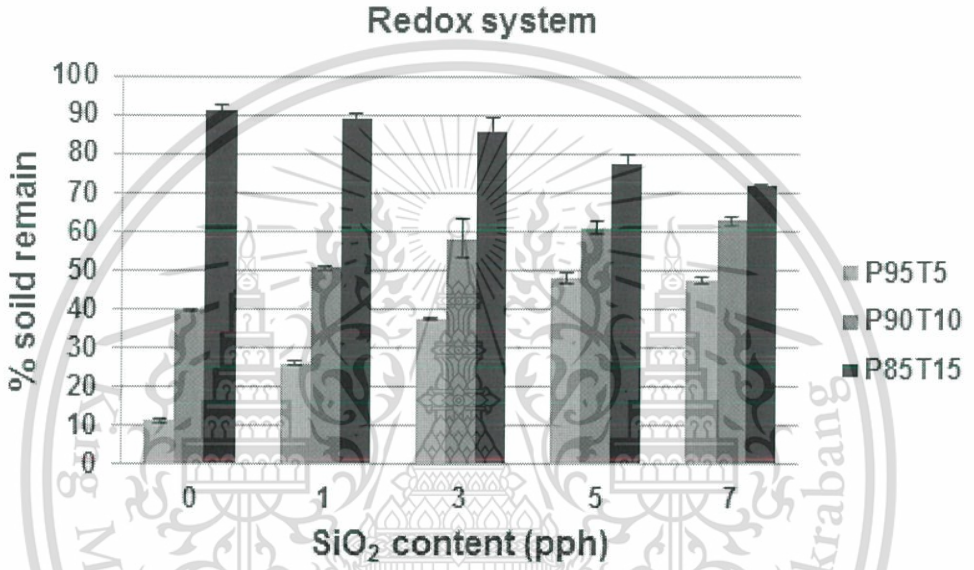

Figure 4.21 The percentage of solid remains of nanosilica contained-PT sheets cured by using redox catalyst and dried at 50 °C after immersed in water at 25 °C for 24 h

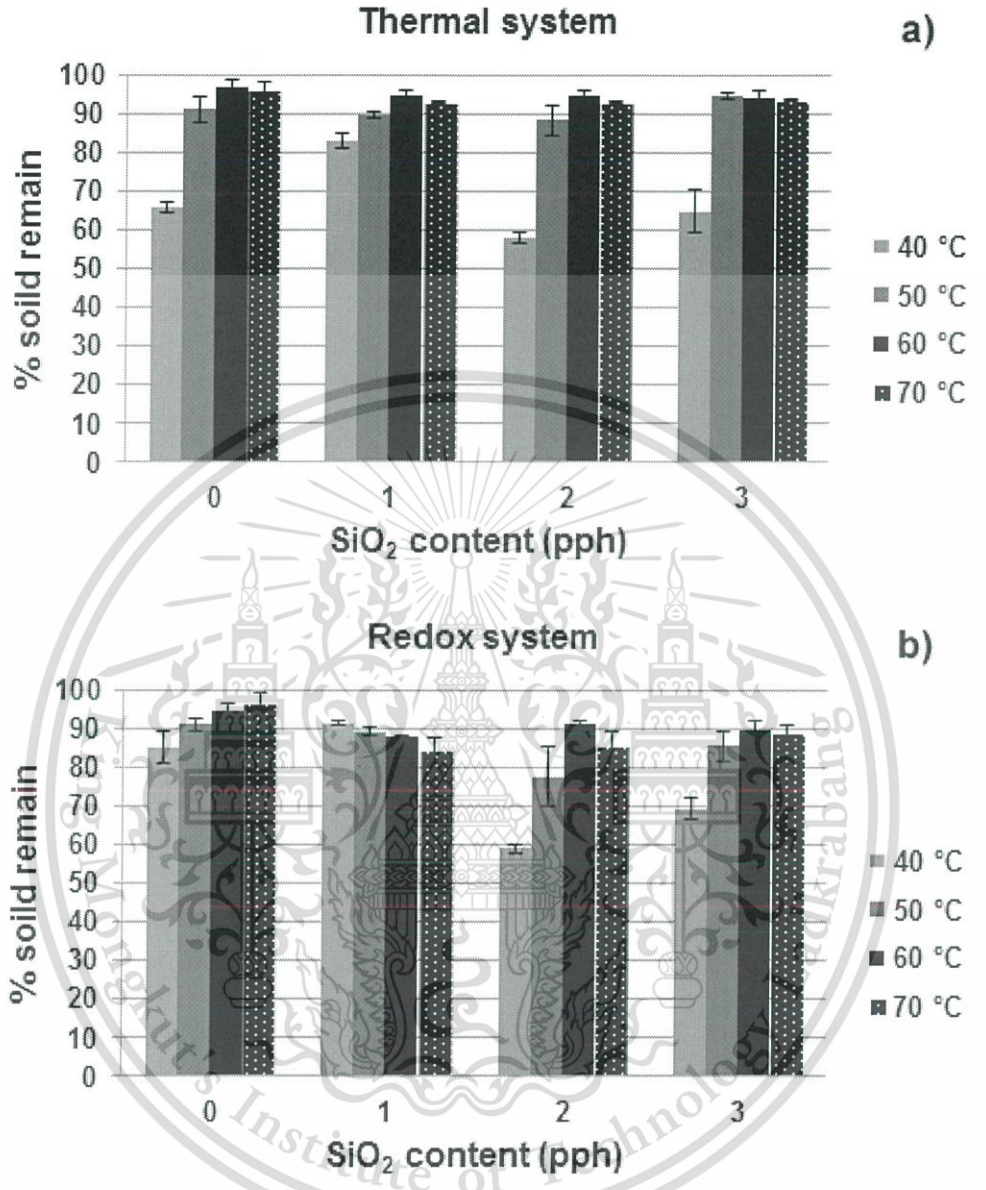

Figure 4.22 The percentage of solid remains of P85T15Si sheets after immersed in water at 25 °C for 24 h; (a) thermal system and (b) redox system.

Figure 4.22 showed % solid remain values as functions of reaction temperature (40 – 70 °C) and amount of nanosilica (0 – 3 pph) cured by using thermal catalyst (Figure 4.22a) and redox catalyst (Figure 4.22b). Neither reaction temperature nor amount of nanosilica affected on the % solid remain of the sheet except for reaction temperature at 40 °C, especially for thermal system. This is because low reaction

temperatures brought about insufficient crosslinking reaction of the sheet resulting in poor water resistant property.

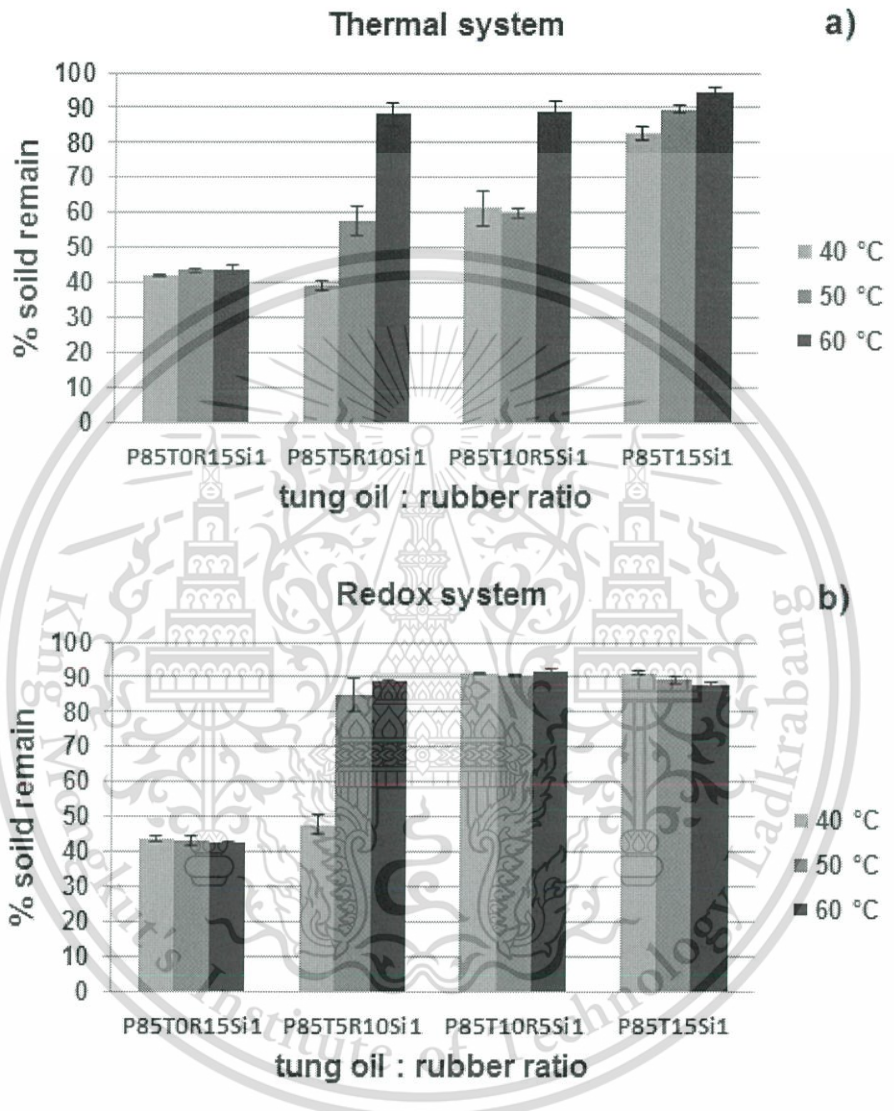

Figure 4.23 The percentage of solid remains of 1 pph nanosilica contained-PTR sheets after immersed in water at 25 °C for 24 h; (a) thermal system and (b) redox system.

For the PTR sheet, nanozinc oxide or nanocalcium carbonate could not be added into PTR sheets. It explained that the positive charge on the surface of nanozinc oxide or nanocalcium carbonate interacted with protein encapsulated rubber latex resulted in the aggregation of rubber. Therefore the sheet thickness was not uniform. In case of nanosilica, 1 pph of nanosilica could add into the mixture to prepare homogeneous PTR sheet. The water resistance of PTR sheets adding nanosilica is shown

in Figure 4.23. The results obviously suggested that the content of tung oil at least 5% is needed in order to gain the reasonable high % solid remain value. It was explained that the crosslink reaction of tung oil retained PVA and rubber structure within its structure leading to the water resistance of PTR sheets. In addition, the % solid remain of PTR sheets cured by using redox system showed better values than those cured by using thermal system, especially at low reaction temperatures. This might be because –C=C- in the rubber structure preferred to react with redox catalyst rather than thermal catalyst where the crosslink reaction occurred and subsequently the network was formed. Thus, the water resistant property was improved. Nevertheless, at 1 pph, the amount of nanosilica exceeded a critical value for PTR sheets. If the amount of nanosilica continued to increase, the aggregates would become larger and could interact with protein encapsulated rubber latex, making the deformation of rubber latex resulting in the poorer compatibility.

Unfortunately, the effects of types of nano-additive on the water resistance and other properties could not properly investigate since the difference in particle sizes. Thus, among all results, the 15% wt. of tung oil and 0-3 pph of nanosilica in the formula gained the better properties. The next part, the PT sheets with 15% wt. of tung oil and 0-3 pph of nanosilica were characterized by SEM and FTIR. DMA results and mechanical properties were also discussed.

4.2.3.2 Scanning electron microscopy (SEM)

SEM images of the cross-section of P85T15-r sheets cured at 60 °C are shown in Figure 4.24. Silicon mapping images from SEM-EDS are demonstrated as the white dot in Figure 4.24 (a) and (c). Moreover, the P85T15Si1-r sheets (Figure 4.24b) showed the quite smooth surfaces similar to the P85T15Si3-r sheets (Figure 4.24d). These images revealed that the silicon atoms are quite uniformly distributed in the whole cross-section. The results indicated that silica could disperse well and had the good compatibility in P85T15-r sheets.

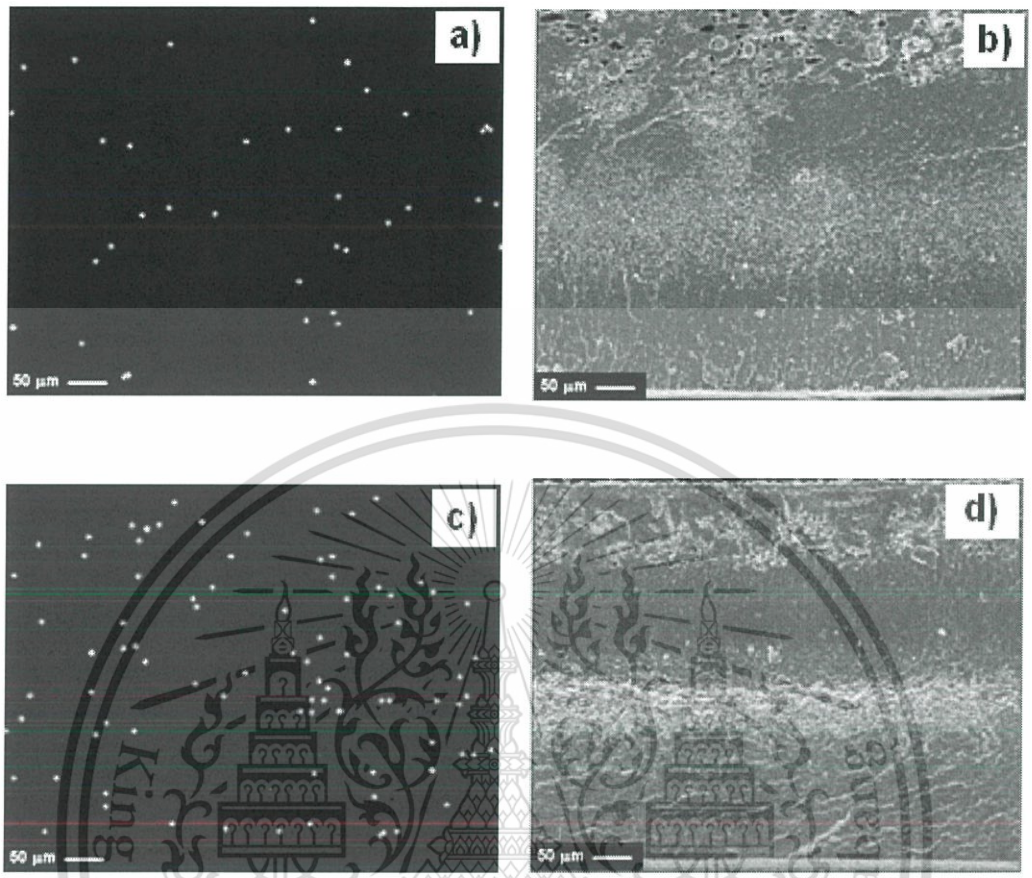

Figure 4.24 Silicon mapping images (left) and SEM images (right) of the same cross-section of P85T15Si-r sheets using various nanosilica contents; (a) and (b) 1 pph magnified 167 times (c) and (d) 3 pph magnified 145 times.

4.2.3.3 Fourier Transformed Infrared spectroscopy (FTIR)

The FTIR spectrum of P85T15-r film cured at room temperature (Figure 4.25a) represents that the absorption peak at about 965 cm^{-1} accredited to the reaction at the double bond of tung oil (conjugated cis: trans -C=C-H bending) disappeared whereas the peak at 992 and 3012 cm^{-1} ascribed to the reaction at the double bond of tung oil (conjugated trans: trans -C=C-H bending and -C=C-H stretching, respectively) still appeared. For P85T15Si-r films, curing at room temperature, all of the peaks related to the reaction at the double bond of tung oil (-C=C-H stretching) creased for the peak at 965 cm^{-1} and decreased in the intensity at 992 and 3012 cm^{-1} when nanosilica 1 pph (P85T15Si1-r film) was applied (Figure 4.25b). Furthermore, these peaks disappeared in P85T15Si3-r film in which 3 pph of nanosilica was added (Figure 4.25 c). It may be suggested that, at ambient temperature, the nanosilica in P85T15Si-r films behaved as a catalyst and induced the crosslinking reaction at unsaturated position of tung oil. For

films curing at 50 °C, the FTIR spectra results were discovered that all absorption peaks at 965 and 992 cm^{-1} attributed to the conjugated double bond in tung oil and the absorption peak at about 3012 cm^{-1} accredited to the double bond of tung oil (-C=C-H stretching) disappeared (Figure 4.25 (d - f)). It can be proved that crosslinking network in the P85T15-r, P85T15Si1-r and P85T15Si3-r films would occur *via* the addition reaction at the double bond of tung oil.

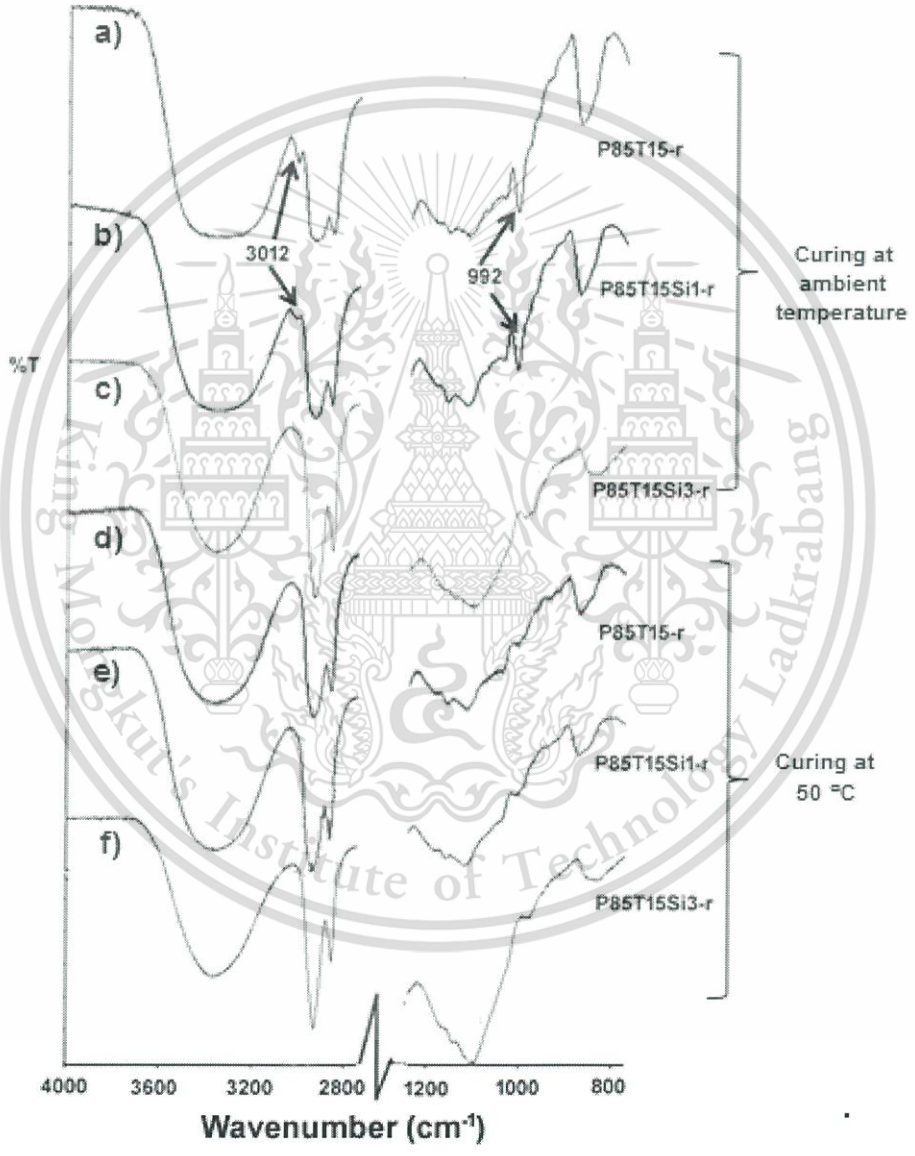

Figure 4.25 FTIR spectra of P85T15-r, P85T15Si1-r and P85T15Si3-r films.

4.2.3.4 Dynamic Mechanical Analysis (DMA)

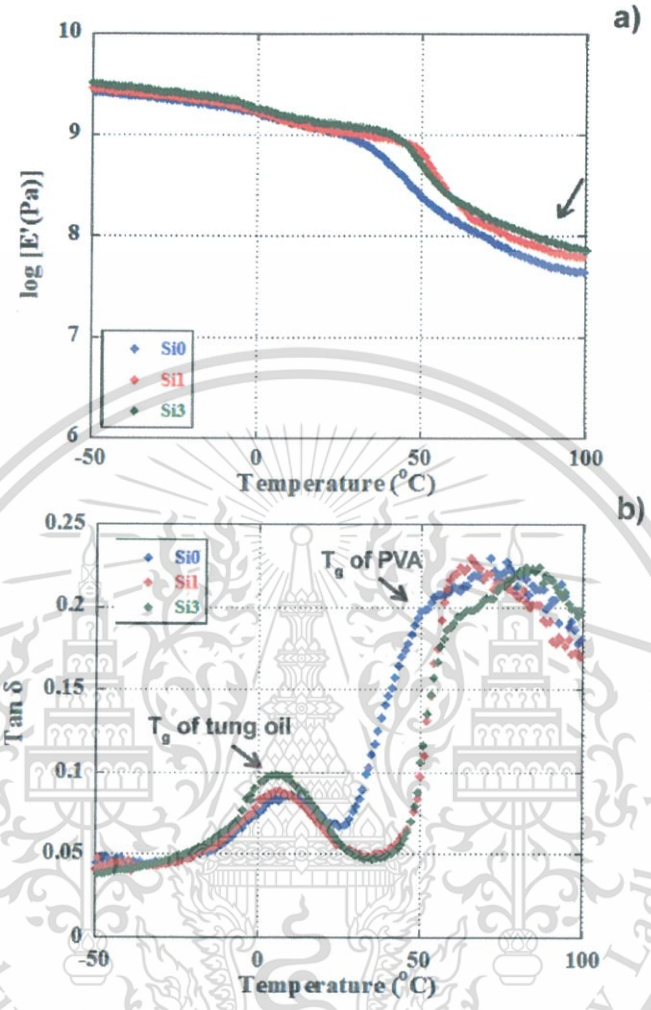

Figure 4.26 Temperature dependence of storage modulus (E′) (a), and tan δ values (T_g) (b) as a function of temperature for P85T15Si-r cured at 50 °C.

The interactions of polymer chains with silica nanoparticles (P85T15Si-r sheets) using various nanosilica contents cured at 50 °C studied as the temperature dependence of E′ and tan δ values are shown in Figure 4.26. In Figure 4.26a, the storage modulus (E′) increased by increasing the nanosilica content. An increase in E′ value meant to the hard movement of the structure of the films. It is not only because of the rigidity of nanosilica but also the degree of crosslink of tung oil and the network structure among silanol groups on the surface of silica, hydroxyl groups of PVA and carbonyl groups of tung oil (see Figure 4.27). From the above reasons, it can be found that P85T15Si3 sheet (3 pph of nanosilica) has the highest storage modulus. As

temperature increased, the components became more mobile and lost their close packing arrangement, leading to the decrease in storage modulus at the glass transition region (see Figure 4.26a).

In term of transition zone (Figure 4.26b), the T_g peaks corresponding to the motion of PVA and tung oil in P85T15Si1 and P85T15Si3 sheets are visible in two regions i.e., at around 10 °C (T_g of tung oil) and 58.1 to 71.0 °C (T_g of PVA). As compared with P85T15-r sheet, the higher shift in temperature of the T_g of PVA for P85T15Si-r sheets proved that crosslinking reaction of the double bond of tung oil occurred along with hydrogen bonds among silanol groups on the surface of silica, carbonyl groups of tung oil and hydroxyl groups of PVA in the P85T15Si-r sheet. Thus the addition of nanosilica in PT sheets reduced the mobility of polymer chains and then caused the formation of immobilized and restricted mobility regions around the nanoparticles.

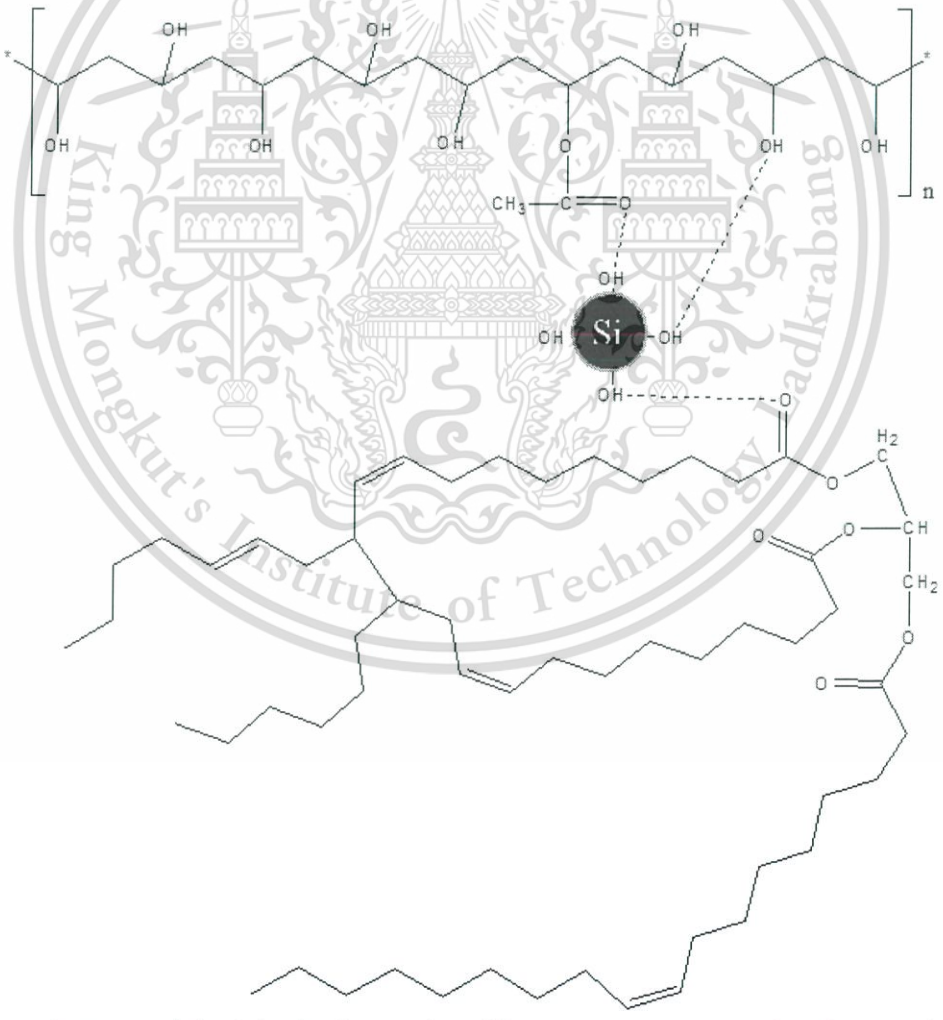

Figure 4.27 Model of the hydrogen bond between PVA, tung oil and nanosilica.

4.2.3.5 Mechanical properties

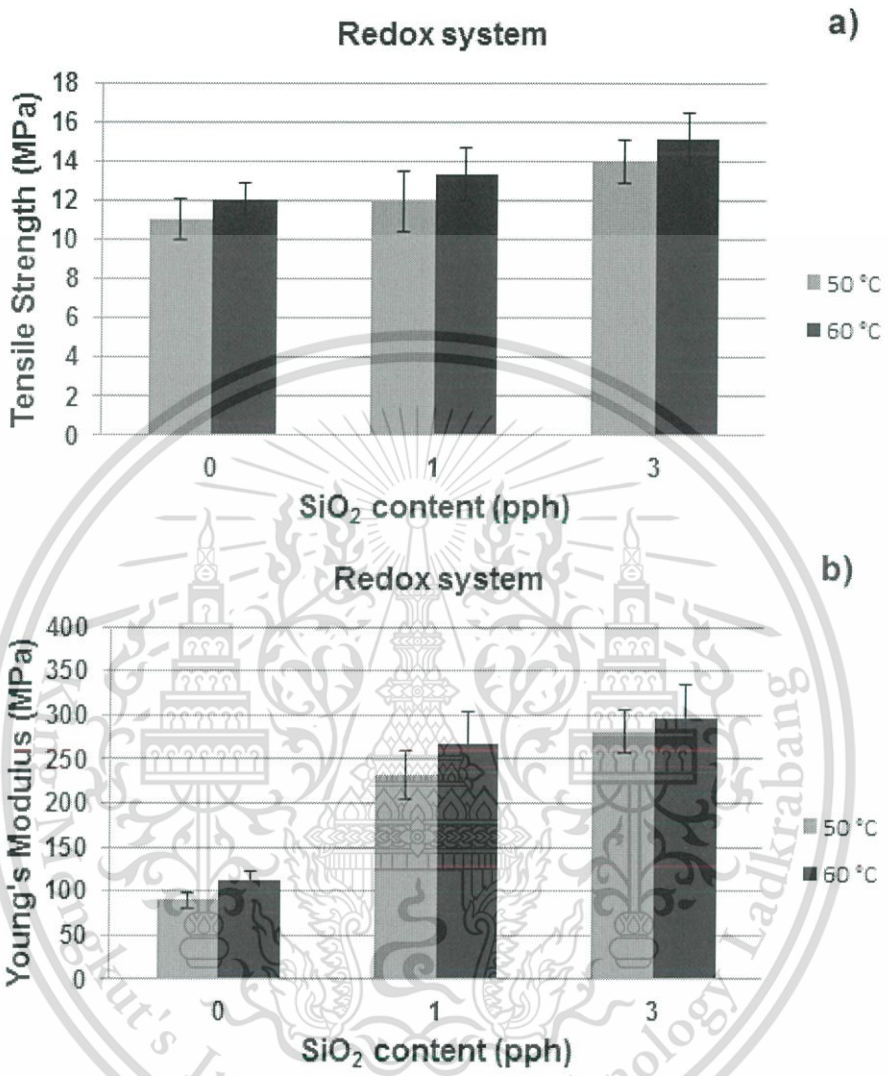

Figure 4.28 Mechanical properties of P85T15Si-r sheets using various nanosilica contents; (a) tensile strength and (b) Young's modulus.

The improvement of their mechanical properties (tensile strength and Young's modulus) of P85T15Si-r sheets using various nanosilica contents would gain in Figure 4.28. Both mechanical properties showed the increase in those values when nanosilica was added. For example, tensile strength of P85T15-r sheets cured at 50 °C increase from 11 MPa to 11.9 MPa (for 1 pph) and 14 MPa (for 3 pph). In the same way, Young's modulus cured at 50 °C went up from 89.8 MPa to 231.6 MPa (for 1 pph) and 281.7 MPa (for 3 pph). The increase in mechanical properties is due to the high surface area of

silica nanoparticles resulting in a high interface with the PVA matrix. This phenomenon allowed the nanosilica to prevent the accumulation of stress and stress transfer from PVA to nanoparticles. Thus, the sheets are hard to deform. However, these values do not linearly increase because nanosilica has high surface energy and they are easy to aggregate, leading to their poor dispersion in polymer matrix and discontinuity between silica phase and polymer. This brought about the defect of the sheet and impeded to yield the theoretical high mechanical properties. With different curing temperatures, these mechanical properties slightly enhanced with increasing curing temperatures. It might be proposed that the crosslinked sheet could be easily formed before nanosilica was assembled to form agglomeration.

4.3 Application of PT and PTR as coating materials

4.3.1 Morphology, contact angles and contact angle change rates of PT and PTR coated paperboard and fiberboard

1 g of selected coating materials was coated on white paperboard and fiberboard (8 cm x 5 cm) and then dried at 50 ^{o}C. It was found that all selected coating materials were easy to apply on white paperboard and fiberboard without sagging and other defects. After coating, the coated materials were subsequently conditioned in a desiccator for at least 7 days at ambient conditions before the measurement was made.

SEM images of the surfaces of uncoated and coated paperboards are shown in Figure 4.29. The base paperboard (Figure 4.29a) shows the expanded nonwoven cellulosic fibrils and the porous surface, whereas the coated paperboard (Figure 4.29b) shows the smooth surface. It suggested that the rough and porous surfaces of the paperboards were filled and covered by coating material. In addition, SEM image of the cross section of the coated paperboard shows the thickness of coated film at about 72 μm (Figure 4.29c).

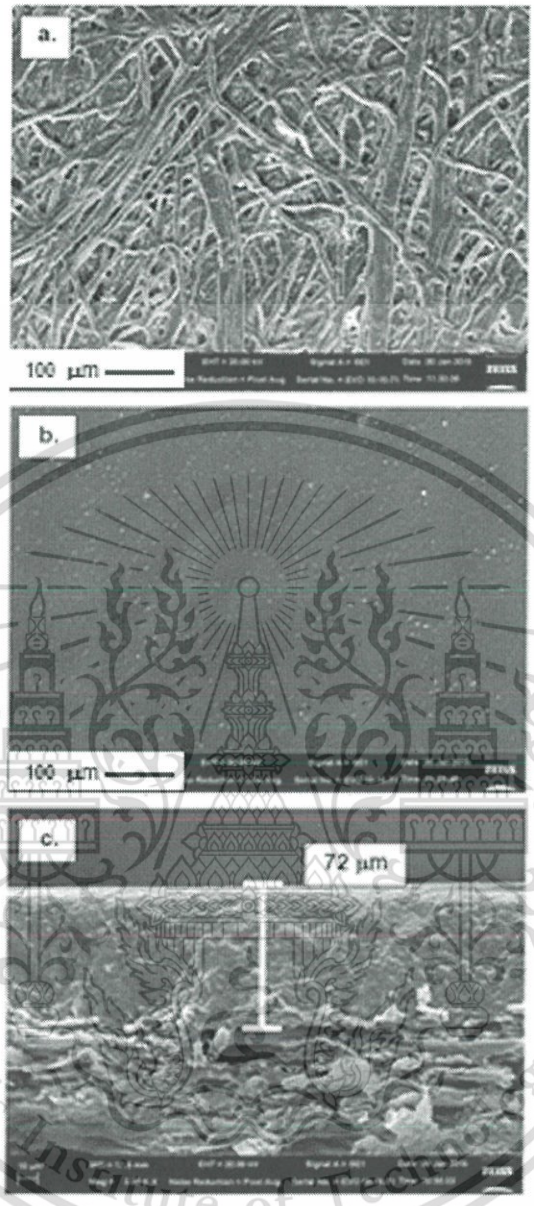

Figure 4.29 SEM micrographs of the paperboards; (a) uncoated surface magnified 1000 times, (b) P85T15-r coated surface magnified 1000 times, and (c) cross section of P85T15-r coated paperboard magnified 3000 times.

Fig 4.30 showed the SEM images of the surfaces of uncoated and coated fiberboards. The base fiberboard (Figure 4.30a) shows the bigger nonwoven cellulosic fibrils and the porous surface, whereas the coated fiberboard (Figure 4.30b) shows some roughness surface. It can be explained that, during coating process, air bubble were trapped within the bigger porous surfaces of the fiberboards bringing about uncertain coated on the material.

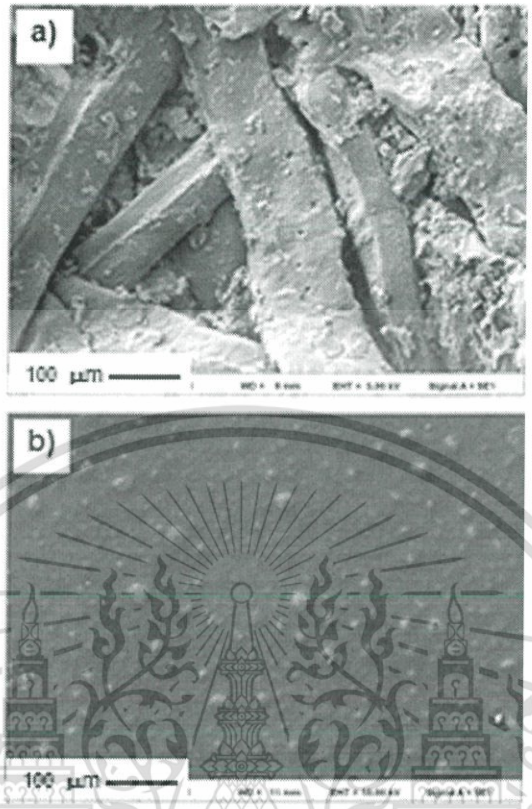

Figure 4.30 SEM micrographs of the fiberboards magnified 1000 times; (a) uncoated surface, and (b) P85T15-r coated surface.

Table 4.1 Initial contact angles of water and contact angle change rates (k) on paperboards coated at 50 °C.

Coating materials	Initial contact angle (deg.)	k (deg/s)	R^2
Uncoated	105.2 ± 8.2	0.095 ± 0.004	0.99
PVA	34.3 ± 0.7	N/A	N/A
P85T15t	93.7 ± 1.5	0.062 ± 0.005	0.99
P85T15r	94.8 ± 0.6	0.060 ± 0.003	0.99
P85T10R5-t	96.2 ± 2.6	0.082 ± 0.013	0.97
P85T10R5-r	97.9 ± 1.9	0.077 ± 0.006	0.97
P85T5R10-t	103.4 ± 1.6	0.072 ± 0.004	0.97
P85T5R10-r	98.6 ± 3.1	0.063 ± 0.005	0.99
P85T0R15-t	74.6 ± 4.4	0.069 ± 0.011	0.98
P85T0R15-r	69.6 ± 3.9	0.062 ± 0.010	0.98

Table 4.2 Initial contact angles of oil and contact angle change rates (k) on paperboards coated at 50 °C.

Coating materials	Initial contact angle (deg.)	k (deg/s)	R^2
Uncoated	N/A	N/A	N/A
P85T15t	55.8 ± 2.9	0.037 ± 0.003	0.99
P85T15r	62.8 ± 7.2	0.016 ± 0.001	0.99

Table 4.3 Initial contact angles of water and contact angle change rates (k) on fiberboards coated at 50 °C.

Coating materials	Initial contact angle (deg.)	k (deg/s)	R^2
Uncoated	129.8 ± 9.4	0.213 ± 0.019	0.98
P85T15t	92.1 ± 2.0	0.063 ± 0.004	0.99
P85T15r	93.8 ± 3.0	0.053 ± 0.008	0.96

The initial contact angle results of water on the paperboards coated at 50 °C are summarized in Table 4.1. An uncoated paperboard showed water contact angle of 105.2° while PVA coated paperboard presented water contact angle of 34.3°. For PT and PTR coated paperboards, the initial contact angles of water on the coated paperboards were 69.6-103.4° laying on between the values of uncoated and PVA coated paperboard, depending on types of coating materials. This suggested the relatively hydrophobic property of PT and PTR coating materials over the surface of the paperboard. It could be pointed that the use of tung oil (P85T15) or the synergy of tung oil and rubber (P85T10R5 and P85T5R10) in coating materials gained higher water contact angle than those using the sole rubber. It is because tung oil contains hydrophobic structures and the crosslinked tung oil resists to water absorption [96]. However, types of catalyst use in coating materials seemed to be no effect on the water contact angle. Similar results occurred when fiberboards were applied instead of paperboards. The results are summarized in Table 4.3. The contact angles of P85T15 coated fiberboards were in the range of 92.1–93.8° less than that of uncoated fiberboard at 129.8°.

For the contact angle of the oil tested, the initial contact angles on the P85T15 coated paperboard were in the range of 55.8–62.8° (Table 4.2). The lower values of

initial contact angles of oil tested suggested that the presence of tung oil within P85T15 coatings material improved oil affinity of those surfaces. Unfortunately, the comparison of contact angle with the fiberboards and uncoated paperboard could not be performed since the oil drop could not stay long on the surface and was immediately absorbed into the surface of the boards. In conclusion, the contact angle results of both liquid drops confirmed that the P85T15 coating materials protected the surfaces of paperboards and fiberboards, yielding better water and oil affinities for printing application.

The contact angle change rates of water or oil on the paperboards and fiberboards are also summarized in Table 4.1 – 4.3. The contact angles of both water drop and oil drop on coated paperboards and fiberboards, including the uncoated ones, tended to decrease at different rates depending on time. These results plainly indicated that the contact angle on the paperboards or fiberboards decreased due to water or oil absorption by the surfaces of substrates and/or evaporation into the atmosphere. In general, the water or oil absorption rate by the paperboards and fiberboards is faster than their evaporation rate over a short time span. Therefore, in this case, the change in contact angle can be used as an indication of the water or oil absorption rates by the paperboards or fiberboards. The linear reversion of the water or oil absorption rates exposed that the linear model was equal to the contact angle change rate with significant high values of the coefficient of determination (R^2) [45].

The results from Table 4.1 indicated that the contact angle change rates (k value) of water tests on coated paperboards decreased from 0.095 deg/s of the uncoated paperboard. The reduction in the k values of water test by PT or PTR coated paperboards is due to the presence of hydrophobic materials i.e., tung oil and rubber. Moreover, tung oil can be crosslinked, resulting in lower water perpetrations, leading to the decrease in the contact angle change for water test. Furthermore, at different catalytic systems, the k values of PT or PTR coated paperboard using redox catalyst presented lower k values compared with those of using thermal catalyst. It indicated that the redox system showed a higher efficiency of crosslinking reaction than thermal system.

With the oil drop applied (Table 4.2), the k values of P85T15 coated paperboard (0.016–0.037 deg/s) were lower than those of the water tests (0.060–0.062 deg/s) (Table 4.1). It could be explained that not only crosslinked tung oil structure but also PVA structure could block the penetration of oil drops resulting in the lower contact angle change for the oil test.

In the case of the fiberboard results (Table 4.3), the k values of the water tests could be improved when the fiberboard was coated with P85T15 coating materials. The k values dramatically reduced from 0.213 deg/s (for uncoated fiberboard) to the range of 0.053–0.063 deg/s (for coated fiberboards). As seen from the results of paperboard and fiberboard, they showed a similar tendency of the contact angle and the k value. This is because they share the same basic structure which is the cellulose.

All results can be confirmed that these coatings could improve the water resistant property on the surfaces of coated paperboards and fiberboards and had better water and oil affinities with lower absorption rate of those surfaces.

4.3.2 Morphology, contact angles and contact angle change rates of nanosilica containing - PT and PTR coated paperboard and fiberboard

1 g of selected coating materials was coated on white paperboard (8 cm x 5 cm). The coated materials were dried at 50 °C. It was found that all selected coating materials were easy to apply on white paperboard and fiberboard without sagging and other defects. After coating, the coated materials were subsequently conditioned in a desiccator for at least 7 days at ambient conditions before the measurement was made.

The initial contact angle results of water and oil on the coated paperboards are summarized in Table 4.4. As compared with P85T15-r coated paperboard, the initial contact angle of water on P85T15Si-r coated paperboard ascended to the range of 98.2-109.5°. The increase in nanosilica content showed an increase in hydrophobicity of the surface of the paperboards. Although nanosilica has the silanol groups which act as hydrophilic surface, the inclusion of nanosilica provides the roughness on top of the surface, which is known to produce hydrophobicity on natural and artificial surfaces [97].

In term of oil contact angle (Table 4.4), the initial contact angle of oil on P85T15Si-r coated paperboard ascended to the range of 68.1-75.2°. The enhancement of contact angle of oil by P85T15Si-r coated paperboard is because nanosilica has the silanol groups which act as hydrophilic groups. However, the effect of hydrophobicity of coating material was more influence than the effect of hydrophilicity of silanol groups of nanosilica as shown in the results of water and oil contact angles.

Table 4.4 Initial contact angles and contact angle change rates (k) on paperboards coated at 50 °C.

Solvent	Coating materials	Nanosilica content (pph)	Initial contact angle (deg.)	k (deg/s)	R^2
Water	P85T15-r	0	94.8 ± 0.6	0.063 ± 0.003	0.99
		1	98.2 ± 0.9	0.060 ± 0.012	0.96
		3	109.5 ± 4.2	0.057 ± 0.017	0.99
Oil		0	62.8 ± 7.2	0.016 ± 0.001	0.99
		1	68.1 ± 0.5	0.017 ± 0.003	0.99
		3	75.2 ± 3.2	0.023 ± 0.006	0.99

The contact angle change rates (k value) of water and oil on the coated paperboards were measured in order to study the hydrophilic/hydrophobic stability of these modified surfaces as shown in Table 4.4. For water contact angle, the k values of P85T15Si-r coated paperboard changed from P85T15-r coated paperboard (0.063 deg/s) to the range of 0.057 - 0.060 deg/s depending on the nanosilica content. The results show that the k values of water on the P85T15Si-r coated paperboard was lower than that with P85T15-r coating material. This may be suggested that the water drop stabilized on the surface of coated paperboards because of the hydrophobic surface by the surface roughness as discussed above this section. In case of oil contact angle, the increase in the k values of the P85T15Si-r coated paperboard indicated that the oil drop spreaded out on the coated surface because of the hydrophobicity of crosslinked tung oil leading to the absorption of oil drops.

SEM images of the surfaces of P85T15-r and P85T15Si-r coated paperboards are shown in Figure 4.31. As compared with the P85T15-r coated paperboard (Figure 4.31a), the P85T15Si1-r and P85T15Si3-r coated paperboard (Figure 4.31 (b) and (c)) show the roughness surface, whereas the P85T15-r coated paperboard shows the smooth surface. It may be suggested that the larger scale roughness arose from the increase in nanosilica contents. The specific structure and roughness of the surface increased the hydrophobicity of the coated paperboard corresponding to the contact angle results.

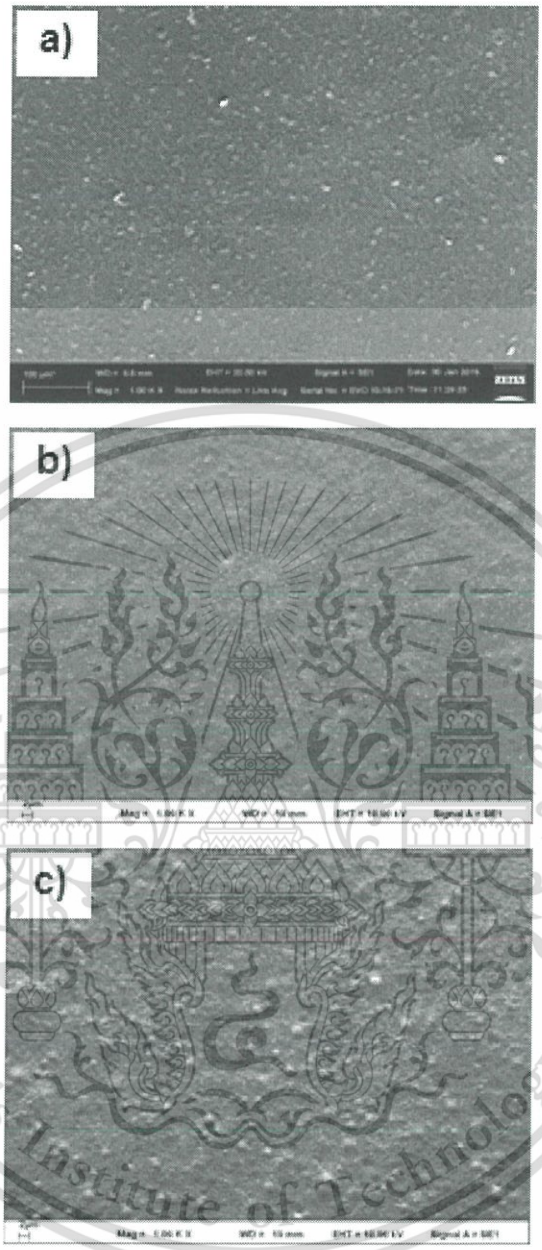

Figure 4.31 SEM micrographs of the coated paperboards with different coating materials magnified 1000 times; (a) P85T15-r, (b) P85T15Si1-r, and (c) P85T15Si3-r.

4.4 Application of PT and PTR as water resistant films

In this part, the water resistant films were prepared. The effects of nanosilica content and photoinitiator on the film properties were studied. In case of nanosilica, the P85T15, P85T15Si1 and P85T15Si3 films (0, 1 and 3 pph of nanosilica in PVA/tung oil films (PT films), respectively) were prepared using thermal and redox catalyst by solution

casting and cured at 50 °C in an oven for 2 h. For studying the photocrosslinking reaction, photoinitiator was added into each PTR mixture including PVA solution and then dried at room temperature to achieve the films. These films were subsequently crosslinked by exposure to light radiation for 10 and 30 min. In comparison, the films without photoinitiator were also prepared. To study the effect of thermal crosslinking reaction, the PVA/tung oil/rubber films (PTR films) cured at 50 °C in an oven for 2 h were also prepared and the results were compared with photocrosslinking reaction. The thickness of the films was controlled at approximately 100 ± 10 μm. These films were subsequently conditioned in a desiccator for at least 7 days at ambient conditions before the measurements were made.

4.4.1 Water resistance testing

4.4.1.1 The effect of nanosilica on the water resistant property of PVA/tung oil/nanosilica films (P85T15Si films)

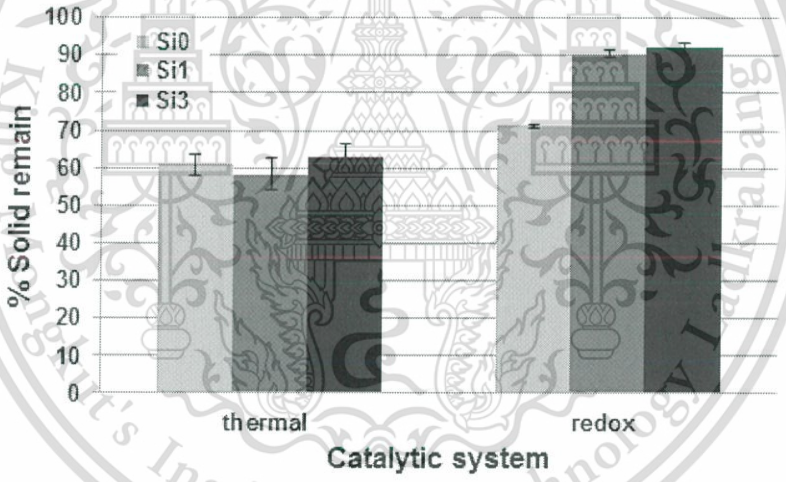

Figure 4.32 The percentage of solid remains of P85T15Si films after immersion in water at 25 °C for 24 h

In this part, water resistance of P85T15Si films was measured in terms of % solid remain as the function of nanosilica content shown in Figure 4.32. Si0, Si1 and Si3 were defined as 0, 1 and 3 pph of nanosilica content in PT films, respectively. It can be seen that the P85T15Si films cured by using redox catalyst at 50 °C (2 h) gained the higher value (~90 %) when the nanosilica was added. It indicated that crosslinking reaction of the double bond of tung oil occurred along with hydrogen bonds among silanol groups on the surface of silica, carbonyl groups of tung oil and hydroxyl groups of PVA in the

P85T15Si-r sheet resulting in better water resistant property, referring to section 4.2.3.1. With the presence of nanosilica, P85T15Si films in redox system gained the increase in the % solid remain up to about 90%, while they were hardly changed in thermal system. It suggested that nanosilica in P85T15Si films with redox system behaved as a catalyst and induced the crosslinking reaction at unsaturated position of tung oil as discussed in section 4.2.3.3. Although P85T15Si3-r film (3 pph of PT sheet in redox system) has the higher value of solid remain (>90%), unfortunately, the original shapes could not be maintained after being soaked in water for 24 h as shown in Figure 4.33.

Figure 4.33 The P85T15Si3-r film crosslinked at 50 °C for 2 h after immersion in water for 24 h

4.4.1.2 The effect of photocrosslinking reaction on the water resistant property of PVA/tung oil/rubber films (PTR films)

For studying the photocrosslinking reaction, PVA and PTR films added with thermal and redox catalysts including photoinitiator were subsequently crosslinked by exposure to light radiation for 10 (p10) and 30 min (p30). In comparison, the films without photoinitiator (np) and the PTR films crosslinked at 50 °C for 2 h (c50) were also prepared. Water resistance of PVA and PTR films was measured in terms of percentage of solid remain shown in Figure 4.34 (a) and (b). It can be seen that the PTR films crosslinked by heat gained relatively low %solid remain values which are similar to those of non-photocrosslinked films because of probably insufficient time for crosslinking at 50 °C (2 h). The % solid remain of PTR films increased when the photoinitiator was added. This was due to an efficiency of the photoinitiator to involve with thermal or redox catalyst in free radical forming. Subsequently, these free radicals abstracted hydrogen at allylic positions and homolytic cleavaged at the double bonds. The network formation was finally occurred among conjugated double bonds of tung oil

and/or double bonds of rubber *via* free radical mechanism. These network structures tied up the molecules together including PVA resulting in the difficulty of the molecules in the photocrosslinked PTR film to move or dissolve into water. As a function of exposure time, the % solid remain of photocrosslinked PTR films improved by prolonging the exposure time which would allow more crosslinking reaction. In terms of tung oil:rubber ratios, the % solid remain of photocrosslinked PTR films raised by increasing tung oil content. It is pointed that the crosslinking reaction occurred at double bonds of tung oil rather than those of rubber. This is because tung oil possesses the conjugated double bonds which their reactivities were relatively high resulting in more crosslinking reaction *via* free radical mechanism than at the non-conjugated double bonds of rubber. The model of network within photocrosslinked PTR films is illustrated in Figure 4.35. As comparing between using thermal and redox catalytic systems, the % solid remains of the PTR films with redox catalyst after exposure to light exhibited slightly higher than those of the films with thermal catalyst at the same condition.

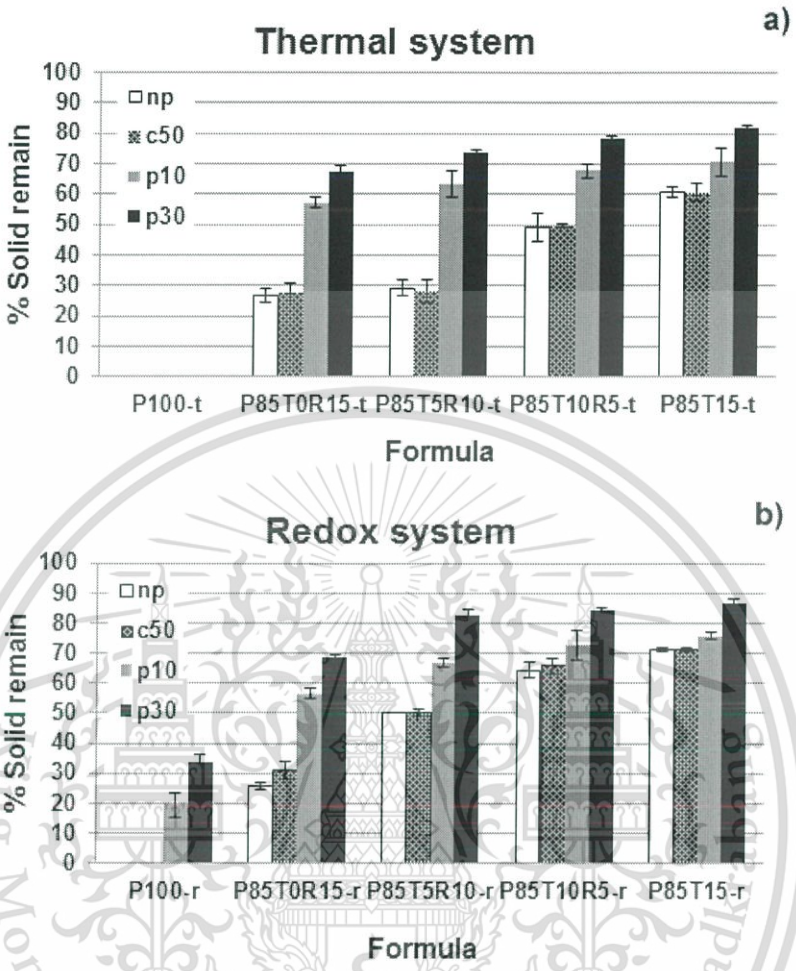

Figure 4.34 The percentage of solid remains of photocrosslinked PTR films after immersion in water at 25 °C for 24 h; (a) thermal system and (b) redox system.

However, the PVA films (without tung oil and rubber) using redox catalyst and exposed to light could gain the % solid remain values but not for the thermal catalyst series. It can be clearly stated that, under light radiation, the crosslinking reaction within PVA itself prefers the cooperation with redox catalytic system to thermal catalytic system. Moreover, it could be seen that crosslinking reaction of the photocrosslinked PTR films would require quite low energy when the photoinitiator was presented with catalytic corporation.

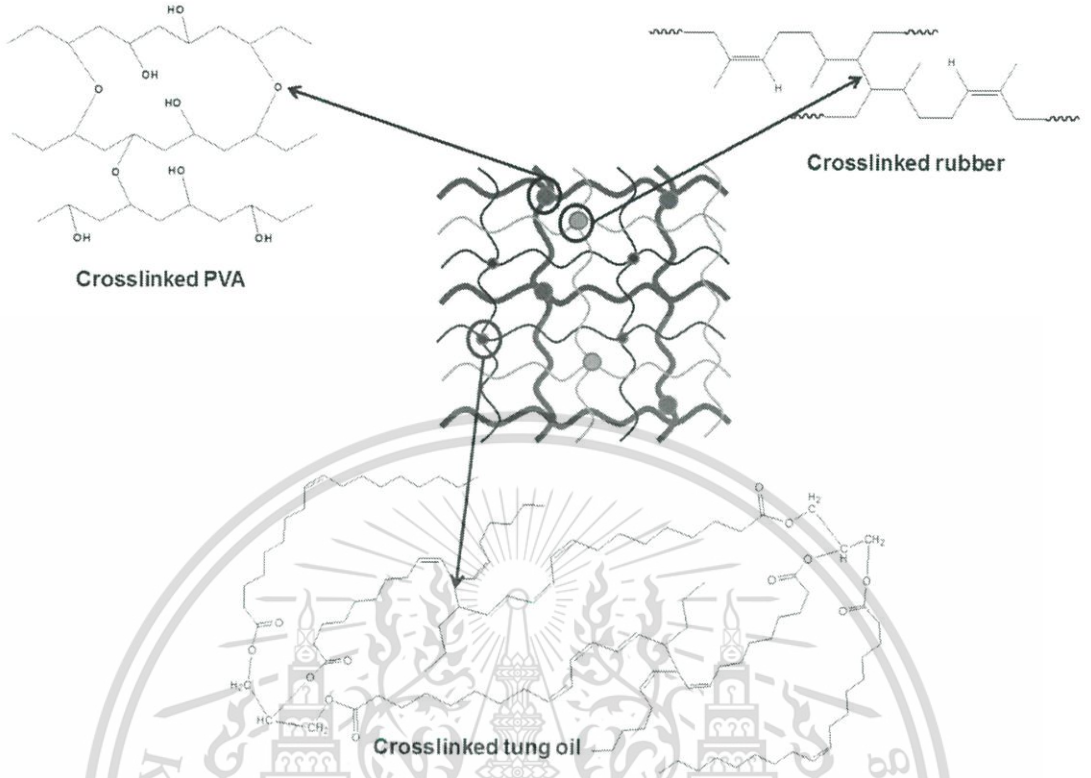

Figure 4.35 Schematic illustration of the photocrosslinked PTR films structures using redox catalyst.

Photographs of P85T0R15-r films after immersion in water for 24 h were showed in Figure 4.36. It was found that some part of P85T0R15-r film crosslinked by heat could dissolve in water as the surrounding water turned to turbidity (see Figure 4.36a) while the P85T0R15-r films prepared by photocrosslinking reaction could form the swelled rectangular shapes (see Figure 4.36b). The swelling degree of the photocrosslinked PTR films could evaluate as exhibited in Figure 4.37. These results decreased when the % solid remain values increased. In general, crosslinking density is one of the factors which can affect to the swelling degree. The presence of tung oil, the longer crosslinking time, the usability of photoinitiator and redox catalyst system caused the reduction of the swelling degree because of the higher crosslinking density within the polymer chains. For example, the PTR films crosslinked by photoinitiator for 30 min (p 30) obtained the slightly lower value of the swelling degree comparing with the films crosslinked by photoinitiator for 10 min (p10). These results suggested that the photocrosslinking reaction nearly completed when the PTR films were crosslinked by light radiation for a long period of time. On the other side, the degradation of the PTR

films might be occurred with increasing the crosslinking time. However, the photocrosslinking reaction for a longer time is not necessary for these PTR films.

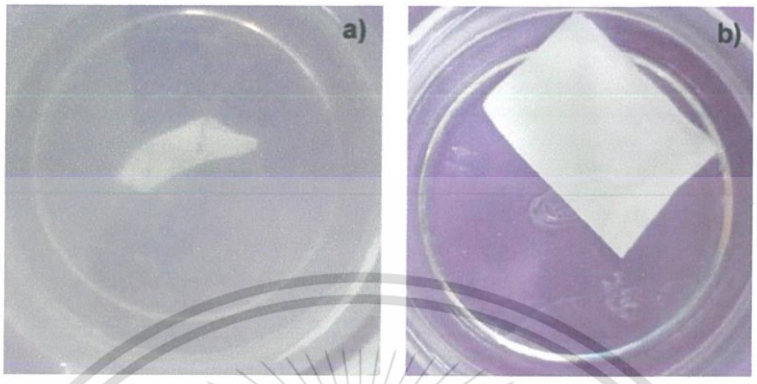

Figure 4.36 The P85T0R15-r films after immersion in water at 25 °C for 24 h; (a) crosslinked at 50 °C for 2 h (c50) and (b) crosslinked by photoinitiator for 10 min (p10).

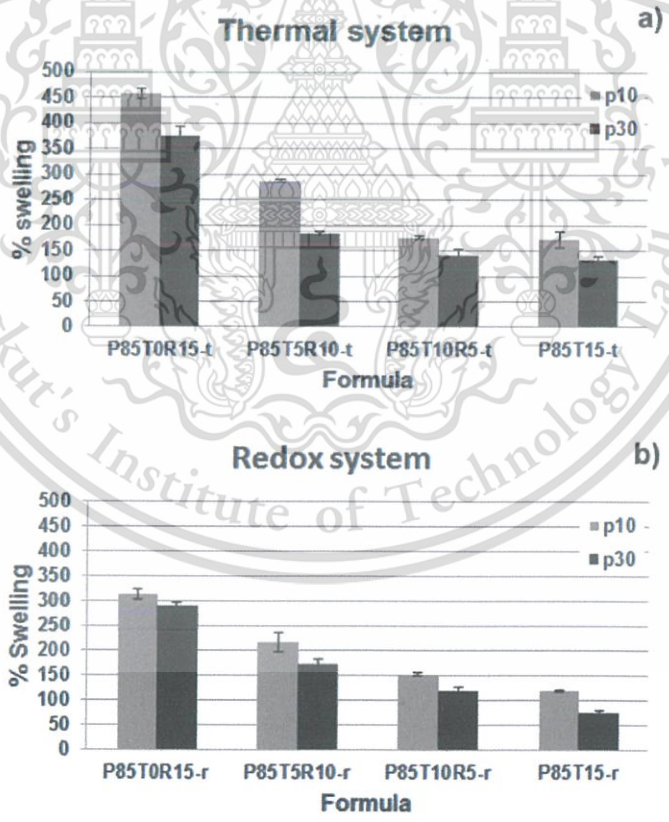

Figure 4.37 The percentage of swelling of photocrosslinked PTR films after immersion in water at 25 °C for 24 h; (a) thermal system and (b) redox system.

Among all results from this part, the PTR films crosslinked by light radiation gained the better properties than the PTR films crosslinked by heat. The next part, the photocrosslinked PTR films were characterized by SEM and FTIR. DMA results and other properties were also discussed.

4.4.2 Fourier Transformed Infrared spectroscopy (FTIR)

The chemical structure of photocrosslinked PTR films was characterized by using FTIR shown in Figure 4.38. An inspection of the -C=**C-H** and -**C=C**-H vibration signals in the structure of rubber and tung oil allowed to follow photocrosslinking reaction. The characteristic peaks corresponding to double bonds of rubber are visible at 3037 cm^{-1} (-C=**C-H** stretching) and 1663 cm^{-1} (-**C=C**-H stretching) while the characteristic peaks corresponding to double bonds of tung oil are visible at 3012 cm^{-1} (-**C=C**-H stretching), 993 cm^{-1} (conjugated trans: trans -C=**C-H** bending) and 966 cm^{-1} (conjugated cis: trans -C=**C-H** bending). The intensities of the peaks related to -**C=C**-H and -C=**C-H** vibration of tung oil and rubber were decreased when the films were exposed to light. Although, almost of the peaks related to -**C=C**-H and -C=**C-H** vibrations of rubber and tung oil still appeared at the similar positions, they decreased in the intensities. It indicated that photoinitiator accelerated thermal and redox catalysts, which subsequently initiated crosslinking reaction at unsaturated positions of rubber and tung oil. In comparison of crosslinking reactivity of double bond presented in rubber and tung oil, the characteristic peaks of tung oil showed sharply decreased, suggesting that the crosslinking reaction at double bond of tung oil was predominant. With using different catalytic systems and prolonging exposure time, the similar intensities of characteristic peaks corresponding to double bonds of rubber and tung oil were obtained meaning that both factors have less effect on the efficiency of photocrosslinking reaction in the PTR films.

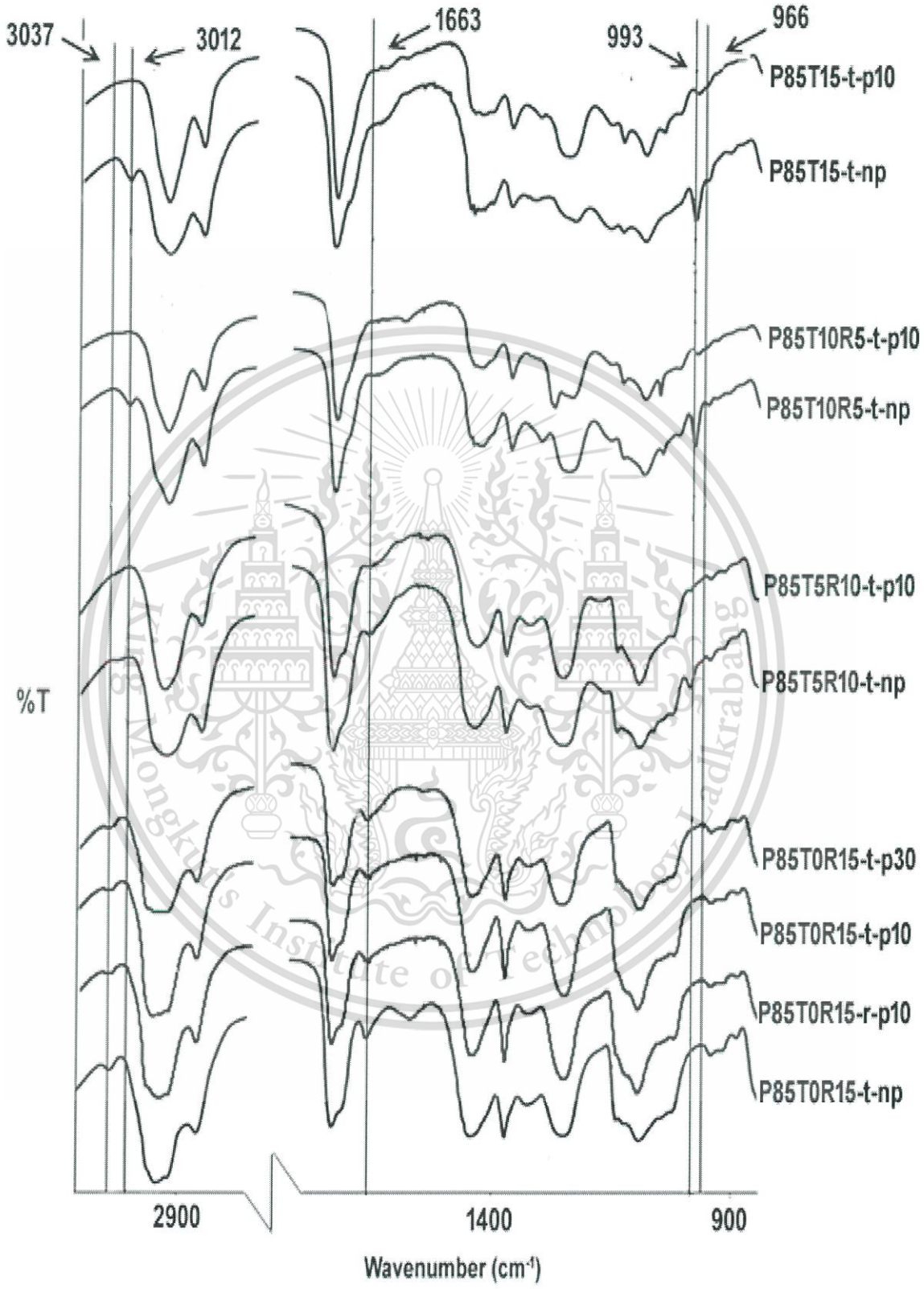

Figure 4.38 FTIR spectra of photocrosslinked PTR films.

4.4.3 Mechanical properties

Tensile strength and Young's modulus of photocrosslinked PTR films are displayed in Figure 4.39 (a) and (b), respectively. It can be seen that, the tensile strengths of photocrosslinked PTR films increased, especially for P85T0R15-r at about 130%. As the same trend, Young's modulus of photocrosslinked PTR films was found to be increase, especially for P85T0R15-r at about 630%. An enhancement in tensile strength and Young's modulus indicated that the formation of network among PVA, rubber and tung oil chains occurred more efficiently in the photocrosslinked PTR films than non-photocrosslinked film, especially in the P85T0R15-r film. Generally, tung oil could be crosslinked itself by oxygen. Therefore the application of light radiation showed less effect on mechanical properties of the tung oil-containing films as seen in case of P85T15-r. Unlike tung oil, the double bonds in rubber chains could not easily reacted when only redox catalyst was applied. It gained relatively less entanglement among all chains in P85T0R15-r film, thus, relatively low mechanical properties. After exposure to light of the film, the occurrence of crosslinking reaction allowed the significant increase of chain entanglement resulting in the sharp enhancement in those mechanical properties. In terms of tung oil:rubber ratios, tensile strength and Young's modulus of photocrosslinked PTR films were found to increase as the tung oil content increase. This is reasonable because the crosslink density in the photocrosslinked PTR films increased with increasing tung oil contents and led to an increase in mechanical properties. In addition, it could be noticed that the presence of photoinitiator could provide feasible economical technique by saving time and energy during crosslinking process.

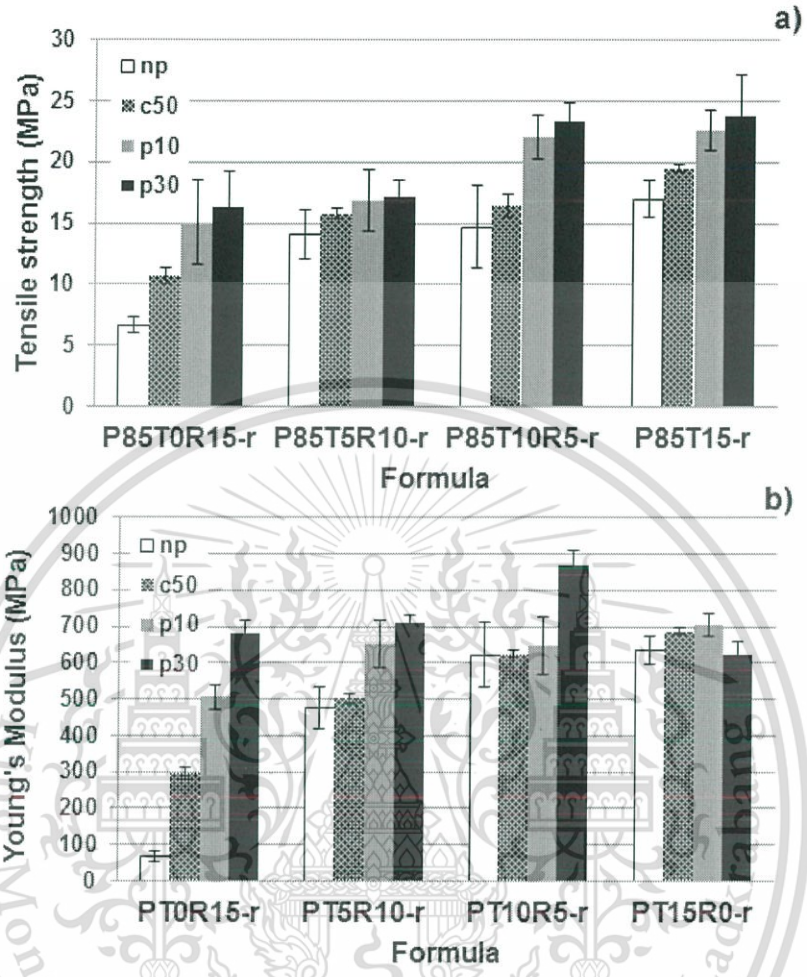

Figure 4.39 Mechanical properties of photocrosslinked PTR films; (a) tensile strength and (b) Young's modulus.

4.4.4 Moisture content

Apart form water resistant properties, moisture content is also necessary for plastic packaging, especially PVA-based materials because of their high water absorption tendency. Moisture content of photocrosslinked PTR films is presented in Figure 4.40. It was found that the equilibrium moisture content in the photocrosslinked PTR films was less than 8%. This can be explained that when tung oil was crosslinked, the crosslinked structures were protected PVA chain from the moisture resulting in the reduction of water absorption. Moreover, the moisture content in the films decreased with increasing tung oil to rubber ratio. This result related to an efficiency of crosslinking reaction through the conjugated double bond of tung oil rather than the double bond of rubber.

However, the use of photoinitiator showed no or less differences in moisture content values comparing to the non-photocrosslinked film.

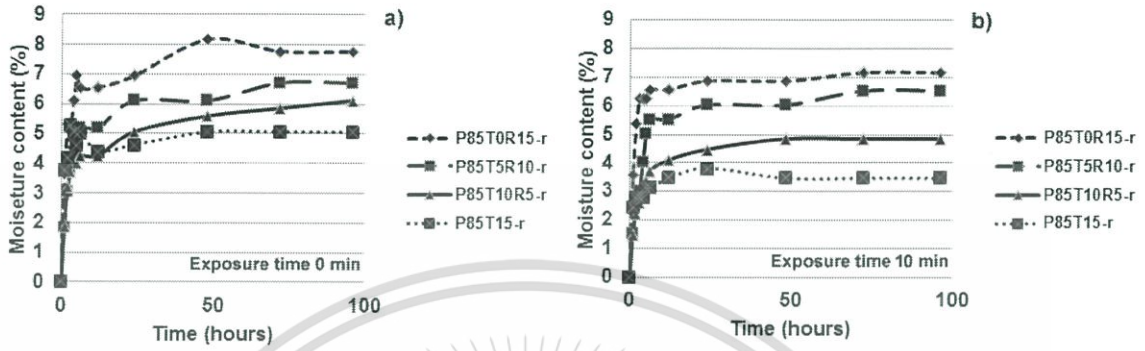

Figure 4.40 The percentage of moisture content of photocrosslinked PTR films at different exposure times; (a) 0 min and (b) 10 min.

4.4.5 Dynamic Mechanical Analysis (DMA)

The tan δ values of photocrosslinked PTR films were determined by DMA, as shown in Figure 4.41 (a)-(d). The T_g peaks of P85T0R15-r-np appeared in two regions, i.e., -69 °C (T_g of rubber) and 87 °C (T_g of PVA). Meanwhile, T_g peaks of P85T15-r-np presented at -1 °C for tung oil and at 86 °C for PVA. As for P85T5R10-r-np and P85T10R5-r-np films, the T_g peaks appeared in three regions as at about -70 °C for rubber, 2 °C for tung oil and 85 °C for PVA. The shift of T_g values of the PTR films were obviously observed when the films were exposed to light. For P85T0R15-r-p10 and P85T15-r-p10 films, only T_g peak of PVA was shifted to higher temperature at about 92 and 100°C, respectively meaning to the more crosslinking reaction among hydroxyl groups of PVA. It seemed that this crosslinking reaction of PVA did not interfere the movement of rubber or tung oil chains as their T_g values did not change. For other films, the raised shifts of T_g of both rubber and PVA occurred. Besides the crosslinked PVA, it could be suggested that PVA and rubber chains were retained within the crosslinked tung oil structures resulting in their cumbersome movement as seen from the shifts of T_g corresponding to the rubber chain in P85T5R10-r-p10 and P85T10R5-r-p10 films. This phenomenon confirmed the efficiency of crosslinking reaction of PVA and tung oil in the PTR films when exposed to light rather than that of the non-photocrosslinked films.

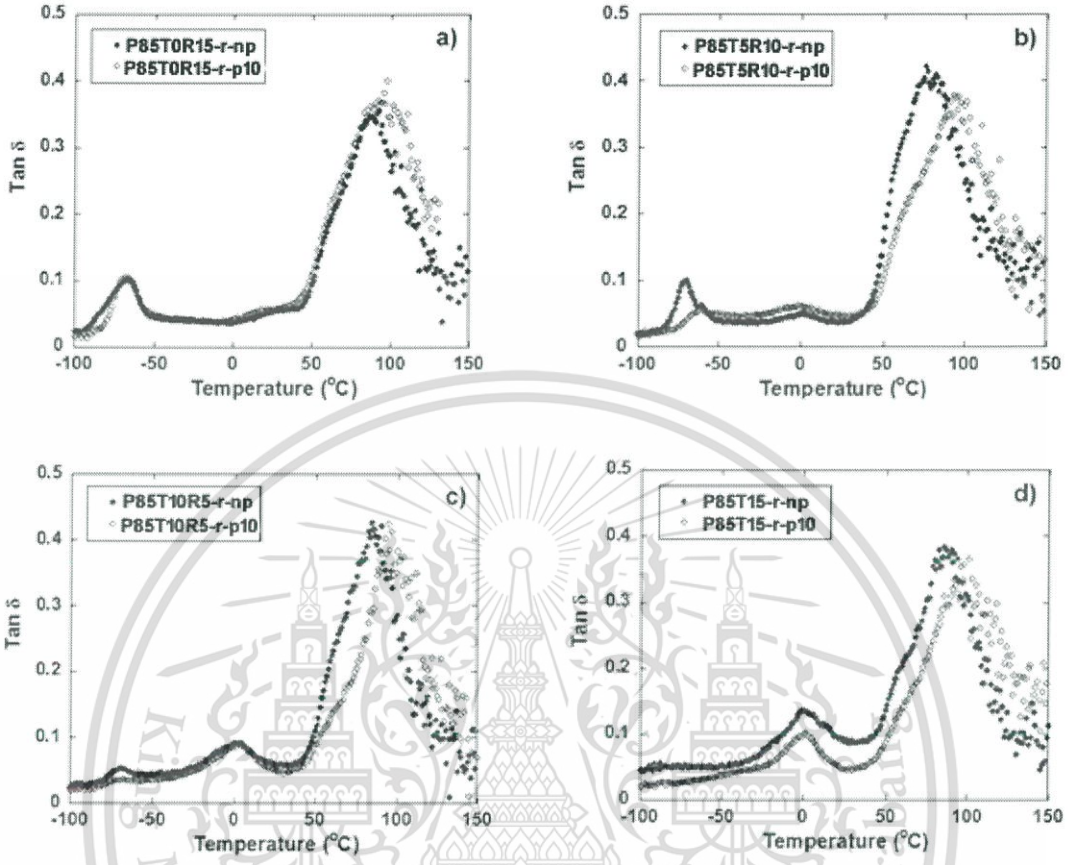

Figure 4.41 Temperature dependence of tan δ values of photocrosslinked PTR films; (a) P85T0R15-r, (b) P85T5R10-r, (c) P85T10R5-r and (d) P85T15-r.

4.4.6 Water vapor permeability (WVP)

Water vapor permeability (WVP) of PVA film and photocrosslinked PTR films was exhibited in Figure 4.42. It was found that WVP value of P85T0R15-r-np was 4.2 x 10^{-4} g/(m·day·kPa) which was lower than that of pure PVA (6.7 x 10^{-4} g/(m·day·kPa)). This is because rubber has excellent moisture barrier properties due to its hydrophobic structure. Therefore, the blend of rubber and PVA could make its film having hydrophobic properties. However, WVP values increased with increasing tung oil content. Although tung oil without proper crosslinking reaction reduced the hydrophilicity of PVA within PTR films, it also increased the void between the interfaces of each part resulting in the increase in the vapor diffusion-path through the film. With the photocrosslinking system, the WVP values of PTR films were in the range of 3.9 x 10^{-4} –4.6 x 10^{-4} g/(m·day·kPa) which are lower than the WVP values of PVA film and non-photocrosslinked PTR films. These results revealed that the WVP values were

significantly affected by light crosslinking. The decrease in the WVP values of photocrosslinked PTR films is because of the increase in crosslink density leading to the tortuosity of the water permeation through the films.

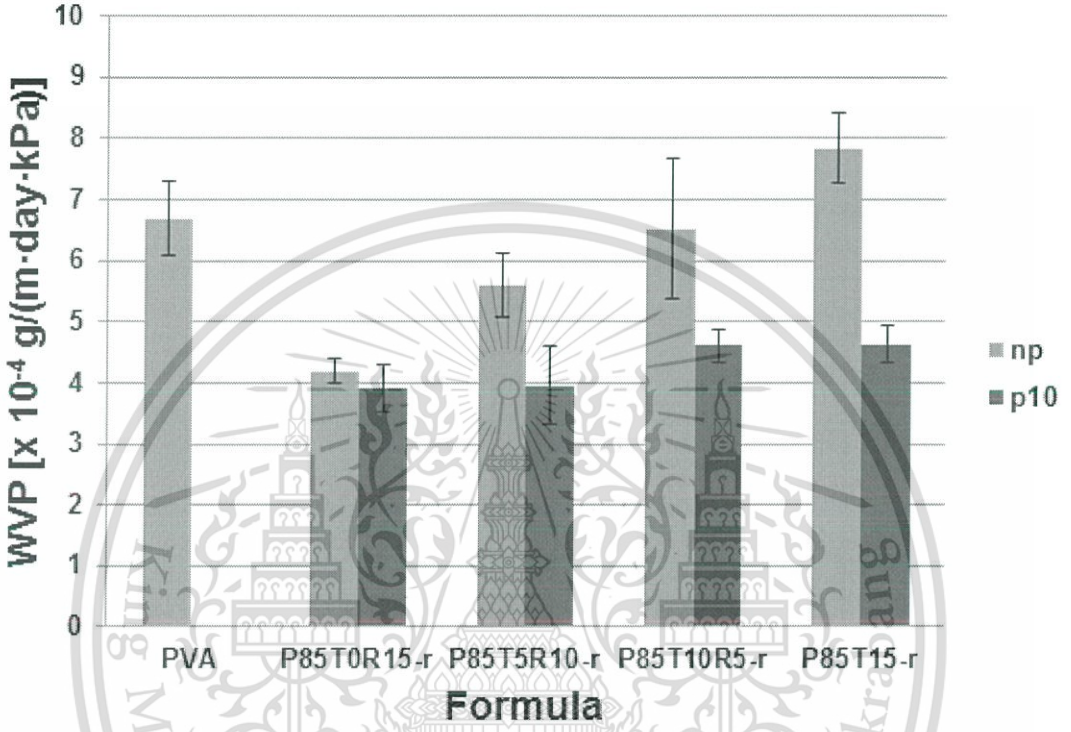

Figure 4.42 Water vapor permeability of PVA and photocrosslinked PTR films.

4.4.7 The initial contact angle

The hydrophilicity of PTR films after crosslinked by light radiation was investigated by static water contact angle. Low contact angle of 29° was obtained for PVA film indicating the hydrophilic nature of PVA. The contact angle values of PTR films reported in Figure 4.43 were significantly higher than that of PVA, pointing that the addition of rubber and tung oil caused an increase in the film surface hydrophobicity. This is due to the hydrophobic nature of rubber and tung oil. Moreover, all of the photocrosslinked PTR films had the water contact angles of over 80°, which were higher values than those of non-photocrosslinked films (<60°). These results pointed to further indication of improved hydrophobic surface properties.

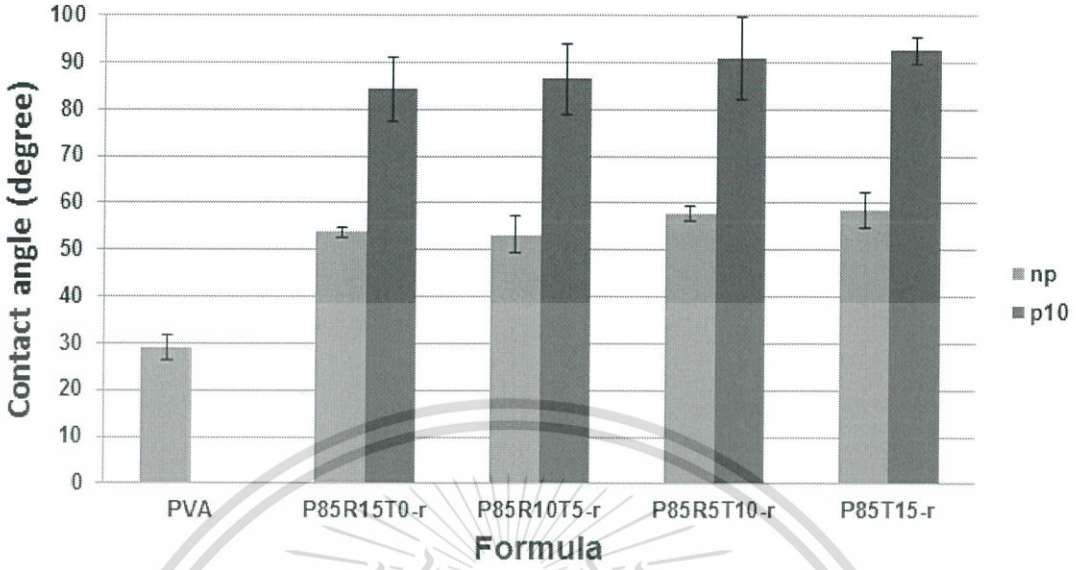

Figure 4.43 The water contact angle of PVA and photocrosslinked PTR films.

Chapter 5
Conclusions and Suggestions

5.1 Conclusions

The modified PVA for coating material and water resistant film applications was successful prepared using tung oil (T) and natural rubber latex (R). The uses of thermal catalyst (KPS) or redox catalyst (KPS and sodium thiosulfate) were applied at various curing temperatures from 30 °C to 80 °C as the initiator for crosslinking reaction. In case of PVA sheets, the crosslinking reaction of PVA itself occurred when using thermal catalyst (≥ 60 °C).

In terms of PVA/tung oil sheets (PT sheet), the % solid remain of the PT sheet showed relatively high values when redox catalyst was applied even at a lower curing temperature (30 °C), while thermal catalyst required higher curing temperatures (>50 °C). FTIR results confirmed the crosslinking reaction of tung oil in PT films.

In case of PVA/tung oil/rubber (PTR), the % solid remain of the PT and PTR sheets showed that water resistance of the sheet was enhanced when tung oil and rubber was incorporated. The tensile results of the PT and PTR sheets revealed the highest tensile strength and the Young's modulus when the relatively high tung oil content was applied. In addition, the synergy of tung oil and rubber in PTR sheets gave better thermal behavior than those using only tung oil or rubber. All results concluded that the increase in crosslink density of PT and PTR structures was obtained by using redox catalytic system, raising curing temperatures or increasing the higher tung oil content.

For the addition of nano-additives, P85T15Si1-r and P85T15Si3-r gained the better thermal and mechanical properties because of the interaction between silanol groups on the surface of silica and hydroxyl groups of PVA along with the crosslinking reaction between the double bonds of tung oil. Their SEM images confirmed that nanosilica dispersed well in PT sheets.

For coating applications, the chosen modified PVA was applied on the paperboard and fiberboard. SEM images of modified PVA coated on paperboards confirmed that the paperboard surfaces were completely covered by PT and PTR film with a thickness of about 72 μm. The water and oil contact angles and absorption rates (k) of the PT and PTR-coated paperboards and fiberboards showed both water and oil

affinities and the decrease in water and oil absorption rates of those substrates by the coating of the PT and PTR-coating substance. In addition, the paperboard coated with nanosilica contained-PT coating materials showed an increase in hydrophobicity of the surface. Among all results, the surface coated by P85T15Si3-r (3 pph of of nanosilica) gained the better hydrophobicity and absorption rates (k).

In case of water resistant film applications, the % solid remain and mechanical properties of the photocrosslinked PTR films showed relatively high values, especially with high tung oil content. Moreover, the results showed that photocrosslinking reaction had more efficient than thermal crosslinking system and the change of tung oil composition would be more effective than prolonging exposure time or varying type of catalysts. All obtained results appeared that the presence of photoinitiator incorporate with redox catalyst improved the properties of PTR films, especially PTR films with the higher rubber content (P85T0R15-r), along with saving time and energy during crosslinking process.

5.2 Suggestions

1. Alternative route to directly modify PVA structure *via* trans-esterification with fatty acids such as oleic acid or linoleic acid for the development of the water resistant property should be studied.

2. The mixing process of the modified PVA and nano-additve should be developed in order to increase the content of nano-additve in the sheet or film.

References

[1] Marin, E., Rojas, J., and Ciro Y. 2012. "A review of polyvinyl alcohol derivatives: Promising materials for pharmaceutical and biomedical applications." **African Journal of Pharmacy and Pharmacology.** 50 : 674–684.

[2] Saxena, S.K. 2014. "Polyvinyl alcohol (PVA)." **Chemical and Technical Assessment (CTA)**, FAO 61st JECFA. 1–3.

[3] Wikipedia. 2013. **Polyvinyl alcohol**. [Online]. Available : http://en.wikipedia.org/wiki/Polyvinyl_alcohol.

[4] Mupalanei, S., and Omidian, H. 2013. "Polyvinyl alcohol in medicine and pharmacy: a perspective." **Journal of Developing Drugs.** 2 : 1-5.

[5] Wang, J., Wang, X., Xu, C., Zhang, M., and Shang, X. 2011. "Preparation of graphene/poly(vinyl alcohol) nanocomposites with enhanced mechanical properties and water resistance." **Polymer International.** 60 : 816-822.

[6] Miranda, T.M.R., Goncalves, A.R., and Amorim, M.T.P. 2001. "Ultraviolet-induced crosslinking of poly(vinyl alcohol) evaluated by principal component analysis of FTIR spectra." **Polymer International.** 50 : 1068-1072.

[7] Shafee, E.E., and Naguib, H.F. 2003. "Water sorption in cross-linked poly(vinyl alcohol) networks." **Polymer.** 44 : 1647-1653.

[8] Bajpai, S.K., Dehariya, P., Saggu, S.P.S. 2015. "Investigation of moisture sorption, permeability, cytotoxicity and drug release behavior of carrageenan/polyvinyl alcohol films." **Journal of Macromolecular Science, Part A: Pure and Applied Chemistry.** 52 : 243-251.

[9] Lim, M., Kwon, H., Kim, D., Seo, J., Han, H., and Khan, S.B. 2015. "Highly-enhanced water resistant and oxygen barrier properties of cross-linked poly(vinyl alcohol) hybrid films for packaging applications." **Progress in Organic Coatings.** 85 : 68-75.

[10] Gaikwad, K.K., Lee, J.Y., and Lee, Y.S. 2016. "Development of polyvinyl alcohol and apple pomace bio-composite film with antioxidant properties for active food packaging application." **Journal of Food Science and Technology.** 53 : 1608-1619.

[11] Kavoosi, G., Nateghpoor, B., Dadfar, S.M.M., and Dadfar, S.M.A. 2014. "Antioxidant, antifungal, water binding, and mechanical properties of poly(vinyl alcohol) film incorporated with essential oil as a potential wound dressing material." **Journal of Applied Polymer Science.** 131 : 1-8.

[12] Nitanan, T., Akkaramongkolporn, P., Rojanarata, T., Ngawhirunpat, T., and Opanasopit P. 2013. ''Neomycin-loaded poly (styrene sulfonic acid-co-maleic acid) (PSSA-MA)/polyvinyl alcohol (PVA) ion exchange nanofibers for wound dressing materials.'' **International Journal of Pharmaceutics.** 448(1) : 71–78.

[13] Sharma, H.O., Alam, M., Riaz, U., Ahmad, S., and Ashraf, S.M. 2007. ''Miscibility studies of polyesteramides of linseed oil and dehydrated castor oil with poly(vinyl alcohol).'' **International Journal of Polymeric Materials and Polymeric Biomaterials.** 56(4) : 437–451.

[14] Minelli, M., Angelis, M.G.D., Doghieri, F., Rocchetti, M., and Montenero, A. 2010. "Barrier properties of organic–inorganic hybrid coatings based on polyvinyl alcohol with improved water resistance." **Polymer Engineering & Science.** 50(1) : 144–153.

[15] Liu, F., Wang, S., Zhang, M., Ma, M., Wang, C., and Li, J. 2013. "Improvement of mechanical robustness of the superhydrophobic wood surface by coating PVA/SiO_2 composite polymer." **Applied Surface Science.** 280 : 686– 692.

[16] Li, J., Suo, J., and Deng, R. 2010. "Structure, mechanical, and swelling behaviors of poly(vinyl alcohol)/SiO_2." **Journal of Reinforced Plastics and Composites.** 29(4) : 1686– 1692.

[17] Shi, B., Wideman, G., and Wang, J.H. 2012. "Improving the processability of water-soluble films based on filled thermoplastic polyvinyl alcohol." **International Polymer Processing.** 27(2) : 231-236.

[18] Zheng, G.Q., Li, X.D., Wang, X.M., Ma, J.F., and Gu, Z.W. 2008. "Structural characteristics of poly(vinyl alcohol)-calcium carbonate composites prepared by sequential method." **Advances in Applied Ceramics.** 107(1) : 46-51.

[19] Wikipedia. 2013. **Natural rubber.** [Online].Available : http://en.wikipedia.org/wiki/Natural_rubber.

[20] Simchareona, W., Amnuaikita, T., Boonmea, P., Taweepredab, W., and Pichayakorna, W. 2012. "Characterization of natural rubber latex film containing various enhancers." **Procedia Chemistry.** 4 : 308-312.

[21] Cacioli, P. 1997. "Introduction to latex and the rubber Industry." **Revue Française d'Allergologie et d'Immunologie Clinique.** 37 : 1173-1176.

[22] Riyajan, S.A., Chaiponban, S., and Tanbumrung, K. 2009. "Investigation of the preparation and physical properties of a novel semi-interpenetrating polymer network based on epoxised NR and PVA using maleic acid as the crosslinking agent" **Chemical Engineering Journal.** 153 : 199–205.

[23] Derksen, J.T.P., Cuperus, F.P., and Kolster, P. 1996. ''Renewable resources in coatings technology: a Review.'' **Progress in Organic Coatings.** 27(1–4) : 45–53.

[24] Derksen, J.T.P., Cuperus, F.P., and Kolster, P. 1995. ''Paints and coatings from renewable resources.'' **Industrial Crops and Products.** 3(4) : 225–236.

[25] Oyman, Z.O., Ming, W., and van der Linde, R. 2005. "Oxidation of drying oils containing non-conjugated and conjugated double bonds catalyzed by a cobalt catalyst." **Progress in Organic Coatings.** 54 : 198–204.

[26] Yang, X., Zhang, S., and Li, W. 2015. ''The performance of biodegradable tung oil coatings.'' **Progress in Organic Coatings.** 85(1) : 216–220.

[27] Wei, S., Pintus, V., Pitthard, V., Schreiner, M., and Song, G. 2011. ''Analytical characterization of lacquer objects excavated from a Chu Tomb in China.'' **Journal of Archaeological Science.** 38(10) : 2667–2674.

[28] Jianprasert, A., Monvisade, P., and Yamaguchi, M. 2016. "Surface improvement on water and oil affinities and absorption rate of PVA/Tung oil-coated paperboard and fiberboard." **Journal of Coatings Technology and Research.** 13 : 345-354.

[29] Jianprasert, A., Monvisade, P., and Yamaguchi, M. 2017. "Study on crosslinked structure and thermal properties of polymer networks based on tung oil and PVA with different catalytic systems" **Macromolecular Symposia.** 372 : 108–114.

[30] Ma, J.W., Cunningham, M.F., McAuley, K.B., Keoshkerian, B., and Georges, M. 2003. ''Nitroxide mediated living radical polymerization of styrene in miniemulsion—modelling persulfate-initiated systems.'' **Chemical Engineering Science.** 58(7) : 1177–1190.

[31] Das, D., Das, R., Mandal, J., Ghosh, A., and Pal, S. 2014. ''Dextrin crosslinked with poly(lactic acid): a novel hydrogel for controlled drug release application.'' **Journal of Applied Polymer Science.** 131(7) : 40039–40050.

[32] Bai, W., Zhang, L., Bai, R., and Zhang, G. 2008. ''A very useful redox initiator for aqueous RAFT polymerization of N-Isopropylacrylamide and acrylamide at room temperature.'' **Macromolecular Rapid Communications.** 29(7) : 562–566.

[33] Lv, P., Bin, Y., Li, Y., Chen, R., Wang, X., and Zhao, B. 2009. "Studies on graft copolymerization of chitosan with acrylonitrile by the redox system." **Polymer.** 50 : 5675–5680.

[34] Bach, T., and Hehn, J.P. 2011. "Photochemical reactions as key steps in natural product synthesis" **Angewandte Chemie International Edition.** 50 : 1000 – 1045.

[35] Schmedlen, R.H., Masters, K.S., and West, J.L. 2002. "Photocrosslinkable polyvinyl alcohol hydrogels that can be modified with cell adhesion peptides for use in tissue engineering." **Biomaterials.** 23 : 4325–4332.

[36] Holik, H. 2006. **Handbook of Paper and Board.** 6th ed. Germany : Wiley.

[37] Bardak, S., Sarı, B., Nemli, G., Kırcı, H., and Baharoğlu, M. 2011. ''The effect of decor paper properties and adhesive type on some properties of particleboard.'' **International Journal of Adhesion & Adhesives.** 31(6) : 412–415.

[38] Nassar, M.A., and Youssef, A.M. 2012. ''Mechanical and antibacterial properties of recycled carton paper coated by PS/Ag nanocomposites for packaging.'' **Carbohydrate Polymers.** 89(1) : 269–274.

[39] Chen, W., Wang, X., Tao, Q., Wang, J., Zheng, Z., and Wang, X. 2013. ''Lotus-like paper/paperboard packaging prepared with nano-modified overprint varnish.'' **Applied Surface Science.** 266 : 319–325.

[40] Samyn, P., Deconinck, M., Schoukens, G., Stanssens, D., Vonck, L., and Van den Abbeeleb, H. 2010. ''Modifications of paper and paperboard surfaces with a nanostructured polymer coating.'' **Progress in Organic Coatings.** 69(4) : 442–454.

[41] Du, Y., Zang, Y-H., and Sun, J. 2014. ''The effects of water soluble polymers on paper coating consolidation.'' **Progress in Organic Coatings.** 77(4) : 908–912.

[42] Aloui, H., Khwaldiaa, K., Slama, M.B., and Hamdi, M. 2011. ''Effect of glycerol and coating weight on functional properties of biopolymer-coated paper.'' **Carbohydrate Polymers.** 86(2) : 1063–1072.

[43] Khwaldia, K., Arab-Tehrany, E., and Desobry, S. 2010. ''Biopolymer coatings on paper packaging materials.'' **Comprehensive Reviews in Food Science and Food Safety.** 9(1) : 82–91.

[44] Li, X., Li, Y., Zhong, Z., Wang, D., Ratto, J.A., Sheng, K., and Sun, X.S. 2009. ''Mechanical and water soaking properties of medium density fiberboard with wood fiber and soybean protein adhesive.'' **Bioresource Technology.** 100(14) : 3556–3562.

[45] Rhima, J-W., Leeb, J-H., and Hong, S-I. 2006. ''Water resistance and mechanical properties of biopolymer (alginate and soy protein) coated paperboards.'' **LWT- Food Science and Technology.** 39(7) : 806–813.

[46] Aulin, C., and Ström, G. 2013. ''Multilayered alkyd resin/nanocellulose coatings for use in renewable packaging solutions with a high level of moisture resistance.'' **Industrial & Engineering Chemistry Research.** 52(7) : 2582–2589.

[47] Selke, S.E.M., Culter, J.D., and Hernandez, R.J. 2004. **Plastics packaging, in: Properties, Processing, Applications and Regulations.** 2nd ed. Munich : Hanser Publishers.

[48] Haitao, C., Ying, L., Xia, G., Weili, L., and Yunjun, L. 2015. "Antioxidant BHT modelling migration from food packaging of high density polyethylene plastics into the food simulant." **Advance Journal of Food Science and Technology**. 9 : 534-538.

[49] Shemesh, R., Krepker, M., Goldman, D., Danin-Poleg, Y., Kashi, Y., Nitzan, N., Vaxman, A., and Segal, E. 2015. "Antibacterial and antifungal LDPE films for active packaging" Polymers advanced technologies. 26 : 110–116.

[50] Pechyen, C., and Ummartyotin, S. 2016. "Development of isotactic polypropylene and stearic acid-modified calcium carbonate composite: a promising material for microwavable packaging." **Polymer Bulletin.** DOI 10.1007/s00289-016-1722-3.

[51] Lloretm, E., Picouet, P.A., Trbojevich, R., and Fernandez, A. 2016. "Colour stability of cooked ham packed under modified atmospheres in polyamide nanocomposite blends." **LWT -Food Science and Technology.** 66 : 582-589.

[52] Galikhanov, M.F., Guzhova, A.A., Efremova, A.A., and Nazmieva, A.I. 2015. "Effect of aluminum oxide coating on structural, barrier and electret properties of polyethylene terephthalate films." **IEEE Transactions on Dielectrics and Electrical Insulation.** 22 : 1492-1496.

[53] Kim, S.W., and Cha, S.J. 2014. "Thermal, mechanical, and gas barrier properties of ethylene–vinyl alcohol copolymer-based nanocomposites for food packaging films: effects of nanoclay loading." **Journal of applied polymer science.** 131 : 1-8.

[54] Madhu, G., Bhunia, H., and Bajpai, P.K. 2014. "Blends of high density polyethylene and poly(L-lactic acid): mechanical and thermal properties." **Polymer Engineering and Science.** 54 : 2155–2160.

[55] Jain, K., Madhu, G., Bhunia, H., Bajpai, P.K., Nando, G.B., and Reddy, M.S. 2015. "Physicomechanical characterization and biodegradability behavior of polypropylene/poly(Llactide) polymer blends." **Journal of Polymer Engineering.** 35 : 407-415.

[56] Sunilkumar, M., Francis, T., Thachil, E.T., and Sujith, A. 2012. "Low density polyethylene– chitosan composites: a study based on biodegradation." **Chemical Engineering Journal.** 204-206 : 114–124.

[57] Ozakia, S.K., Monteirob, M.B.B., Yanoc, H., Imamurac, Y., and Souza, M.F. 2005. "Biodegradable composites from waste wood and poly(vinyl alcohol)" **Polymer Degradation and Stability.** 87 : 293–299.

[58] Liu, X., Zhang, X., Long, K., Zhu, X., Yang, J., Wu, Y., Luo, S., and Yang, S. 2012. "PVA wood adhesive modified with sodium silicate cross-linked copolymer" **International Conference on Biobase Material Science and Engineering (BMSE).** 108-1110.

[59] Imam, S.H., Gondon, S.H., Mao, L., and Chen, L. 2001. "Environmentally friendly wood adhesive form a renewable plant polymer:characteristics and optimization" **Polymer Degradation and Stability**. 73 : 529-533.

[60] Krumova, M., LÓpez, D., Benavente, R., Mijangos, C., and Pereña, J.M. 2000. "Effect of crosslinking on the mechanical and thermal properties of poly(vinyl alcohol)" **Polymer.** 41 : 9265–9272.

[61] Wikipedia. 2013. **Tung oil.** [Online]. Available : http://en.wikipedia.org/wiki/Tung_oil.

[62] Master Garden Products. 2013. **Tung oil.** [Online]. Available : http://www.mastergardenproducts.com/tungoil.htm.

[63] Gui-zhuan, X., Bai-liang, Z., Sheng-yong, L., and Jim-zhi, Y. 2006. "Study on immobilized lipase catalyzed transesterification reaction of tung Oil." **Agricultural Sciences in China.** 11 : 859-864.

[64] Chumchuen, W. 2010. "Development of formaldehyde-free wood adhesive from Poly (vinyl alcohol) Modified with tung oil." Polymer Technology programs, Faculty of science, King Mongkut's Institute of Technology Ladkrabang. [Thai version]

[65] Tongsuk R., Ternwanna N. and Pulsawang P. 2009. "Preparation of formaldehyde-free wood adhesive using PVA and tung oil" Chemistry programs, Faculty of science, King Mongkut's Institute of Technology Ladkrabang. [Thai version]

[66] Lakkanapornwisit P. 2012. "Effect of silica on mechanical properties of particle board using formaldehyde free adhesive" Polymer Technology programs, Faculty of science, King Mongkut's Institute of Technology Ladkrabang. [Thai version]

[67] Robert, O. 2000. **Polymer Science and Technology.** New York : CRC Press.

[68] Shaikh, A.S., and Gohil, C.J. 2016. "Photochemical reaction: A lightning phenomena." **International Journal of Pharmaceutical Chemistry and Analysis.** 3(3) : 104-109.

[69] Wikipedia. 2013. **Potassium persulfate.** [Online]. Available : http://en.wikipedia.org/wiki/Potassium_persulfate.

[70] Wikipedia. 2013. **Elbs persulfate oxidation.** [Online]. Available : http://en.wikipedia.org/wiki/Elbs_persulfate_oxidation.

[71] Wikipedia. 2013. **Sodium thiosulfate.** [Online]. Available : http://en.wikipedia.org/wiki/Sodium_thiosulfate.

[72] Riyajan, S.A., Sasithornsonti, Y., and Phinyocheep, P. "Effect of potassium persulphate on the physical property of PVA" Proceedings of the 7th IMT-GT UNINET and the 3rd International PSU-UNS Conferences on Bioscience.

[73] Işıklan N. and Kurşun F. 2013. "Synthesis and characterization of graft copolymer of sodium alginate and poly(itaconic acid) by the redox system." **Polymer Bulletin.** 70 : 1065–1084.

[74] Bai, H., Li, Y., Wang, W., Chen, G., Rojas, O.J., Dong, W., and Liu, X. 2015. "Interpenetrated polymer networks in composites with poly(vinyl alcohol), micro- and nano-fibrillated cellulose (M/NFC) and polyHEMA to develop packaging materials." **Cellulose.** 22 : 3877–3894.

[75] Wikipedia. 2013. **Silicon dioxide.** [Online]. Available : http://en.wikipedia.org/wiki/Silicon_dioxide.

[76] Wikipedia. 2013. **Calcium carbonate.** [Online]. Available : http://en.wikipedia.org/wiki/Calcium_carbonate.

[77] Wikipedia. 2013. **Zinc oxide.** [Online]. Available : http://en.wikipedia.org/wiki/Zinc_oxide.

[78] Sawai, J., Yamamoto, O., Ozkal, B., and Nakagawa, Z. 2007. "Antibacterial activity of carbon-coated zinc oxide particles." **Biocontrol Science.** 12(1) : 15-20.

[79] Kale, G., Kijchavengkul, T., Auras, R., Rubino, M., Selke, S.E., and Singh, S.P. 2007. "Compostability of bioplastic packaging materials: an overview." **Macromolecular Bioscience.** 7 : 255-277.

[80] Kirwan, M. J., and Strawbridge, J. W. 2003. "Plastics in food packaging" **Food Packaging Technology.** 174-240.

[81] Bohlmann, G. M. 2004. "Biodegradable packaging life-cycle assessment." **American Institute of Chemical Engineers.** 23 : 253–357.

[82] Tracton, A.A. 2006. **Coatings Technology Handbook.** New York : Taylor & Francis Group.

[83] Holik, H. 2006. **Handbook of Paper and Board.** 6th ed. Germany : Wiley.

[84] Rhima, J.W., Leeb, J.H., and Hong, S.I. 2006. "Water resistance and mechanical properties of biopolymer (alginate and soy protein) coated paperboards." **LWT.** 39 : 806–813.

[85] Huang, H-D., Ren, P-G., Chen, J., Zhang, W-Q., Ji, Xu., and Li, Z-M. 2012. "High barrier graphene oxide nanosheet/poly(vinyl alcohol) nanocomposite films." **Journal of Membrane Science.** 409– 410 : 156– 163.

[86] Musetti, A., Paderni, K., Fabbri, P., Pulvirenti, A., Al-Moghazy, M., and Fava, P. 2014. "Poly(vinyl alcohol)-based film potentially suitable for antimicrobial packaging applications" **Journal of Food Science.** 79 : E577- E582.

[87] Jansson, A., and Järnström, L. 2006. "Barrier and film properties of plastisol coatings, a water free coating application based on mixtures of starch, poly(vinyl alcohol) and poly(alkyl methacrylate)." **Nordic Pulp & Paper Research Journal.** 21 (5) : 690-696.

[88] Miller, G.D., Jones, R.B., and Boylan, J.R. 1998. "Polyvinyl alcohol-a specialty polymer for paper and paperboard." **TAPPI Notes.** 14.

[89] ASTM D 882 Committee on standard. 2012. "Standard Test Method for Tensile Properties of Thin Plastic Sheeting." Philadephia : American Society for Testing and Materials.

[90] ASTM D 4092 Committee on standard. 2013. "Standard Terminology for Plastics: Dynamic Mechanical Properties." Philadephia : American Society for Testing and Materials.

[91] ASTM E96/E96M Committee on standard. 2015. "Standard Test Methods for Water Vapor Transmission of Materials." Philadephia : American Society for Testing and Materials.

[92] ASTM D 7334 Committee on standard. 2013. "Standard Practice for Surface Wettability of Coatings, Substrates and Pigments by Advancing Contact Angle Measurement." Philadephia : American Society for Testing and Materials.

[93] Schönemann, A., and Edwards, H.G.M. 2011. ''Raman and FTIR microspectroscopic study of the alteration of Chinese tung oil and related drying oils during ageing.'' **Analytical and Bioanalytical Chemistry.** 400(4) : 1173–1180.

[94] Agostini, D.L.S., Constantino, C.J.L., and Job A.E. 2008. "Thermal degradation of both latex and latex cast films forming membranes : combined TG/FTIR investigation." **Journal of Thermal Analysis and Calorimetry.** 91(3) : 703–707.

[95] Riyajan, S.A., and Sasithornsonti, Y. 2013. "Chemical Crosslink Degradable PVA Aqueous Solution by Potassium Persulphate." Journal of Polymers and the Environment. 21 : 472-478.

[96] Rakotonirainy, A.M., and Padua, G.W. 2001. "Effects of lamination and coating with drying oils on tensile and barrier properties of zein films." **Journal of Agricultural and Food Chemistry.** 49 : 2860-2863.

[97] Teisala, H., Tuominen, M., Aromaa, M., Mäkelä, J.M., Stepien, M., Saarinen, J.J., Toivakka, M., and Kuusipalo, J. 2010. "Development of superhydrophobic coating on paperboard surface using the Liquid Flame Spray." **Surface & Coatings Technology.** 205 : 436–445.

Appendix

Appendix A : Water resistant property

Table A-1 % solid remain of modified PVA sheets.

Formula	Curing temperatures					
	Room temp.	40 °C	50 °C	60 °C	70 °C	80 °C
P100	0	0	0	0	0	0
P100-t	0	0	0	54.4±1.6	57.9±2.2	81.3±0.1
P100-r	0	0	0	0	0	34.8±3.5
P95T5	0.4±0.1	0.4±0.1	0.8±0.1	1.0±0.4	4.13±0.11	6.0±0.2
P95T5-t	0.9±0.1	1.1±0.2	1.3±0.4	78.6±0.4	84.7±0.6	89.6±0.4
P95T5-r	1.3±0.3	5.4±1.4	11.4±0.3	26.6±0.1	32.0±0.35	48.8±0.5
P90T10	2.2±0.1	3.4±0.6	6.8±0.5	11.4±1.4	15.6±0.4	19.2±0.6
P90T10-t	5.4±4.9	7.3±0.5	8.0±0.6	87.8±1.0	92.1±0.1	93.1±0.3
P90T10-r	31.4±0.3	38.4±1.3	39.8±0.3	46.3±0.3	83.4±0.2	91.1±0.1
P85T15	15.4±4.9	22.1±1.5	22.9±1.4	29.8±0.9	43.5±5.5	52.3±1.9
P85T15-t	67.1±3.5	65.7±1.4	90.9±3.6	96.6±2.2	96.4±1.9	94.9±1.7
P85T15-r	85.2±3.8	85.1±4.1	91.1±1.7	94.7±1.9	96.9±2.3	93.1±1.7
P85T10R5	32.5±5.2	35.7±2.2	45.9±1.1	51.6±1.0	54.5±2.5	38.5±2.1
P85T10R5-t	48.7±5.9	50.4±5.2	54.8±2.5	93.5±1.3	94.7±1.3	92.8±2.0
P85T10R5-r	85.6±0.5	83.7±1.1	90.1±2.8	87.2±4.8	89.6±2.9	89.7±2.4
P85T5R10	28.0±0.7	33.5±2.0	33.6±3.3	45.4±3.6	48.2±0.4	37.9±4.3
P85T5R10-t	33.7±2.1	37.3±1.0	40.4±3.9	55.5±0.9	96.1±2.2	94.7±2.1
P85T5R10-r	79.1±2.4	80.6±0.2	79.9±7.1	87.3±3.7	82.9±6.4	80.0±0.4
P85T0R15	7.2±1.3	18.5±0.6	25.8±3.9	36.4±1.9	37.6±1.9	20.4±3.6
P85T0R15-t	25.6±3.0	27.4±1.5	29.1±8.1	41.4±2.7	56.3±2.6	72.3±6.7
P85T0R15-r	23.8±2.0	36.9±1.0	37.9±4.6	41.3±4.1	46.3±7.7	32.1±2.9

Table A-1 (Cont.)

Formula	Curing temperatures			
	40 °C	50 °C	60 °C	70 °C
P85T15Si1-t	82.7±1.9	89.7±1.0	94.4±1.2	92.6±0.3
P85T15Si1-r	91.3±0.5	89.2±1.2	87.8±0.6	84.8±3.0
P85T15Si2-t	58.1±1.4	88.2±4.0	94.6±1.0	93.0±0.3
P85T15Si2-r	58.9±1.3	77.7±7.9	91.3±0.9	85.7±3.3
P85T15Si3-t	64.9±5.7	94.5±1.0	94.1±1.5	93.5±0.2
P85T15Si3-r	69.2±2.9	85.4±4.0	89.6±2.7	89.0±1.7
P85T15Ca1-t	34.5±1.1	48.6±1.1	75.8±3.0	81.5±0.3
P85T15Ca1-r	52.1±0.2	54.7±0.4	60.3±2.2	56.3±0.5
P85T15Ca2-t	36.4±0.2	52.6±0.3	59.0±1.8	65.7±5.9
P85T15Ca2-r	53.6±0.1	54.1±0.2	55.6±0.5	61.6±4.7
P85T15Ca3-t	44.8±2.9	60.2±0.8	59.2±1.1	63.7±4.2
P85T15Ca3-r	54.3±0.2	56.1±0.4	56.9±0.7	57.3±1.2
P85T15Zn1-t	22.4±0.7	27.2±3.2	27.4±5.9	36.3±2.5
P85T15Zn1-r	41.1±0.8	44.4±2.2	56.1±0.8	58.3±5.3
P85T15Zn2-t	34.9±3.7	49.6±3.8	58.5±2.5	56.6±2.8
P85T15Zn2-r	53.9±1.7	53.0±2.1	58.6±2.3	55.7±1.8
P85T15Zn3-t	49.4±2.3	52.7±0.9	54.6±3.2	62.6±0.9
P85T15Zn3-r	57.7±0.4	59.1±0.5	58.4±0.1	59.6±0.5
P85T0R15Si1-t	42.0±0.3	43.5±0.7	43.6±1.3	N/A
P85T0R15Si1-r	43.8±0.8	43.2±1.4	42.4±0.4	
P85T5R10Si1-t	39.2±1.2	57.4±4.2	88.0±3.3	
P85T5R10Si1-r	47.8±2.9	85.2±4.8	88.9±0.2	
P85T10R5Si1-t	61.3±5.0	59.7±1.3	88.6±3.4	
P85T10R5Si1-r	91.1±0.2	90.6±0.4	91.9±0.7	

Table A-1 (Cont.)

Formula	Curing temperature
	50 °C
P85T15Si5-r	77.6±2.5
P85T15Si7-r	71.6±0.3
P90T10Si1-r	50.7±0.6
P90T10Si3-r	58.3±4.9
P90T10Si5-r	60.9±1.7
P90T10Si7-r	62.7±0.9
P95T5Si1-r	26.2±0.5
P95T5Si3-r	37.7±0.2
P95T5Si5-r	48.1±1.5
P95T5Si7-r	47.3±0.8

Table A-2 % solid remain of modified PVA films.

Formula	Curing conditions			
	Room temp.	Cured at 50 °C	Exposure time 10 min	Exposure time 30 min
P100-t	0	0	0	0
P100-r	0	0	19.4± 4.3	33.8± 2.4
P85T0R15-t	26.6± 2.3	28.0± 2.9	57.2± 1.6	67.2± 2.3
P85T0R15-r	25.8± 0.9	30.9± 3.1	56.7± 1.9	68.9± 0.8
P85T5R10-t	29.1± 2.6	28.3± 3.7	63.3± 4.1	73.9± 0.5
P85T5R10-r	50.3± 0.1	50.3± 1.2	66.9± 1.4	82.5± 2.1
P85T10R5-t	49.4± 4.6	49.7± 0.5	67.7± 2.4	78.4± 0.8
P85T10R5-r	64.5± 2.6	65.6± 2.6	72.6± 5.0	84.4± 1.1
P85T15-t	60.7± 1.7	60.8± 2.9	70.7± 4.6	81.9± 0.7
P85T15-r	71.2± 0.7	71.2± 0.6	75.8± 1.2	86.5± 1.6
P85T15Si1-t	N/A	58.4± 4.3	N/A	
P85T15Si1-r		90.6± 1.1		
P85T15Si3-t		62.9± 3.3		
P85T15Si3-r		92.1± 1.4		

Table A-3 % swelling of modified PVA films.

Formula	Curing conditions			
	Room temp.	Cured at 50 °C	Exposure time 10 min	Exposure time 30 min
P100-t	N/A			
P100-r				
P85T0R15-t	N/A		457.8± 8.9	375.8± 16.2
P85T0R15-r			314.6± 8.9	290.7± 7.4
P85T5R10-t			287.1± 2.9	182.1± 5.5
P85T5R10-r			217.7± 19.8	173.5± 9.1
P85T10R5-t			175.3± 3.6	140.4± 12.3
P85T10R5-r			153.8± 3.9	120.6± 6.4
P85T15-t			172.5± 15.4	131.0± 7.0
P85T15-r			120.9± 2.2	75.8± 5.4
P85T15Si1-t			N/A	
P85T15Si1-r				
P85T15Si3-t				
P85T15Si3-r				

Appendix B : Mechanical properties

Table B-1 Tensile strength (MPa) of modified PVA sheets.

Formula	Curing temperatures			
	40 °C	50 °C	60 °C	70 °C
P85T0R15-t	5.4± 0.6	8.5± 0.5	8.6± 0.3	8.6± 0.5
P85T0R15-r	6.3± 0.2	11.0± 1.0	12.1± 0.8	12.1± 1.2
P85T5R10-t	5.0± 0.4	7.1± 0.4	10.4± 0.7	13.5± 0.9
P85T5R10-r	9.1± 0.5	11.6± 0.4	11.9± 0.4	12.6± 0.3
P85T10R5-t	7.7± 0.8	9.7± 1.2	10.1± 0.6	10.9± 1.2
P85T10R5-r	11.0± 0.3	11.1± 0.5	11.9± 0.7	11.9± 0.5
P85T15-t	6.7± 0.3	7.2± 0.4	9.5± 1.1	9.5± 0.4
P85T15-r	9.4± 0.7	10.5± 0.6	10.9± 0.4	11.6± 0.3
P85T15Si1-t	6.8±1.0	8.9±1.6	10.6±0.9	14.1±0.4
P85T15Si1-r	8.3±0.4	11.9±1.5	13.3±1.3	17.3±0.4
P85T15Si3-t	7.2±1.0	9.3±1.5	10.4±1.8	14.6±2.2
P85T15Si3-r	7.0±0.4	14.0±1.1	15.1±1.3	17.7±0.5

Table B-2 Young's modulus (MPa) of modified PVA sheets.

Formula	Curing temperatures			
	40 °C	50 °C	60 °C	70 °C
P85T0R15-t	54.8±6.5	79.8±9.0	79.7±8.7	91.9±9.8
P85T0R15-r	56.3±7.3	65.2±7.9	82.4±5.2	91.2±4.0
P85T5R10-t	107.1±9.4	111.9±12.6	113.0±6.3	122.3±13.0
P85T5R10-r	56.8±12.0	73.7±3.8	74.1±3.6	91.4±2.3
P85T10R5-t	47.4±5.5	93.8±6.4	121.3±12.8	120.7±12.5
P85T10R5-r	73.6±7.3	109.7±5.8	119.8±5.8	120.1±2.7
P85T15-t	69.3±10.6	98.9±8.2	103.3±11.9	113.3±6.4
P85T15-r	44.8±3.5	89.8±8.2	111.9±11.0	119.7±7.7
P85T15Si1-t	108.2±12.4	251.8±19.3	274.5±60.7	368.4±10.5
P85T15Si1-r	113.1±13.7	231.6±27.1	267.1±37.8	371.6±24.8
P85T15Si3-t	116.8±11.4	283.5±75.3	330.0±96.1	415.9±13.9
P85T15Si3-r	104.2±7.9	281.7±23.6	296.9±38.9	406.2±48.6

Table B-3 Tensile strength (MPa) of modified PVA films.

Formula	Curing conditions			
	Room temp.	Cured at 50 °C	Exposure time 10 min	Exposure time 30 min
P85T0R15-r	6.6± 0.7	10.7± 0.7	15.1± 3.4	16.3± 2.9
P85T5R10-r	14.1± 2.0	15.8±0.4	16.9±2.5	17.2±1.4
P85T10R5-r	14.7±3.4	16.4±0.9	22.1±1.8	23.4±1.4
P85T15-r	17.0±1.5	19.6±0.3	22.6±1.7	23.7±3.4

Table B-4 Young's modulus (MPa) of modified PVA films.

Formula	Curing conditions			
	Room temp.	Cured at 50 °C	Exposure time 10 min	Exposure time 30 min
P85T0R15-r	69.5±14.4	295.4±15.1	505.9±34.1	681.2±35.8
P85T5R10-r	475.1±57.8	502.2±14.1	652.1±64.9	708.9±24.4
P85T10R5-r	622.0±87.9	624.5±10.9	647.9±80.3	866.9±43.4
P85T15-r	636.5±38.1	689.2±10.5	703.4±30.6	621.3±37.4

Appendix C : Dynamic Mechanical Analysis

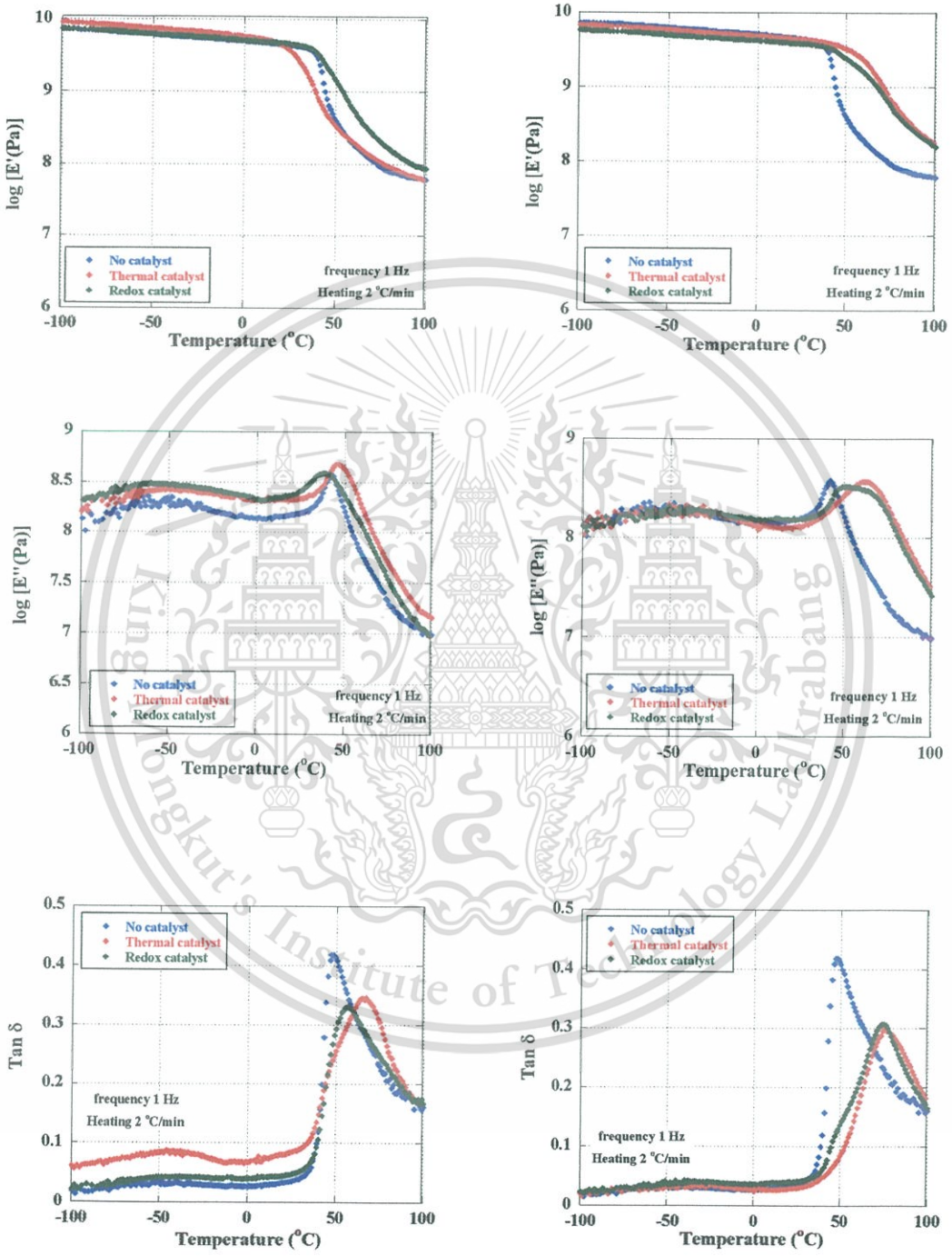

Figure C-1 Temperature dependence of E', E" and tan δ values for PVA sheets (P100) for different catalytic systems cured at 60 °C (left) and cured at 80 °C (right).

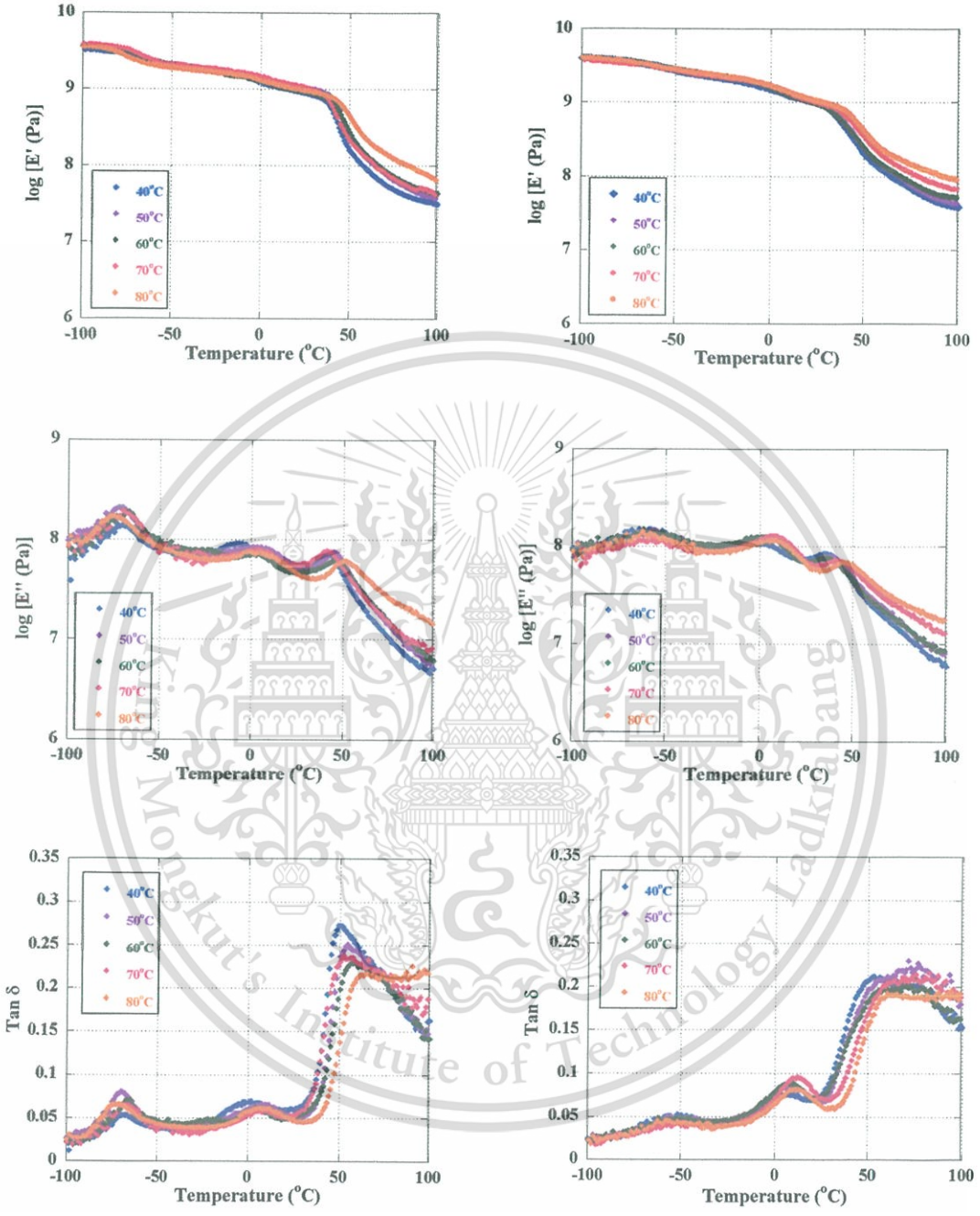

Figure C-2 Temperature dependence of E', E" and tan δ values for P85T15 sheets for different curing temperatures cured by using thermal catalyst (left) and cured by using redox catalyst (right).

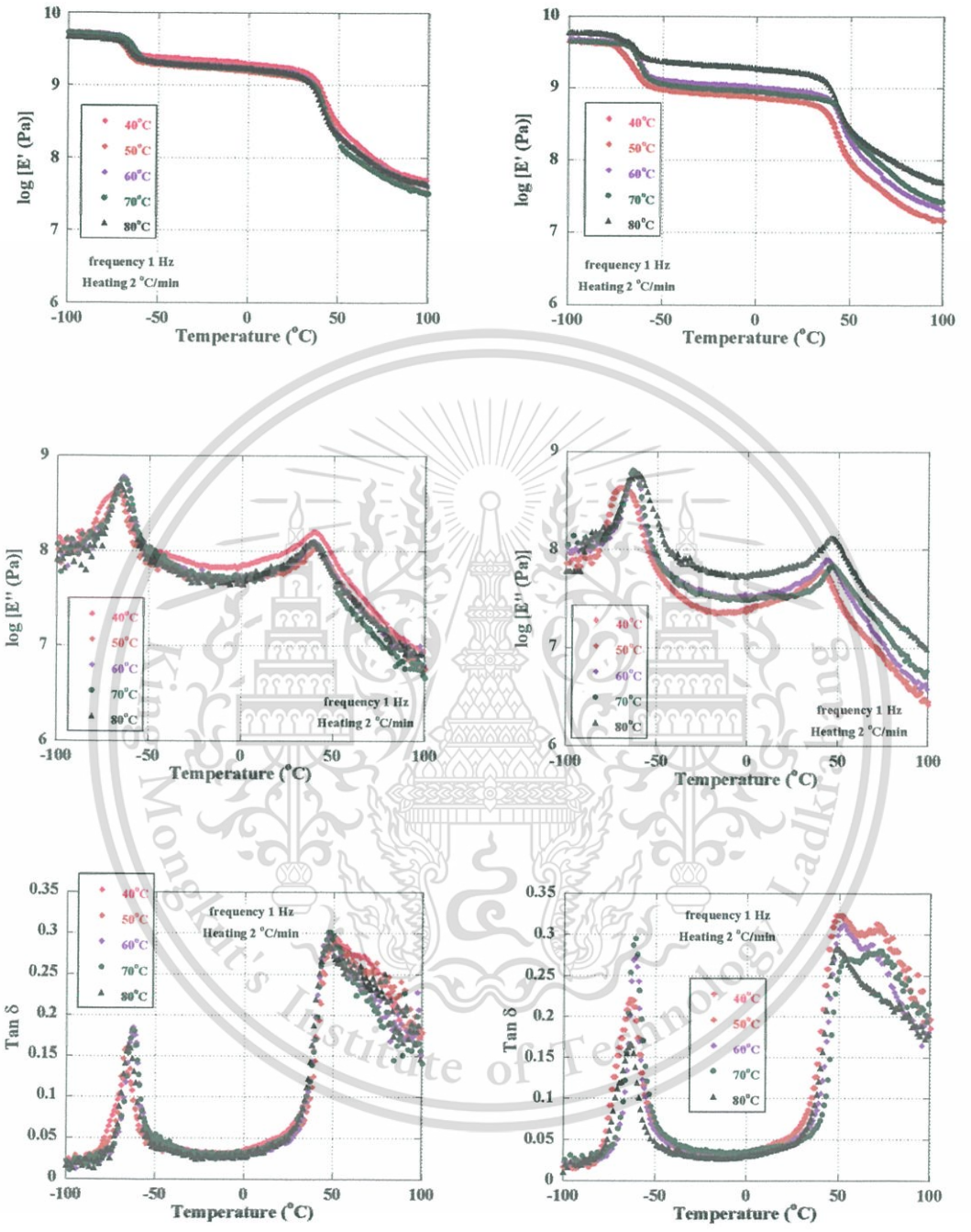

Figure C-3 Temperature dependence of E', E" and tan δ values for P85T0R15 sheets for different curing temperatures cured by using thermal catalyst (left) and cured by using redox catalyst (right).

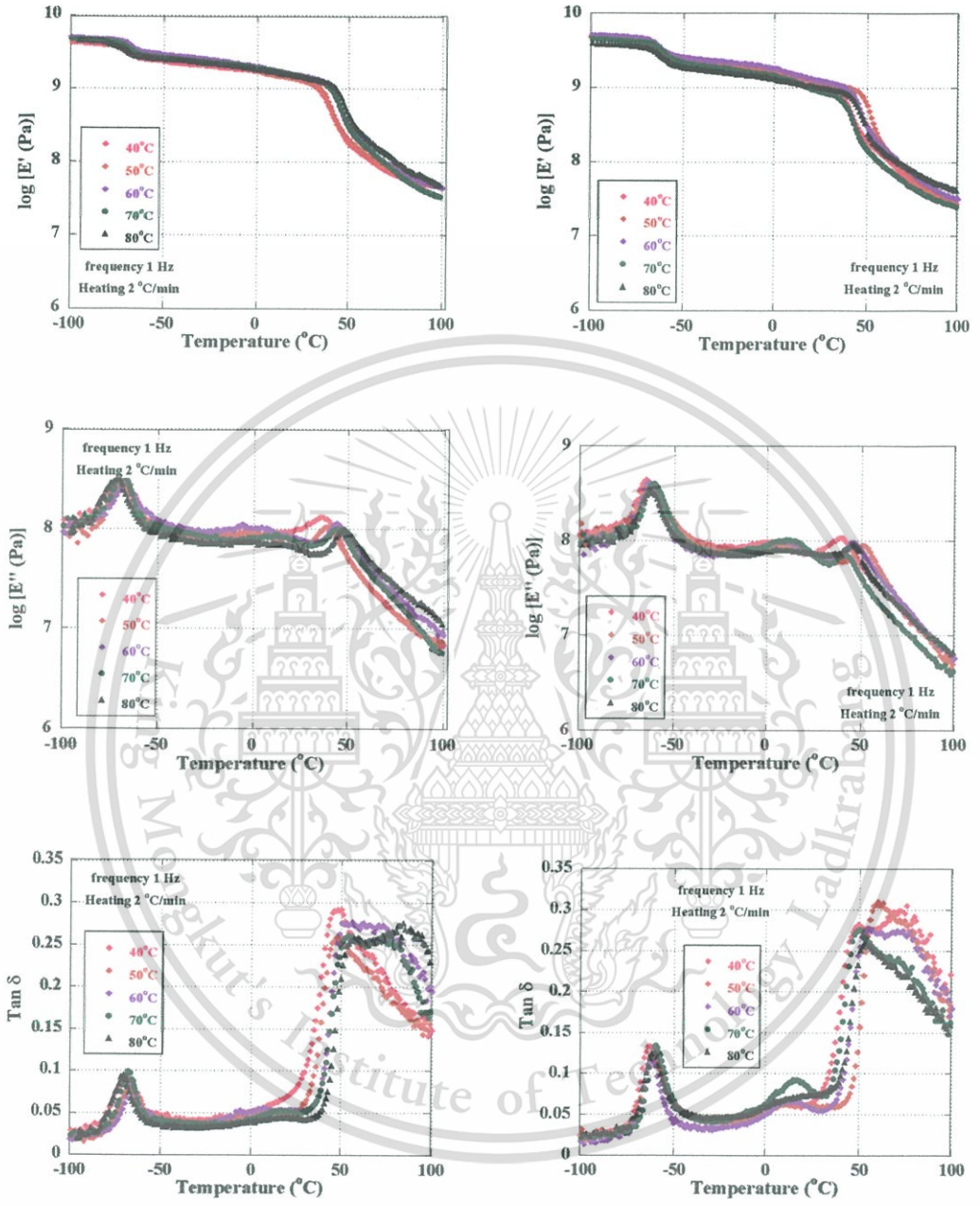

Figure C-4 Temperature dependence of E', E" and tan δ values for P85T5R10 sheets for different curing temperatures cured by using thermal catalyst (left) and cured by using redox catalyst (right).

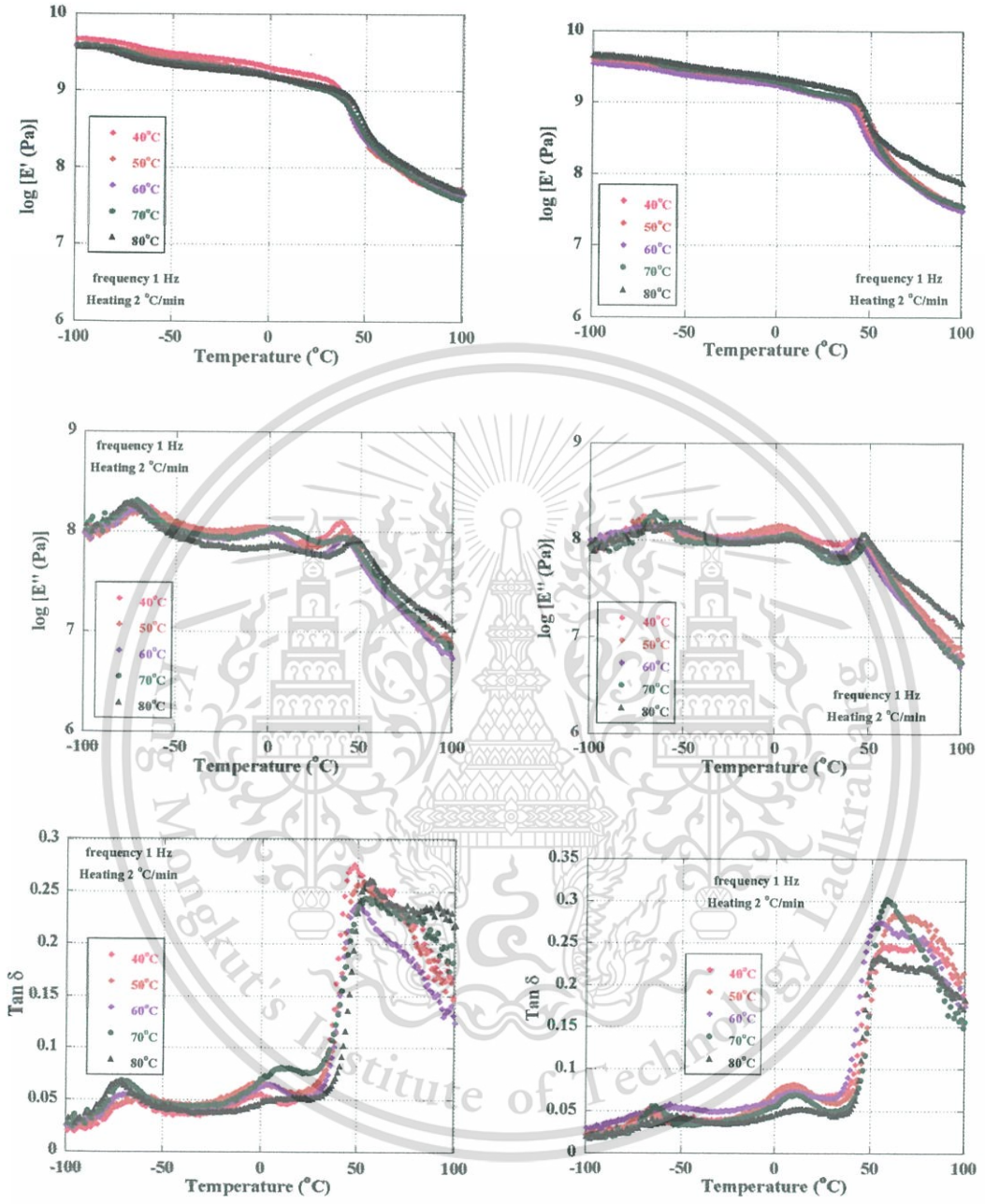

Figure C-5 Temperature dependence of E', E" and tan δ values for P85T10R5 sheets for different curing temperatures cured by using thermal catalyst (left) and cured by using redox catalyst (right).

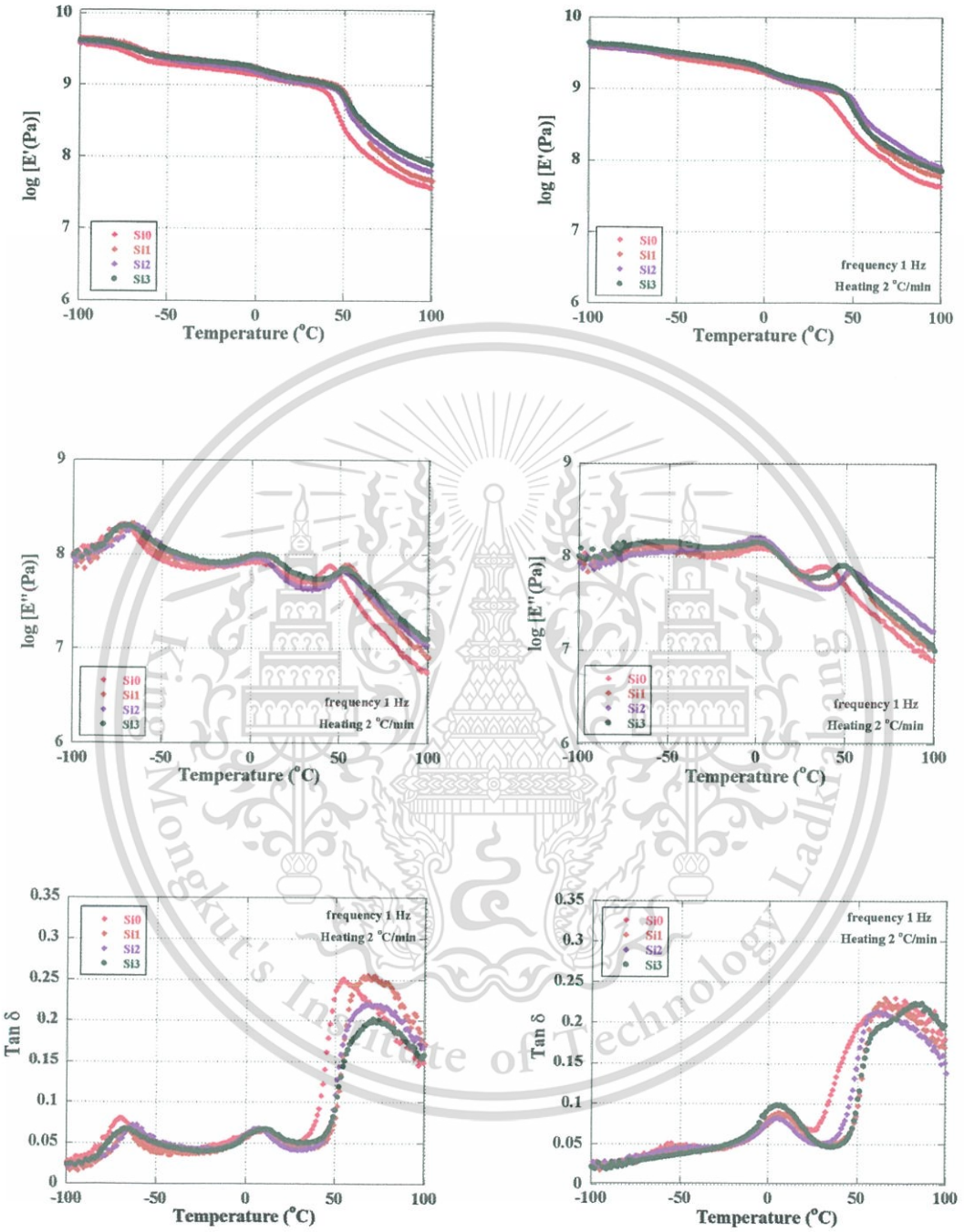

Figure C-6 Temperature dependence of E', E" and tan δ values for P85T15Si sheets using different nanosilica content cured at 50 °C by using thermal catalyst (left) using redox catalyst (right).

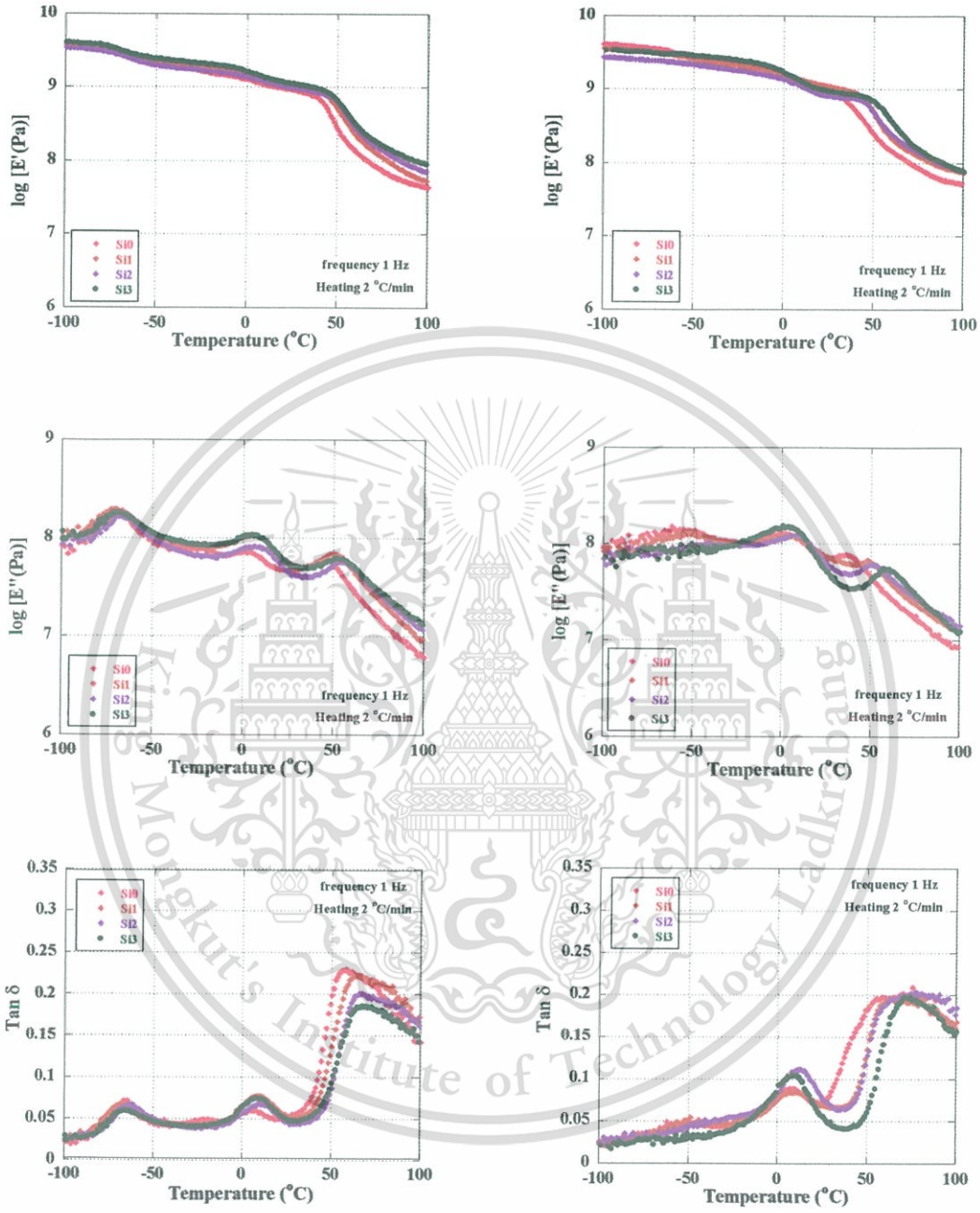

Figure C-7 Temperature dependence of E', E" and tan δ values for P85T15Si sheets using different nanosilica content cured at 60 °C by using thermal catalyst (left) and using redox catalyst (right).

Appendix D : Water and oil contact angles

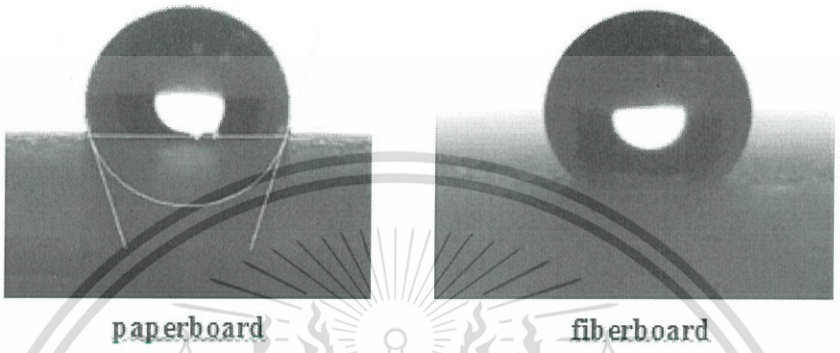

Figure D-1 Water contact angle on the surface of paperboard and fiberboard

Figure D-2 Oil contact angle on the surface of coated paperboards and fiberboard with different coating materials at 50 °C.

PVA-coated paperboard

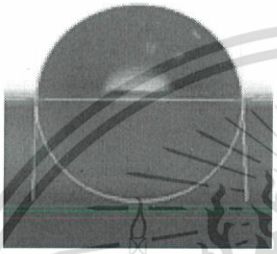

P85T15-t-coated paperboard

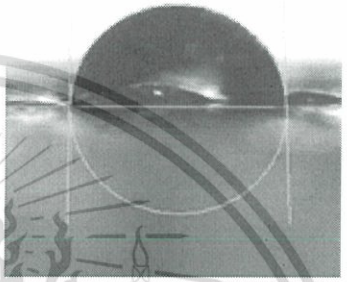

P85T15-t-coated fiberboard

P85T15-r-coated paperboard

P85T15-r-coated fiberboard

Figure D-3 Water contact angle on the surface of coated paperboards and fiberboard with different coating materials at 50 °C.

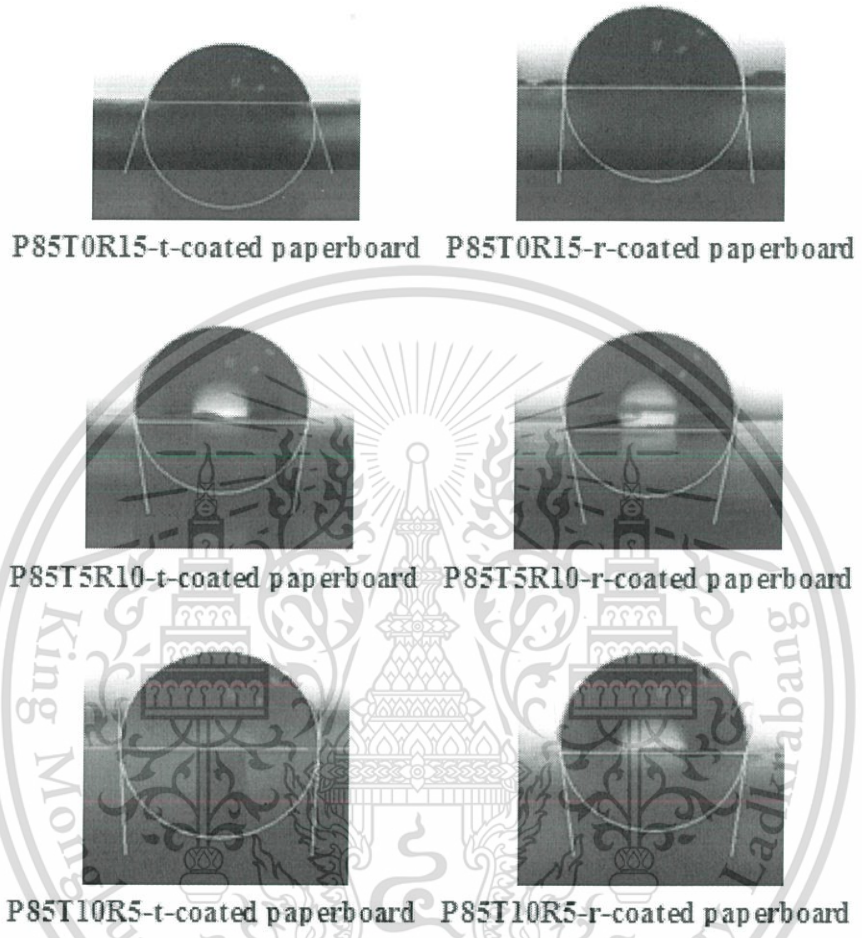

Figure D-4 Water contact angle on the surface of coated paperboards with different coating materials at 50 °C.

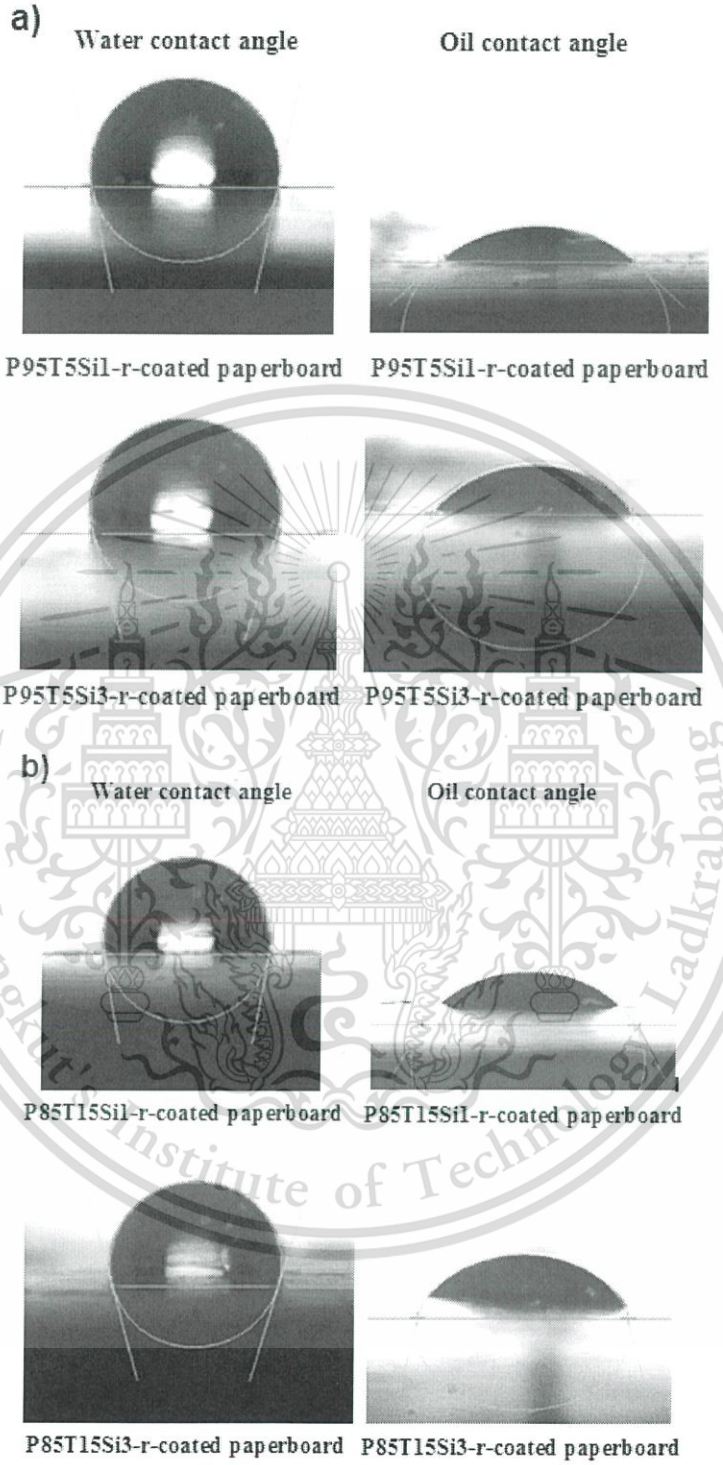

Figure D-5 Water contact angle on the coated paperboards with different coating materials at 50 °C; (a) P95T5Si-r, and (b) P85T15Si-r.

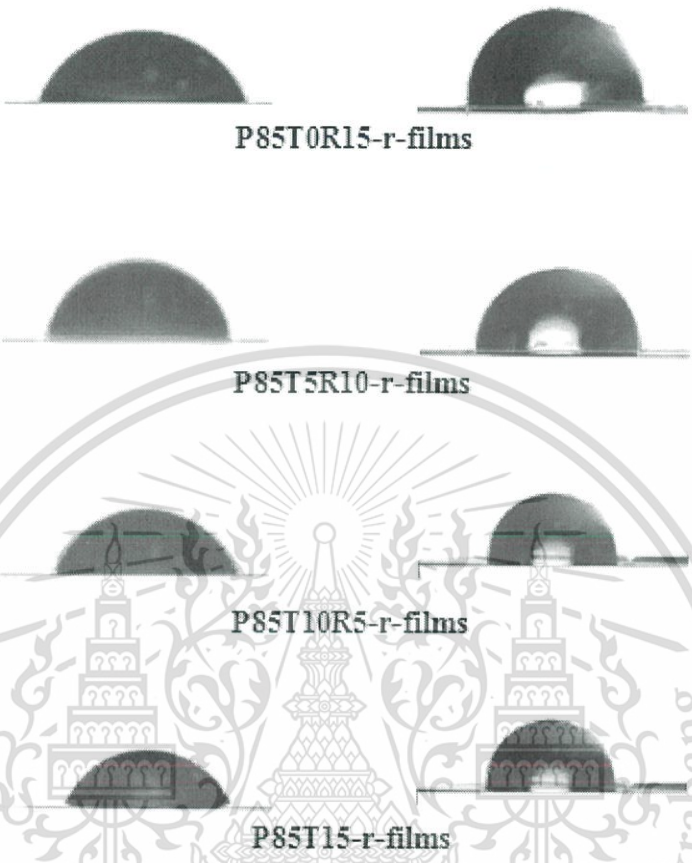

Figure D-6 Water contact angle on the surface of photocrosslinked PTR films for different curing conditions ; dried at room temperature (left) and with exposure time 10 min (right).

Appendix E : Moisture content

Table E-1 % Moisture content of modified PVA films dried at room temperature.

Time (h.)	P85T0R15-r	P85T5R10-r	P85T10R5-r	P85T15-r
0	0	0	0	0
1	3.67	1.83	1.86	3.74
2	5.31	3.05	3.19	4.18
3	5.31	3.66	3.72	5.27
4	6.12	3.96	3.99	5.05
5	6.94	4.27	3.99	4.62
6	6.53	5.18	4.26	5.05
12	6.53	5.18	4.26	4.40
24	6.94	6.10	5.05	4.62
48	8.16	6.10	5.59	5.05
72	7.76	6.71	5.90	5.05
96	7.76	6.71	6.11	5.05

Table E-2 % Moisture content of modified PVA films with exposure time 10 min.

Time (h.)	P85T0R15-r	P85T5R10-r	P85T10R5-r	P85T15-r
0	0	0	0	0
1	3.58	1.51	1.49	2.43
2	5.37	2.51	2.24	2.78
3	6.27	3.02	2.61	2.78
4	6.27	4.02	2.99	2.78
5	6.27	5.03	3.36	3.13
6	6.57	5.53	3.73	3.13
12	6.57	5.53	4.10	3.47
24	6.87	6.03	4.48	3.82
48	6.87	6.03	4.85	3.47
72	7.16	6.53	4.85	3.47
96	7.16	6.53	4.85	3.47

Appendix F : Water vapor permeability (WVP)

Table F-1 Water vapor permeability (WVP) of modified PVA films with exposure time 10 min.

Formula	Curing conditions	Water Vapor Transmission Rate (WVTR) [g/(m^2*day)]	Water vapor permeability (WVP) [x 10^{-4} g/(m*day*kPa)]
PVA	Dried at room temperature	15.83±2.18	6.69±0.62
P85T0R15-r		11.54±0.55	4.20±0.20
P85T5R10-r		13.11±2.41	5.60±0.53
P85T10R5-r		14.76±0.72	6.53±1.16
P85T15-r		15.06±0.75	7.84±0.58
PVA	Exposure time 10 min	-	-
P85T0R15-r		13.97±1.01	3.93±0.39
P85T5R10-r		11.34±1.68	3.96±0.65
P85T10R5-r		13.73±3.40	4.61±0.28
P85T15-r		14.69±0.22	4.64±0.30

Author Biography

Name : Miss Apichaya Jianprasert

Date of Birth : 2 September 1982

Place of Birth : Bangkok, Thailand

Address : 39/9 Village No.6, Thawihong 2 Village, Thepharak Road, Amphur Muang, Samutprakarn, 10270

Educations :

- Senior High School, Wattana Wittaya Academy
- Bachelor's degree of Science , Industrial Chemistry, Faculty of Science, King Mongkut's Institute of Technology Ladkrabang, Thailand
- Master's degree of Science, Polymer Technology, Faculty of Science, King Mongkut's Institute of Technology Ladkrabang, Thailand

Research Topics :

Bachelor's degree : Hydroxyapatite/poly(ethylene terephthlate) (HAp/PET) and Calciumsilicate/poly(ethylene terephthlate) composites (CS/PET) : Preparation, Compressive Strength and Bioactivity.

Master's degree: Effect of Epoxidised Soybean Oil and LLDPE Grafted Maleic Anhydride on Properties of LDPE/Organo-Montmorillonite Nanocomposites.

Publications :

1. **A. Jianprasert,** P. Siriphannon, S. Rukchonlatee and C. Ritvirulh, "*Effect of Compatibilizer on Properties of LDPE/Organo-Montmorillonite Nanocomposites*", **Proceeding of The Thai Institute of Chemical Engineering and Applied Chemistry Annual Conference ,** TIChE17, Thailand. (2007)
2. S. Suebwongnat, **A. Jianprasert**, P. Siriphannon, P. Monvisade, "*Calcium silicate/poly(ethylene terephthalate) biomaterials via ring-opening polymerization*", Journal of Polymer Research, Vol.19, Issue 10 (2012)

3. **A. Jianprasert** and P. Monvisade, "*Improvement of Water Resistance of Formaldehyde-free Adhesive Film Based on PVA/Tung Oil/Natural Rubber Latex*", **Proceeding of 14th RGJ-Ph.D. Congress**, Pattaya, Thailand (2013)

4. **A. Jianprasert** and P. Monvisade, "*Improvement of Water Resistance of Formaldehyde-free Adhesive Film Based on PVA/Tung oil/Natural Rubber Latex*", **Proceeding of 2013 International Symposium on Technology for Sustainability,** ISTS2013, Hong Kong, China

5. N. Oonkasem, P. Monvisade and **A. Jianprasert**, "*Development of Formaldehyde-free Adhesive from Poly(vinyl alcohol) Modified with Tung oil and Natural Rubber Latex for Particle Board*", **Proceeding of 2013 International Symposium on Technology for Sustainability,** ISTS2013, Hong Kong, China

6. **A. Jianprasert**, P. Monvisade and M. Yamaguchi, "*Combination of Tung oil and Natural Rubber Latex in PVA as Water Based Coatings for Paperboard Application*", MATEC Web of Conferences, Vol.30 (2015)

7. **A. Jianprasert**, P. Monvisade, M. Yamaguchi, "*Surface improvement on water and oil affinities and absorption rate of PVA/Tung oil-coated paperboard and fiberboard*", Journal of Coatings Technology and Research, Vol.13, Issue 2 (2016)

8. **A. Jianprasert**, P. Monvisade, M. Yamaguchi, "*Study on Crosslinked Structure and Thermal Properties of Polymer Networks Based on Tung Oil and PVA with Different Catalytic Systems*", Macromolecular Symposia, Vol.372, (2017)